Catalytic carboxylation of sp^2 and sp^3 C-H bonds with CO_2 under atmospheric pressure conditions: An integrated experimental and theoretical study

Paltu Kumar Giri, Pooja Rani, Manpreet Kaur, T. J. Dhilip Kumar and C. M. Nagaraja*

Department of Chemistry, Indian Institute of Technology Roapr, Rupnagar 140001, Punjab, India, Tel:91-1881-242229, Email:cmnraja@iitrpr.ac.in

Table of Contents

Materials and Methods

All reagents used in this study were commercially available and used as received without further purification. The $AgNO_3$, CuI, 1H-pyrazole-4-carbaldehyde, 2′-Bromoacetophenone, 4,4',4"-(1,3,5-triazine-2,4,6-triyl)trianiline (TAPT), 1-(2-bromophenyl)ethan-1-one and Phenylacetylene were purchased from Sigma Aldrich Chemical Co. The phase purity of the

COF samples was confirmed by powder XRD analysis, recorded on a PAN Analytical's X'PERT PRO diffractometer using Cu K_α radiation (k = 1.542 Å; 40 kV, 20 MA). Fourier transform infrared (FT-IR) spectra of the samples were recorded on a Perkin-Elmer FT-IR spectrometer. The UV−Vis (Diffuse Reflectance) spectra were recorded on a Shimadzu spectrophotometer using $BaSO_4$ as a reference. The metal content of Ag in the framework was determined by Agilent's microwave-plasma atomic emission spectrometer (MP-AES). The X-ray photoelectron spectroscopy (XPS) analyses were performed on a Thermo Fisher Scientific NEXSA photoemission spectrometer using Al Kα (1486.6 eV) X-ray radiation, and analysis of the obtained data was performed using Avantage software. Thermogravimetric analysis (TGA) of Ag_3-TAPT-COF was carried out on a Mettler Toledo Thermogravimetric Analyzer in the air atmosphere (flow rate of 30 $mL.min^{-1}$) in the temperature range of 30-800 °C (heating rate of 10 °C min^{-1}). ^1H and ^{13}C NMR spectra were recorded in $CDCl_3$ and DMSO-d_6 on a JEOL JNM-ECS 400 spectrometer operating at 400 MHz and 101 MHz, respectively.

Experimental Section

Synthesis of Ag_3L_3

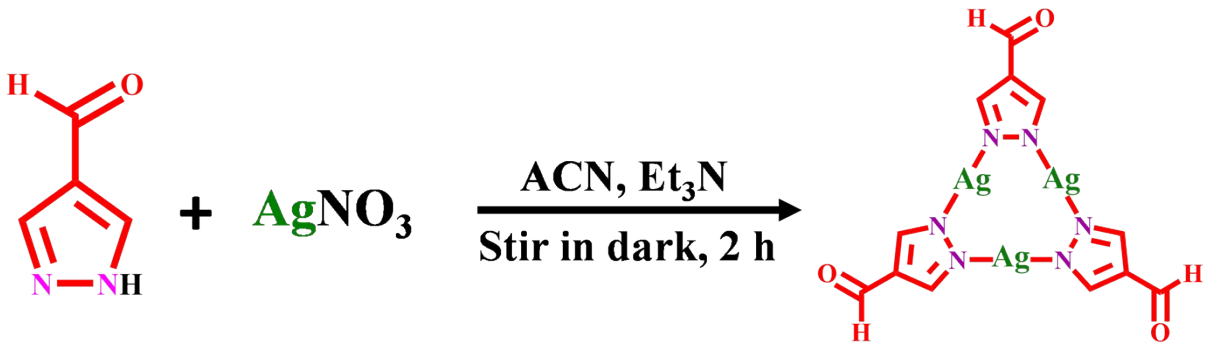

Scheme S1 Synthesis of Ag_3L_3 cluster.

A mixture of ligand, 1H-pyrazole-4-carbaldehyde (HL) (48 mg, 0.5 mmol), $AgNO_3$ (85 mg, 0.5 mmol), 15 mL acetonitrile, and 0.2 mL triethylamine were taken in a 20 mL Schlenk tube. Then, the resulting mixture was stirred for 2 h in the dark. Afterward, the product obtained was washed with acetonitrile and absolute ethanol and filtered to give a white crystalline powder of Ag_3L_3. Further, the formation of Ag_3L_3 was confirmed by ^1H, ^{13}C NMR and FT-IR analyses. Importantly, the PXRD pattern of the formed trinuclear complex was well matched with the reported literature, suggesting the formation of Ag_3L_3 cluster (Scheme S1 and Fig.s S1-S4), (94.07 mg, yield: 71.5% based on $AgNO_3$). ^1H NMR (400 MHz, DMSO-d_6) δ (ppm) 9.84 (s, 1H), 8.20 (s, 2H). ^{13}C NMR (101 MHz, DMSO-d_6) δ (ppm) 184.85, 143.68, 123.10.

The yield and selectivity of the carboxylated product are determined by using the following formula.

$$\text{Isolated Yields (\%)} = \frac{\text{Amount of desired product obtained}}{\text{Amount of starting materials used}} \text{ X } 100$$

$$\text{Selectivity (\%)} = \frac{\text{Moles of desired product obtained}}{\text{Moles of all product formed}} \text{ X } 100$$

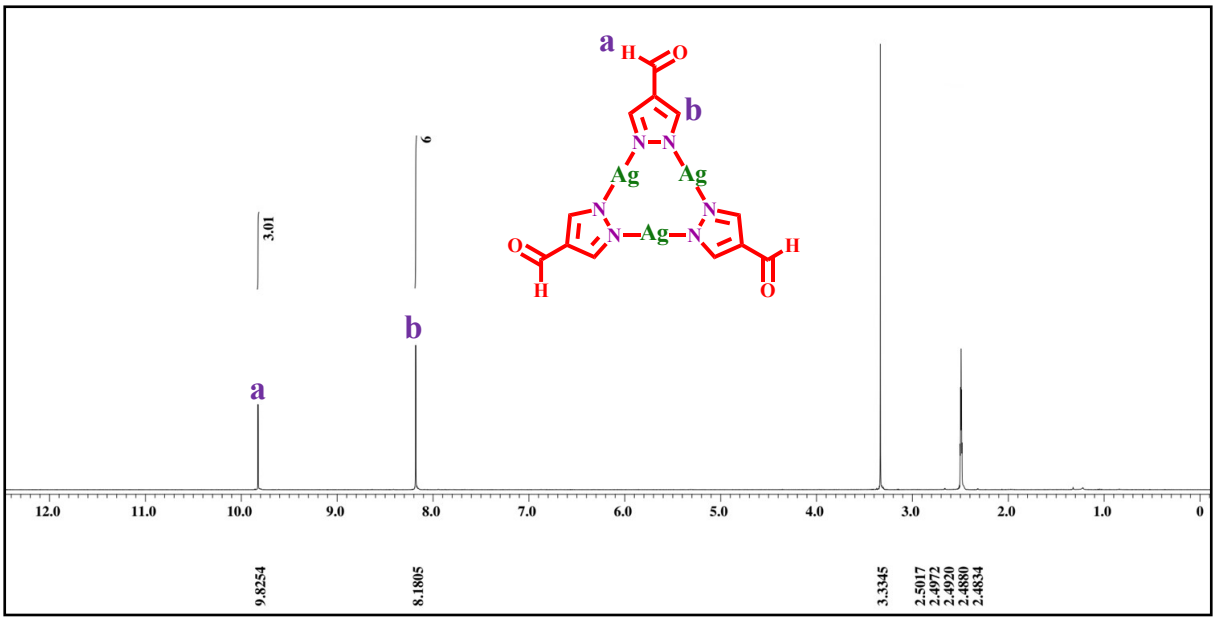

Fig. S1 ^{1}H-NMR (400 MHz, DMSO-d_6) spectrum of Ag_3L_3 cluster.

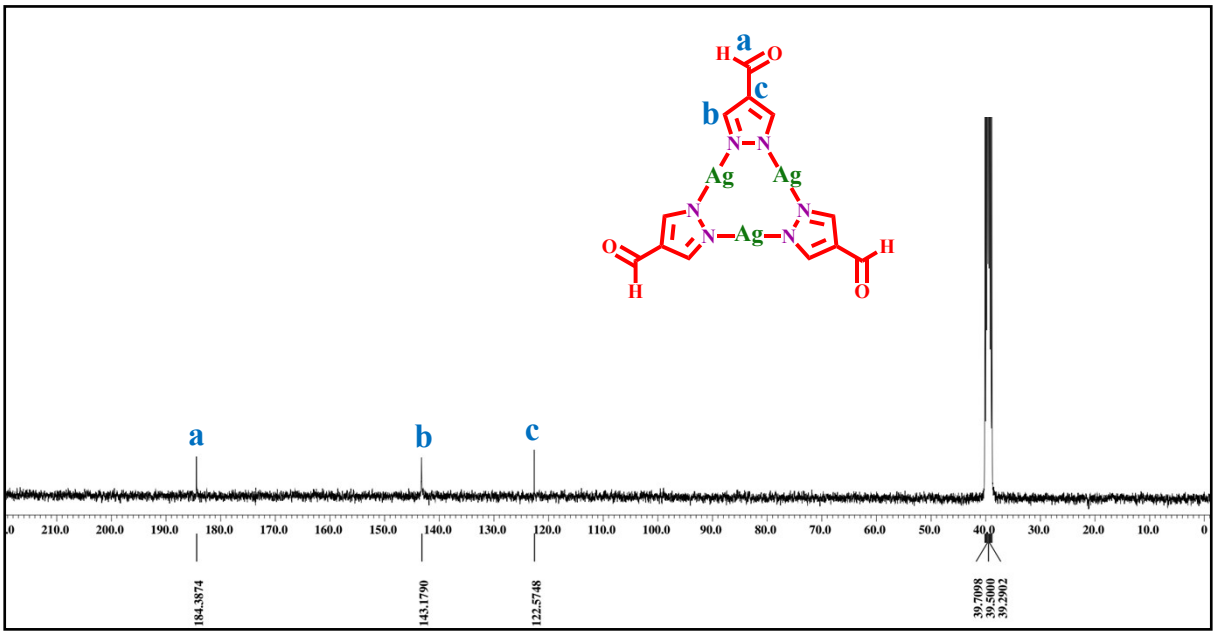

Fig. S2 ^{13}C-NMR (101 MHz, DMSO-d_6) spectrum of Ag_3L_3 cluster.

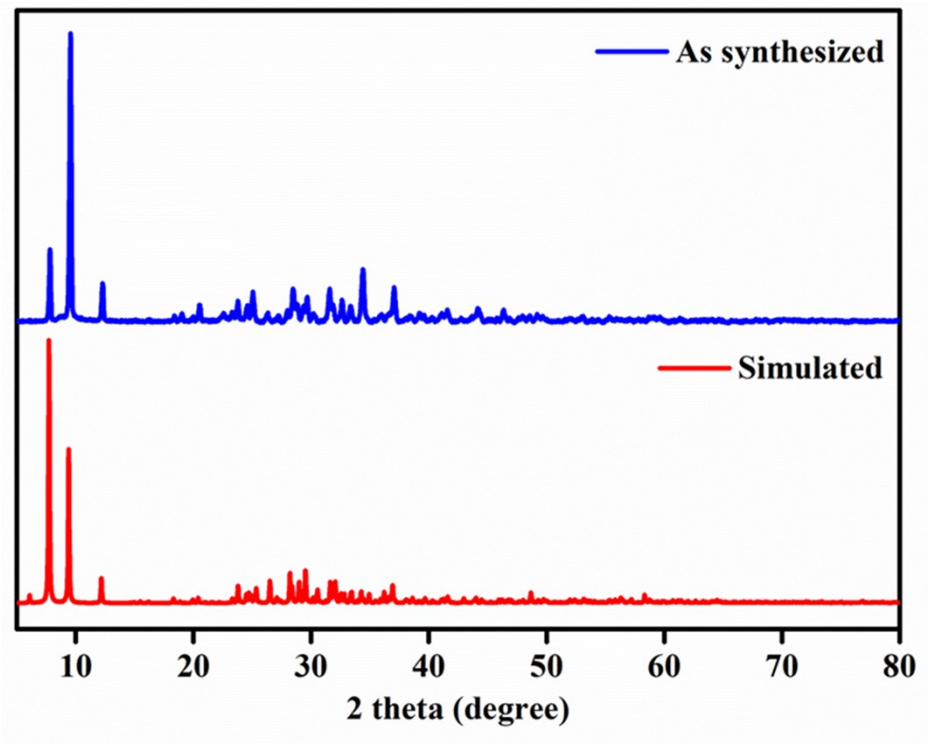

Fig. S3 PXRD patterns of Ag_3L_3 cluster (Blue line: experimental pattern; and red line: simulated pattern from single crystal data), proving the phase purity of Ag_3L_3 cluster.

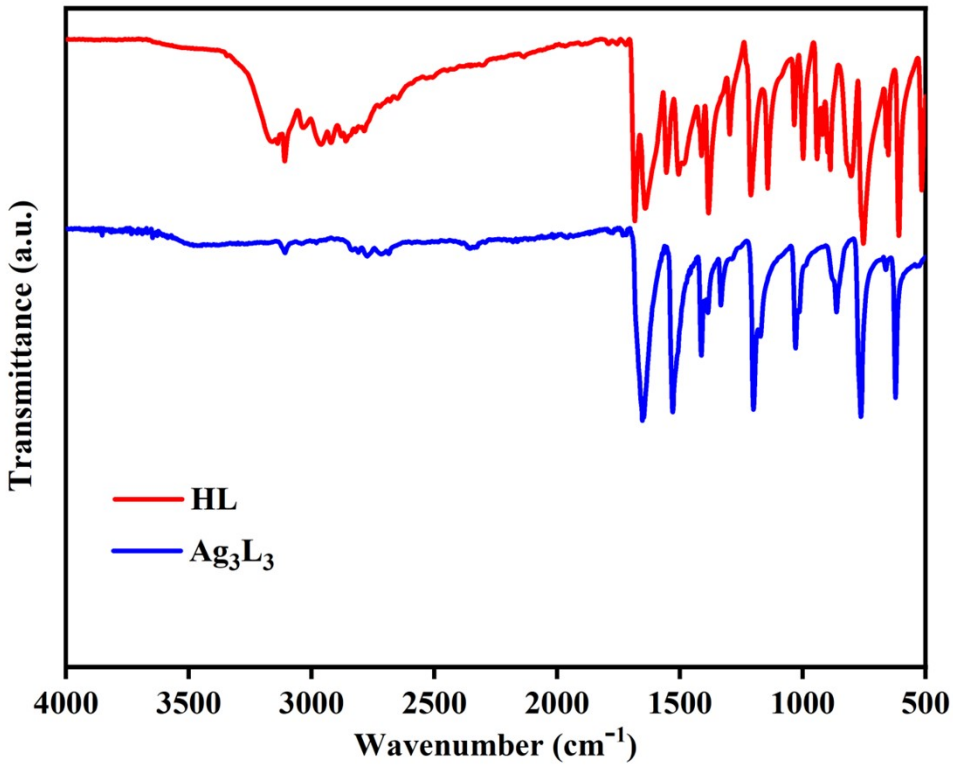

Fig. S4 FT-IR spectra of Ag_3L_3 cluster and 1H-pyrazole-4-carbaldehyde (HL).

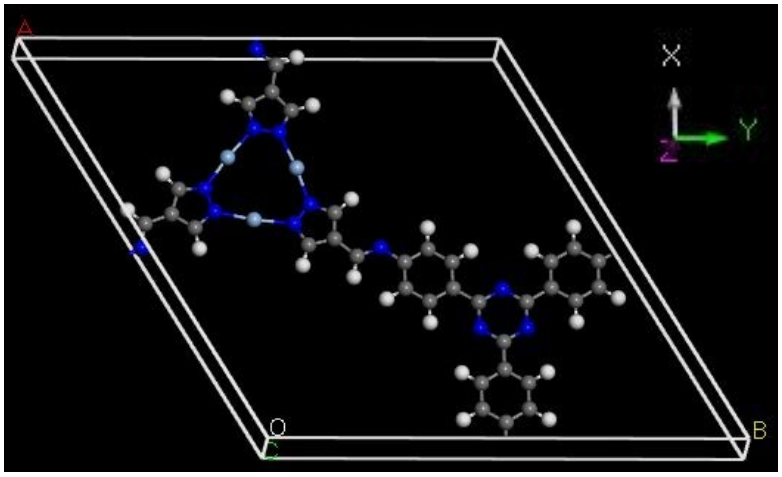

Fig. S5 Unit cell of Ag_3-TAPT-COF.

Catalyst Preparation

Synthesis of Ag_3-TAPT-COF

The Ag_3-TAPT-COF was synthesized according to the reported literature.[1] A 10 mL Schlenk tube was charged with Ag_3L_3 (30.45 mg, 0.05 mmol), 4,4',4''-(1,3,5-triazine-2,4,6-triyl)trianiline (TAPT) (17.7 mg, 0.05 mmol), benzyl alcohol (0.5 mL), 1,2-dichlorobenzene (0.5 mL), and 0.1 mL of 6 M trifluoroacetic acid. The tube was flash-frozen at 77 K in a liquid nitrogen bath and degassed with three freeze-pump-thaw cycles. After warming to room temperature and ultrasonic microwave treatment for 30 min, the mixture was heated at 65 °C for 8 h. The obtained solid was isolated by filtration, washed, and solvent-exchanged with methanol to afford TAPT Ag_3-TAPT-COF (41.2 mg, 87% yield) with a molecular formula of $[C_{33}H_{21}Ag_3N_{12}]_n$.

Catalytic CO_2 Fixation to sp^2 C–H Bonds of 4-Hydroxy-2-pyridones

All catalytic carboxylation reactions were carried out in a 50 mL Schlenk tube. Prior to use, the Ag_3-TAPT-COF catalyst was activated at 90 °C under vacuum for 12 h. In a typical experiment, the activated catalyst (10 mg), 4-Hydroxy-2-pyridones (1 mmol), and LiHMDS (1.5 mmol) were added to the Schlenk tube, followed by 5 mL of DMF as the reaction solvent.

The mixture was then stirred at 50 °C under an atmospheric pressure of CO_2 for 12 h. After completion of the reaction, the catalyst was separated by centrifugation and quenched by adding a saturated solution of NH_4Cl at room temperature. Then, the reaction mixture was acidified with 1M HCl to adjust the pH to approximately 1. The product was extracted with ethyl acetate, washed with brine, and dried over anhydrous Na_2SO_4. The solvent was removed under reduced pressure using a rotary evaporator to afford the corresponding carboxylic acid as a solid product. The crude product was recrystallized from ethanol to afford the pure product, which was characterized by both ^1H and ^{13}C NMR spectroscopy.

Synthesis of 1-(2-(phenylethynyl)phenyl)ethan-1-one

1-(2-(phenylethynyl)phenyl)ethanone was synthesised following a previously reported procedure with minor modifications.[2] In a typical procedure, 2′-Bromoacetophenone (0.27 ml, 2.0 mmol, 1.0 equiv.), phenylacetylene (0.22 ml, 2.0 mmol, 1.0 equiv.), $PdCl_2(PPh_3)_2$ (28.1 mg, 0.04 mmol, 0.02 equiv.), and CuI (7.618 mg, 0.04 mmol, 0.02 equiv.) were added into an oven-dried Schlenk flask, evacuated, and backfilled with nitrogen (3 times). Anhydrous DMF (5.6 ml, 0.33 M) and triethylamine (0.84 ml, 6.0 mmol, 3 equiv.) were injected sequentially into the flask. The reaction mixture was heated in an oil bath at 50 °C, under a nitrogen atmosphere, and kept stirring for 12 h. Then, the mixture was cooled to room temperature, diluted with diethyl ether, and filtered through a pad of Celite. The filtrate was poured into distilled water, and the aqueous layer was extracted with diethyl ether (3 times). The combined organic layers were dried over Na_2SO_4, filtered, and concentrated under reduced pressure. The product was isolated by column chromatography (silica gel, hexane: EtOAc 98:2).

Catalytic CO_2 Fixation to sp^3 C–H Bonds of 1-(2-(phenylethynyl)phenyl)ethan-1-one

The carboxylation of the sp^3 C–H bond of 1-(2-(phenylethynyl)phenyl)ethan-1-one with CO_2 was conducted in a 50 mL Schlenk tube under 1 atm of CO_2 (using a balloon). Before the reaction, the catalyst was thoroughly activated in a vacuum oven at 80 °C for 12 h. Subsequently, the catalyst (10 mg) and 1-(2-(phenylethynyl)phenyl)ethan-1-one(2.0 mmol) were introduced into the tube under vacuum, followed by the addition of DBU (2.5 mmol). The Schlenk tube was filled with CO_2 at 1 atm (using a balloon). Then, DMF (5 mL) was added under constant stirring and heating at 50 °C for 24 h. Then, the reaction was quenched with H_2O at RT. Further, the solution was acidified to pH 1 using concentrated HCl and stirred for 30 min. After extraction of the product with ethyl acetate (3 times), the combined organic phases were dried over anhydrous Na_2SO_4, filtered, and concentrated using rotavap. The crude product was purified by washing with Hexane: ethyl acetate (95:5, V:V) and subsequently characterized by NMR spectroscopy.

Computational Details

Density functional theory (DFT) calculations were carried out within the Kohn–Sham framework using the generalized gradient approximation (GGA), specifically the Perdew–Burke–Ernzerhof (PBE) exchange–correlation functional. Molecular geometries were optimized with the double-numeric polarized (DNP) basis set. As GGA functionals typically underestimate weak long-range interactions such as van der Waals (vdW) forces, Grimme's dispersion correction (DFT-D) was incorporated to improve the accuracy of the computations. During electronic relaxation, self-consistent field (SCF) convergence criteria of 1×10^{-5} Ha for the total energy and 2×10^{-3} Ha $Å^{-1}$ for the gradient were applied. A maximum atomic displacement threshold of 0.005 Å was also enforced to ensure reliable optimization. Transition states were located using the combined linear synchronous transit and quadratic synchronous transit (LST/QST) approach.

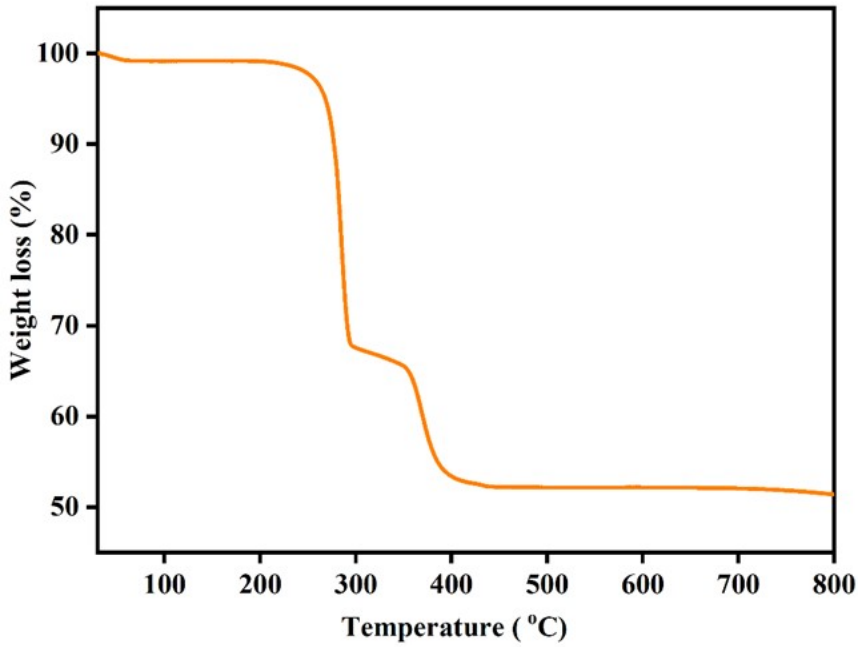

Figure S6. TGA plot of Ag_3 cluster.

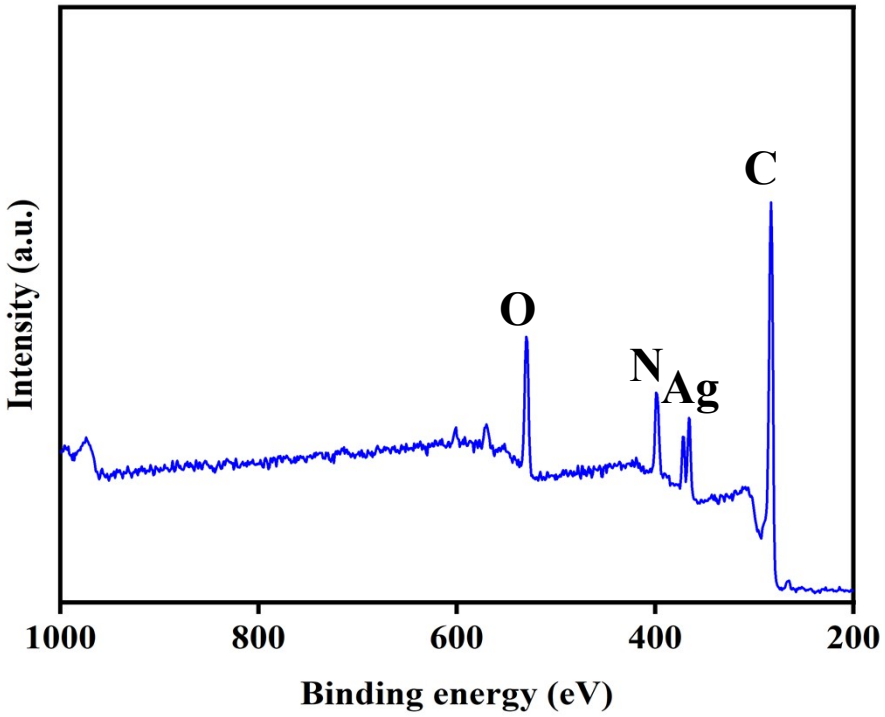

Fig. S7 XPS survey spectra of Ag_3-TAPT-COF.

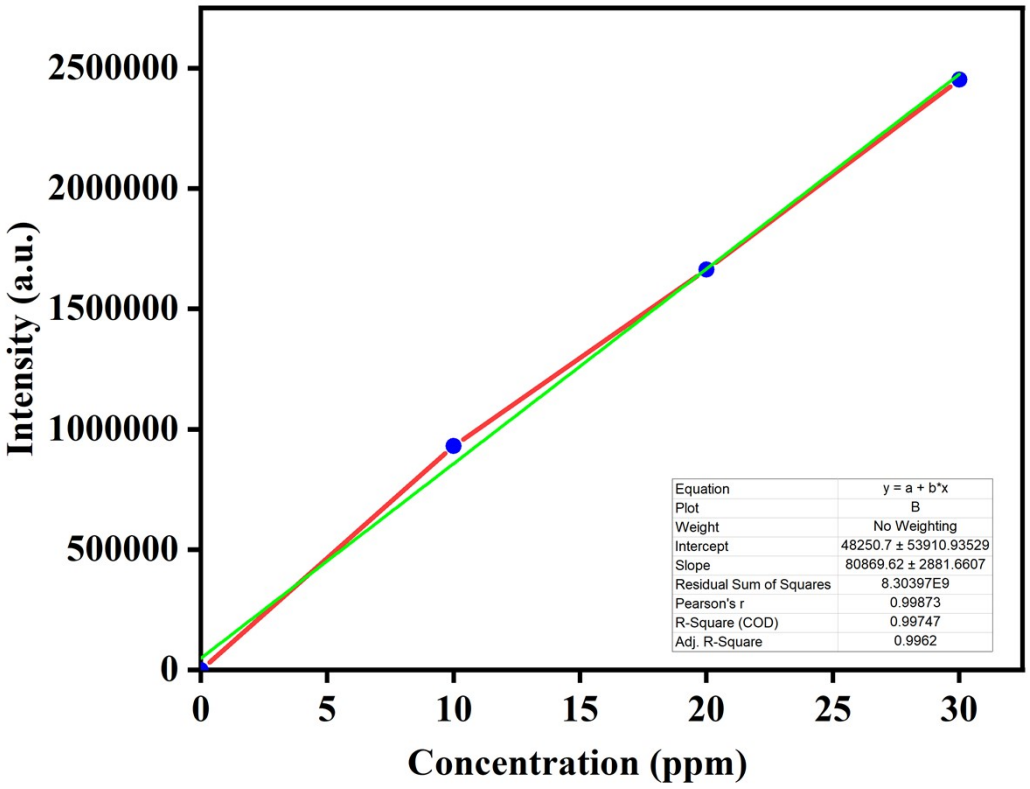

Fig. S8 MP-AES calibration curve for the estimation of Ag content in Ag_3-TAPT-COF.

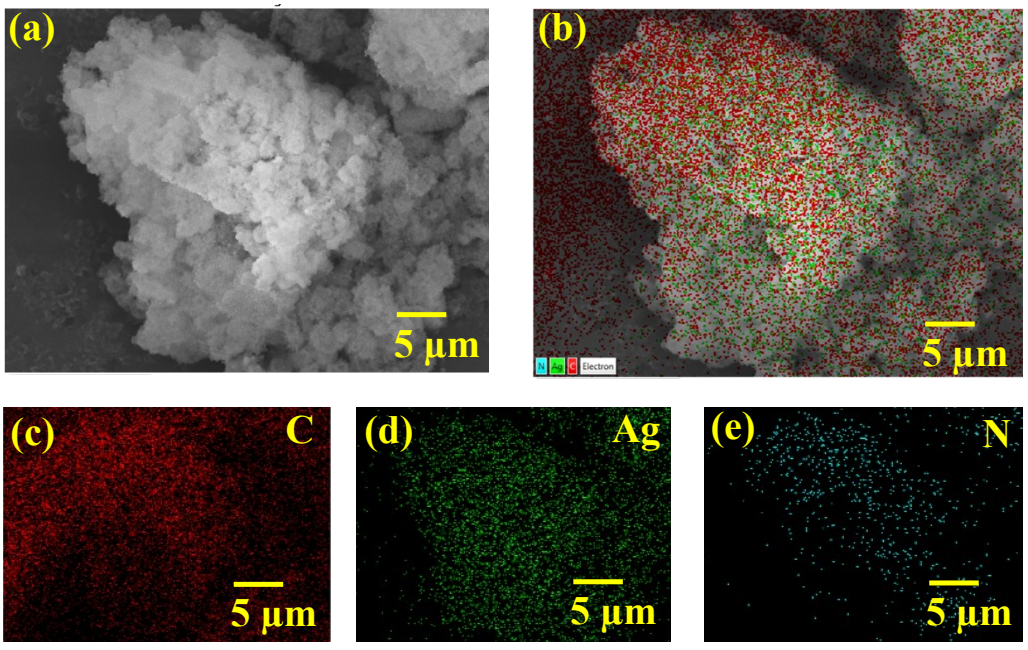

Fig. S9 (a) FE-SEM image of Ag_3-TAPT-COF, (b) Elemental mapping representing (c) C (red), (d) Ag (green), and (e) N (cyan).

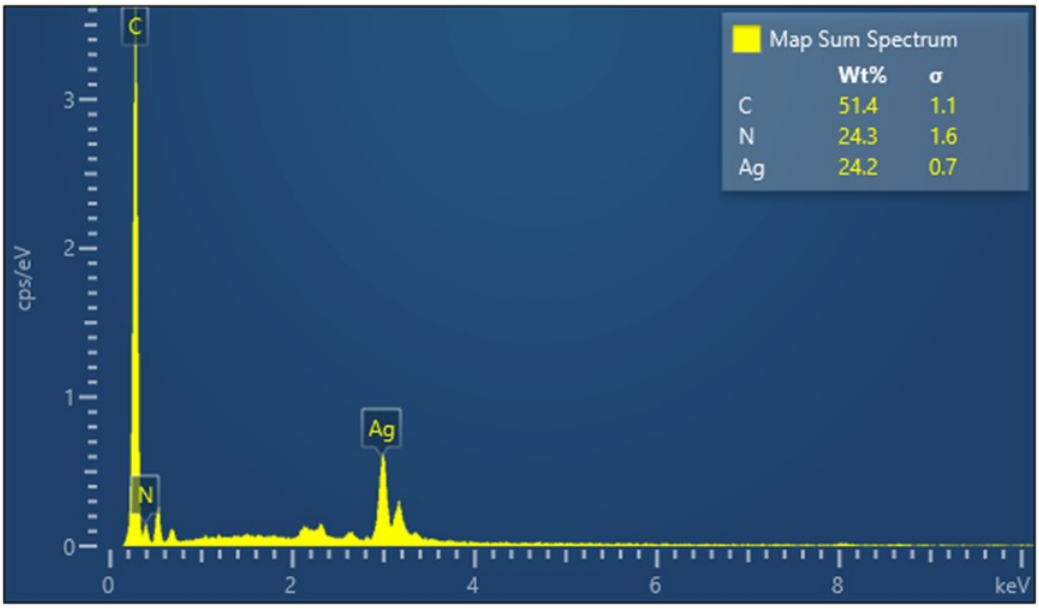

Fig. S10 EDX spectra of Ag_3-TAPT-COF.

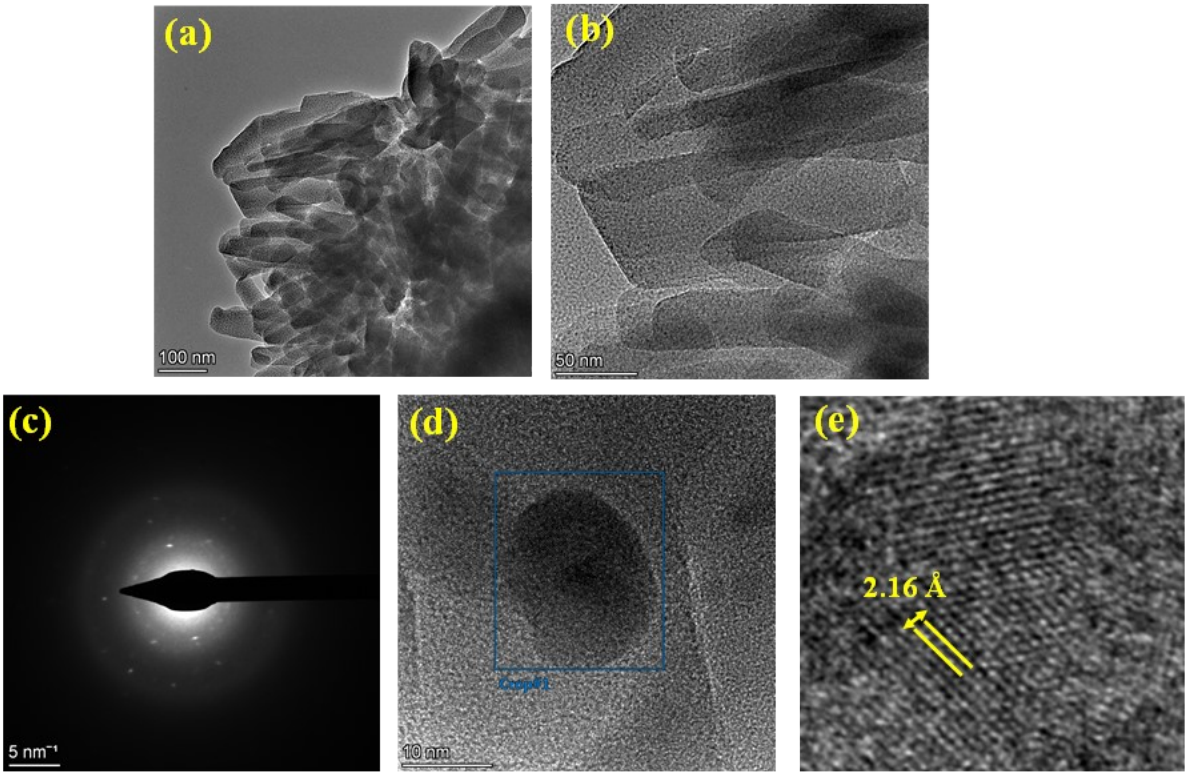

Fig. S11 (a and b) HR-TEM images. (c) SAED pattern and (d and e) lattice fringes of Ag_3-TAPT-COF.

Gas adsorption measurements

Gas adsorption measurements of the samples were performed on Quantachrome's QUADRASORB-SI automatic volumetric instrument using ultrapure (99.995%) N_2, CH_4, and CO_2 gases. Before adsorption measurements, the COF sample (~ 0.10 g) was activated by heating at 120 °C under vacuum (18 m Torr) for 24 h. The N_2 adsorption measurements were carried out at 77K, and the CO_2 adsorption measurements were performed at 273 K and 298 K. The 273 and 298 K temperatures were achieved using a water chiller with appropriate coolants. Whereas 77K was achieved using liquid nitrogen.

Analysis of gas adsorption isotherms

The Clausius-Clapeyron equation[3] was used to calculate the enthalpies of carbon dioxide adsorption. Using the Langmuir-Freundlich equation, an accurate fit was retrieved to predict the carbon dioxide adsorbed at saturation. A modified Clausius-Clapeyron equation was used for calculation.

$$ln(P1/P2) = \Delta H_{ads}(T2 - T1/R.T1.T2) \quad \text{.....(1)}$$

P_1 and P_2 = Pressures for isotherms at 273K and 298K, respectively.

T_1 and T_2 = Temperatures for isotherms at 273K and 298K, respectively.

ΔH_{ads} = Enthalpy of adsorption.

R = Universal gas constant (8.314 J/K/mol).

The pressure is a function of the amount of gas adsorbed, which was determined using the Langmuir-Freundlich fit.

$$Q/Q_m = B.P^{(1/t)}/1 + (B.P^{(1/t)}) \quad \text{.....} (2)$$

where Q = moles of gas adsorbed.

Q_m = moles of gas adsorbed at saturation.

B and t = constants.

P = Pressure.

By rearranging equation (2), we get equation (3)

$$P = [(Q/Q_m)/\{B - (B.(Q/Q_m)\}]^t \quad \text{.....(3)}$$

Substituting equation (3) into equation (1), we get

$$\Delta H_{ads} = \{R.T1.T2/(T2 - T1)\}.ln\frac{[(Q/Q_{m1})/\{B - (B.Q/Q_{m1})\}]^{t1}}{[(Q/Q_{m2})/\{B - (B.Q/Q_{m2})\}]^{t2}} \quad \text{.....(4)}$$

In equation (4), subscripts 1 and 2 represent data corresponding to 273K and 298K for carbon dioxide gas.

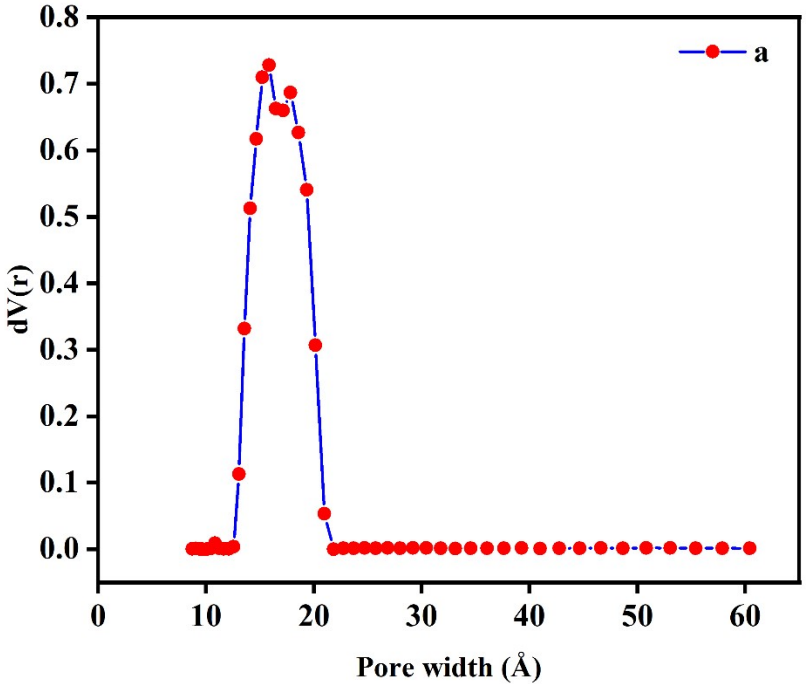

Fig. S12 Pore size distribution plot of Ag_3-TAPTT-COF.

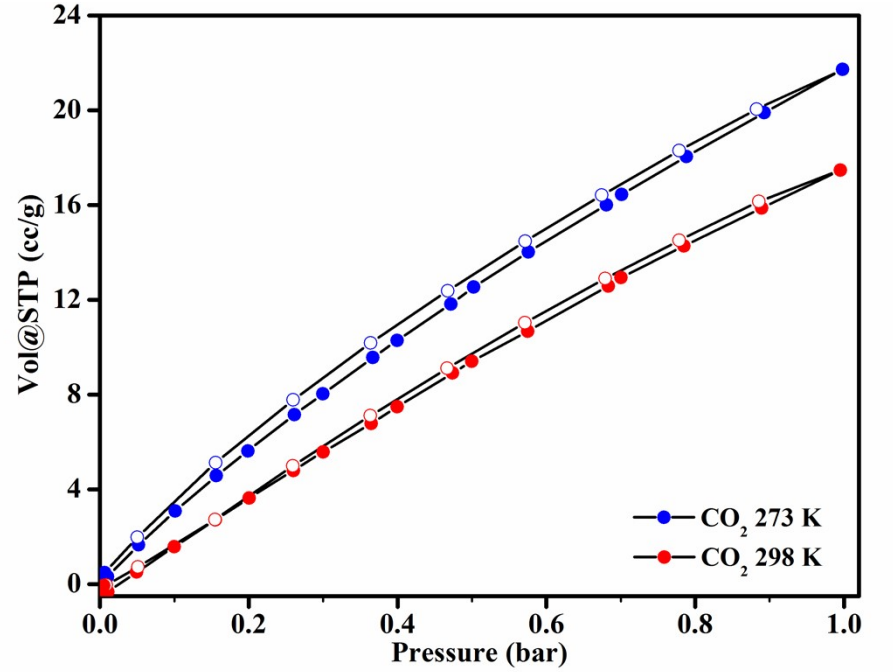

Fig. S13 CO_2 sorption isotherms for Ag_3-TAPT-COF at 273/298 K.

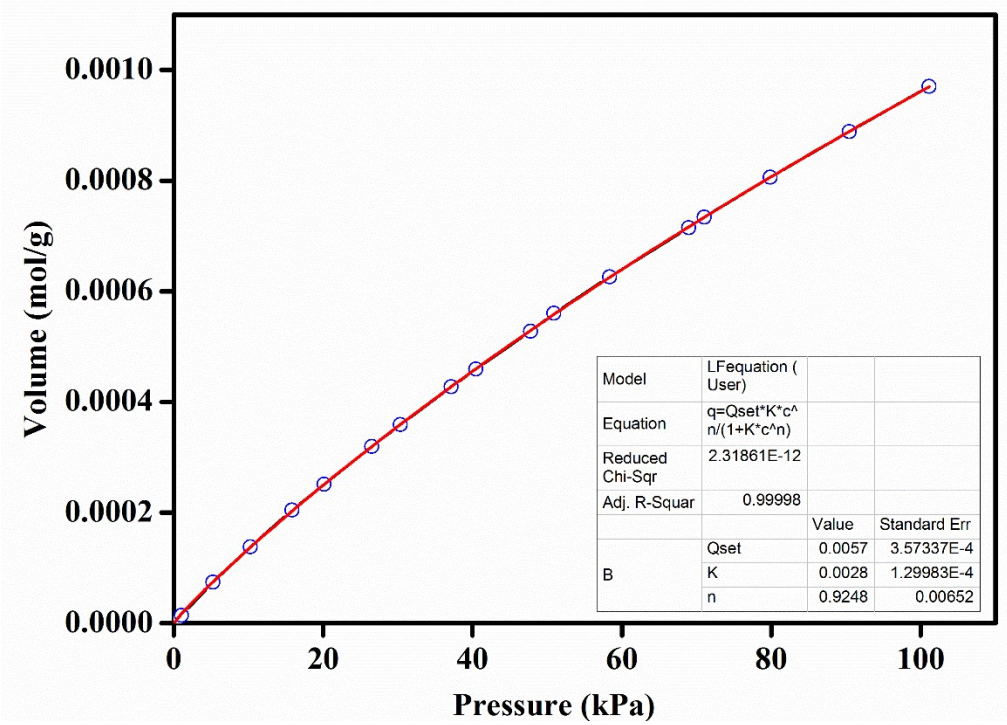

Fig. S14 Carbon dioxide adsorption isotherm of Ag_3-TAPT-COF carried out at 273 K. The solid line shows the best fit to the data using the Langmuir-Freundlich equation.

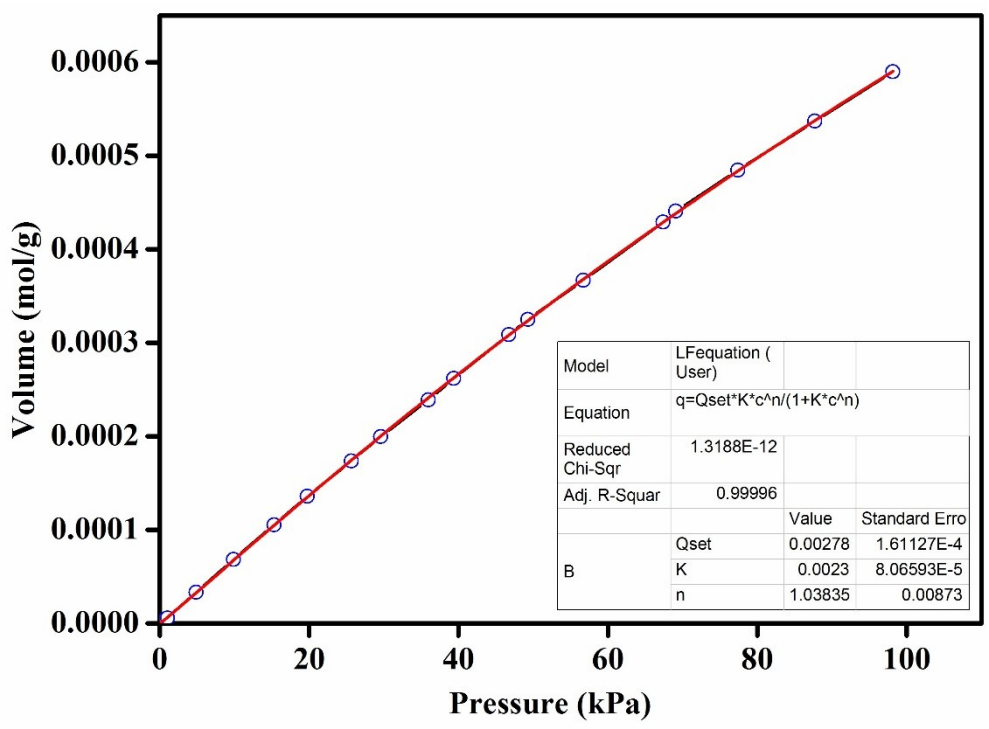

Fig. S15 Carbon dioxide adsorption isotherm of Ag_3-TAPT-COF carried out at 298 K. The solid line shows the best fit to the data using the Langmuir-Freundlich equation.

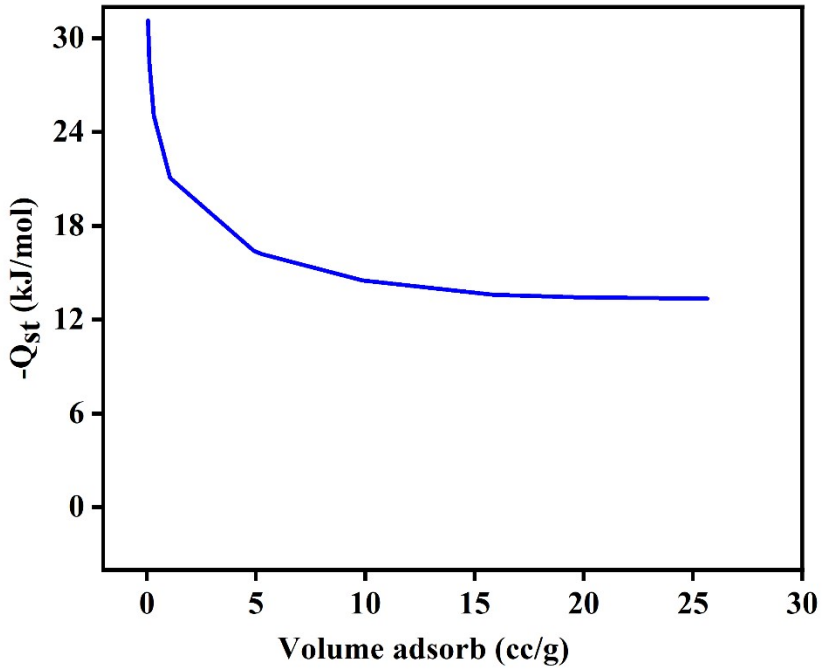

Fig. S16 Enthalpy of carbon dioxide adsorption for Ag_3-TAPT-COF determined using the Clausius-Clapeyron equation.

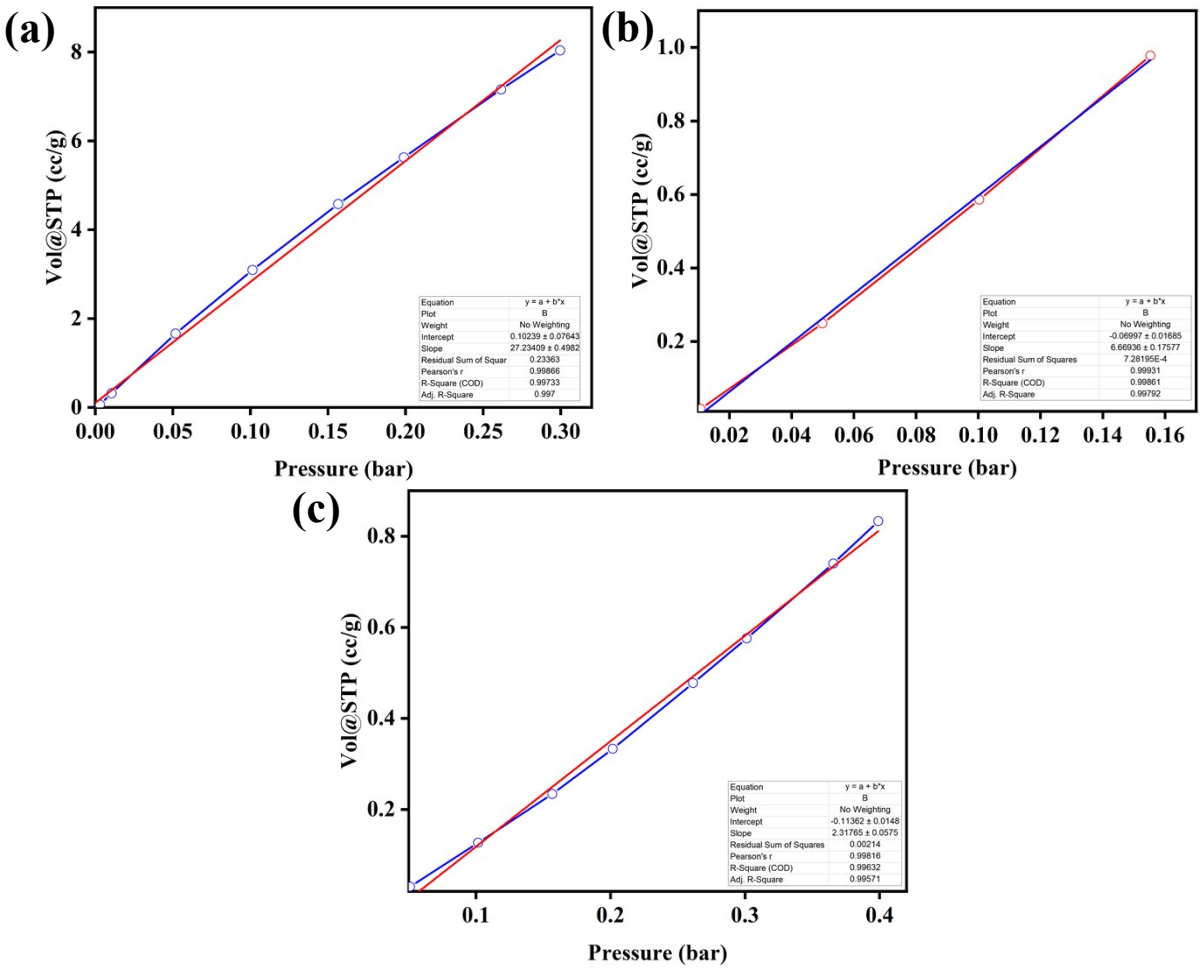

Fig. S17 Calculation of Henry gas selectivity constants for gases (a) CO_2, (b) CH_4, and (c) N_2.

Table S1 Optimization of catalytic reaction conditions for the carboxylation of 4-Hydroxy-6-methyl-2-pyridone-3-acid using 4-Hydroxy-6-methyl-2-pyridone and CO_2 catalyzed by Ag_3-TAPT-COF.

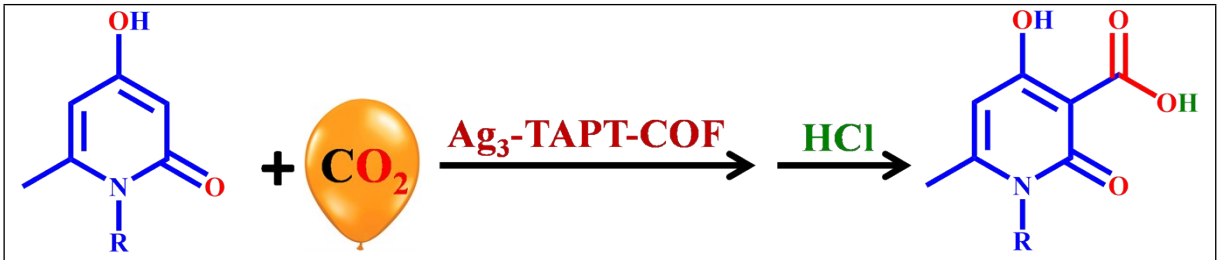

S. No.	Catalyst	Base	Temp. (°C)	Time (h)	Yield (%) [b]
1.	Ag_3-TAPT-COF	-	50	12	-
2.	-	LiHMDS	50	12	10
3.	Ag_3-TAPT-COF	K_2CO_3	40	12	30
4.	Ag_3-TAPT-COF	Cs_2CO_3	40	12	51
5.	Ag_3-TAPT-COF	KO^{t}Bu	50	12	45
6.	Ag_3-TAPT-COF	LiHMDS	50	8	63
7.	Ag_3-TAPT-COF	LiHMDS	50	12	85
8[c].	Ag_3-TAPT-COF	LiHMDS	50	12	trace

Reaction Conditions: 4-hydroxy-6-methyl pyridin-2(1H)-one (1 mmol, 125 mg), LiHMDS (1.5 mmol), 50 °C, 12 h, DMF (5mL), Catalyst (Ag_3-TAPT-COF) 10 mg, and CO_2 balloon. [c]N_2 (balloon).

Table S2 Characterization data of pyridone acids obtained by coupling of 4-hydroxy-2-pyridone with CO_2 catalyzed by Ag_3-TAPT-COF.

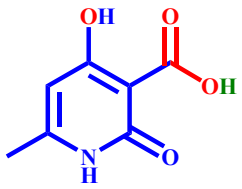	**4-hydroxy-6-methyl-2-oxo-1,2-dihydropyridine-3-carboxylic acid** ^{1}H NMR (400 MHz, DMSO-d_6) δ (ppm) = 15.74 (s, 1H), 13.05 (s, 1H), 12.66 (s, 1H), 6.20 (s, 1H), 2.24 (s, 3H). ^{13}C NMR (101 MHz, DMSO-d_6) δ (ppm) = 173.43, 172.46, 166.10, 102.13,94.55, 19.64.
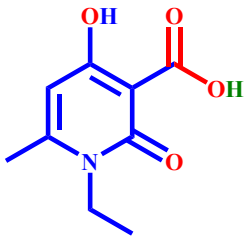	**1-ethyl-4-hydroxy-6-methyl-2-oxo-1,2-dihydropyridine-3-carboxylic acid** ^{1}H NMR (400 MHz, DMSO-d_6) δ (ppm) = 15.73 (s, 1H), 13.02 (s, 1H), 6.36 (s, 1H), 4.01 (q, 2H), 2.46 (s, 3H), 1.17 (t, 3H). ^{13}C NMR (101 MHz, DMSO-d_6) δ (ppm) =172.35, 171.41, 165.17, 154.01, 102.79, 94.84, 19.98, 12.98.
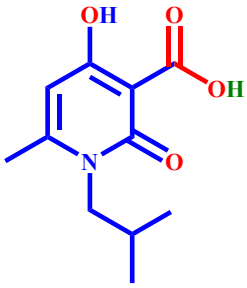	**4-hydroxy-1-isobutyl-6-methyl-2-oxo-1,2-dihydropyridine-3-carboxylic acid** ^{1}H NMR (400 MHz, DMSO-d_6) δ (ppm) = 15.74 (s, 1H), 13.04 (s, 1H), 6.38 (s, 1H), 3.83-3.85 (d, 2H), 2.46 (s, 3H), 2.01 – 2.12 (m, 1H), 0.84 – 0.83 (d, 6H). ^{13}C NMR (101 MHz, DMSO-d_6) δ (ppm) = 172.23, 171.33, 165.81, 154.63, 103.01, 94.80, 50.61, 27.50, 20.70, 19.76.
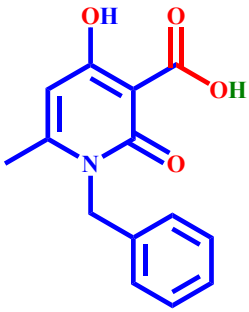	**1-benzyl-4-hydroxy-6-methyl-1,2-dihydropyridine-3-carboxylic acid** ^{1}H NMR (400 MHz, DMSO-d_6) δ (ppm) = 15.48 (s, 1H), 13.11 (s, 1H), 7.28 – 7.34 (t, 2H), 7.22 – 7.28 (t, 2H), 7.11 – 7.13 (d, 2H), 6.42 (s,1H), 5.31 (s, 2H), 2.33 (s, 3H). ^{13}C NMR (101 MHz, DMSO-d_6) δ (ppm) = 172.31, 171.08, 165.78, 154.64, 135.69, 129.02, 127.65, 126.25, 103.20, 95.14, 46.95, 20.49.

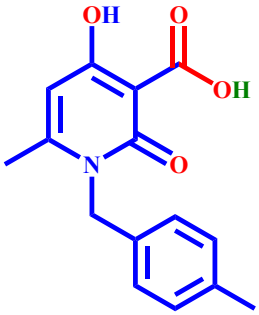	**4-hydroxy-6-methyl-1-(4-methylbenzyl)-2-oxo-1,2-dihydropyridine-3- carboxylic acid** ^{1}H NMR (400 MHz, DMSO-d_6) δ (ppm) = 15.50 (s, 1H), 13.10 (s, 1H), 7.11 – 7.12 (d, 2H), 7.00 – 7.02 (d, 2H), 6.41 (s, 1H), 5.25 (s, 2H), 2.33 (s, 3H), 2.23 (s, 3H). ^{13}C NMR (101 MHz, DMSO-d_6) δ (ppm) = 172.24, 171.96, 165.69, 154.61, 136.80, 132.58, 129.46, 126.28, 103.06, 95.00, 46.71, 20.67, 20.33.
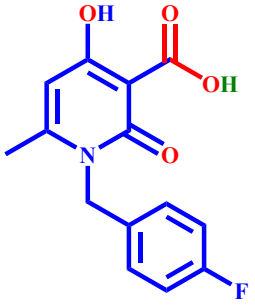	**1-(4-fluorobenzyl)-4-hydroxy-6-methyl-2-oxo-1,2-dihydropyridine-3- carboxylic acid** ^{1}H NMR (400 MHz, DMSO-d_6) δ (ppm) = 15.43 (s, 1H), 13.10 (s, 4H), 7.11 –7.21 (m, 4H), 6.41 (s, 1H), 5.27 (s, 2H), 2.33 (s, 3H). ^{13}C NMR (101 MHz, DMSO-d_6) δ (ppm) = 173.43, 172.46, 166.10, 102.13,94.55, 19.64.
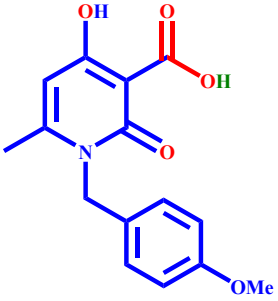	**4-hydroxy-1-(4-methoxybenzyl)-6-methyl-2-oxo-1,2-dihydropyridine-3- carboxylic acid** ^{1}H NMR (400 MHz, DMSO-d_6) δ (ppm) = 15.52 (s, 1H), 13.10 (s, 1H), 7.08 – 7.10 (d, 2H), 6.85 – 6.88 (d, 2H), 6.40 (s, 1H), 5.23 (s, 2H), 3.67 (s, 3H), 2.35 (s, 3H). ^{13}C NMR (101 MHz, DMSO-d_6) δ (ppm) = 172.29, 171.95, 165.68, 158.50, 127.87, 127.68, 114.06, 55. 27, 46.39, 20.29
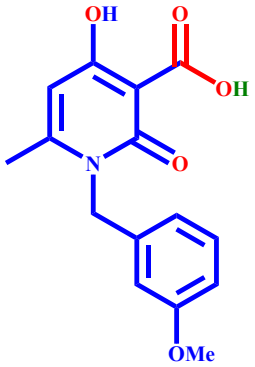	**4-hydroxy-1-(3-methoxybenzyl)-6-methyl-2-oxo-1,2-dihydropyridine-3-carboxylic acid** ^{1}H NMR (400 MHz, DMSO-d_6) δ (ppm) = 15.48 (s, 1H), 13.14 (s, 1H), 7.22 – 7.26 (t, 1H), 6.83 – 6.86 (dd, 1H), 6.72 (s, 1H), 6.63-6.65 (d, 1H), 6.44 (s, 1H), 5.29 (s, 2H), 3.70 (s, 3H), 2.35 (s, 3H).^{13}C NMR (101 MHz, DMSO-d_6) δ (ppm) = 172.18, 171.91, 165.65, 159.56, 154.56, 132.20, 130.10, 117.96, 112.67, 112.19, 103.04, 94.98, 55.07, 46.74, 20.29.

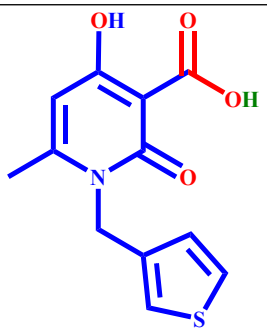	**4-hydroxy-6-methyl-2-oxo-1-(thiophen-3-ylmethyl)-1,2-dihydropyridine-3-carboxylic acid** ^{1}H NMR (400 MHz, DMSO-d_6) δ (ppm) = 15.39 (s, 1H), 13.06 (s, 1H), 7.47 – 7.48 (d, 1H), 7.22 – 7.27 (t, 1H), 7.14 –7.15 (d, 1H), 6.40 (s, 1H), 5.41 (s, 2H), 3.70 (s, 3H), 2.31 (s, 3H).

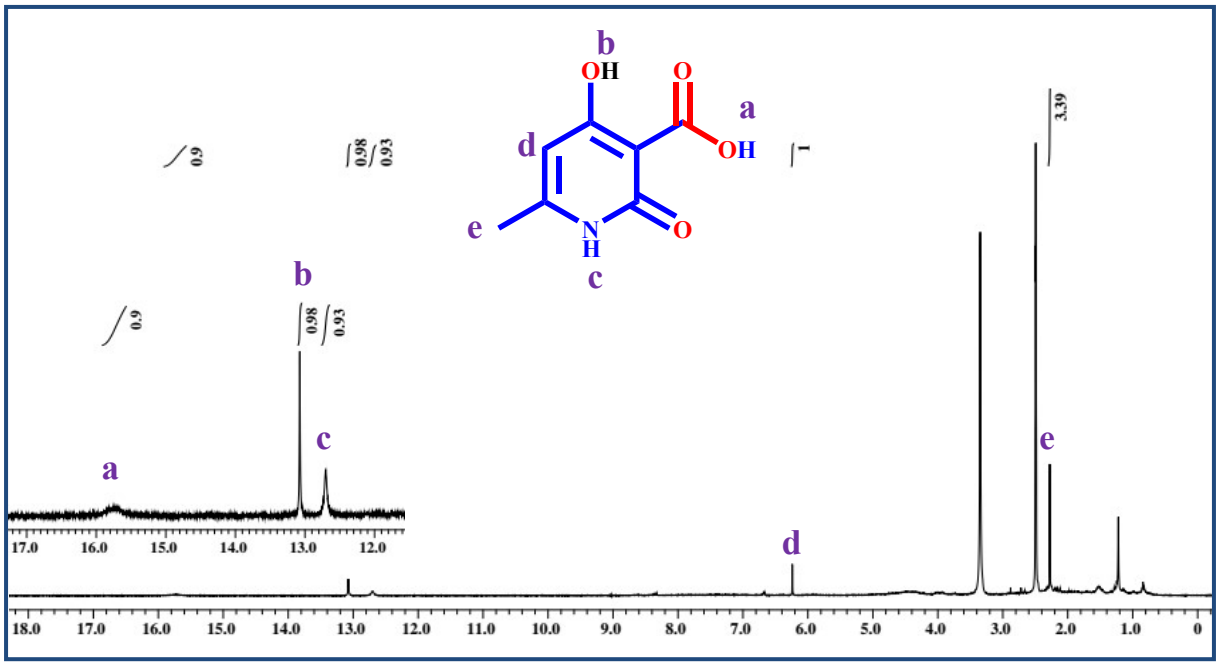

Fig. S18 ^{1}H NMR (DMSO-d_6, 400 MHz) spectrum of 4-hydroxy-6-methyl-2-oxo-1,2-dihydropyridine-3-carboxylic acid obtained from carboxylation of 4-hydroxy-6-methylpyridin-2(1H)-one by Ag_3-TAPT-COF under optimized conditions.

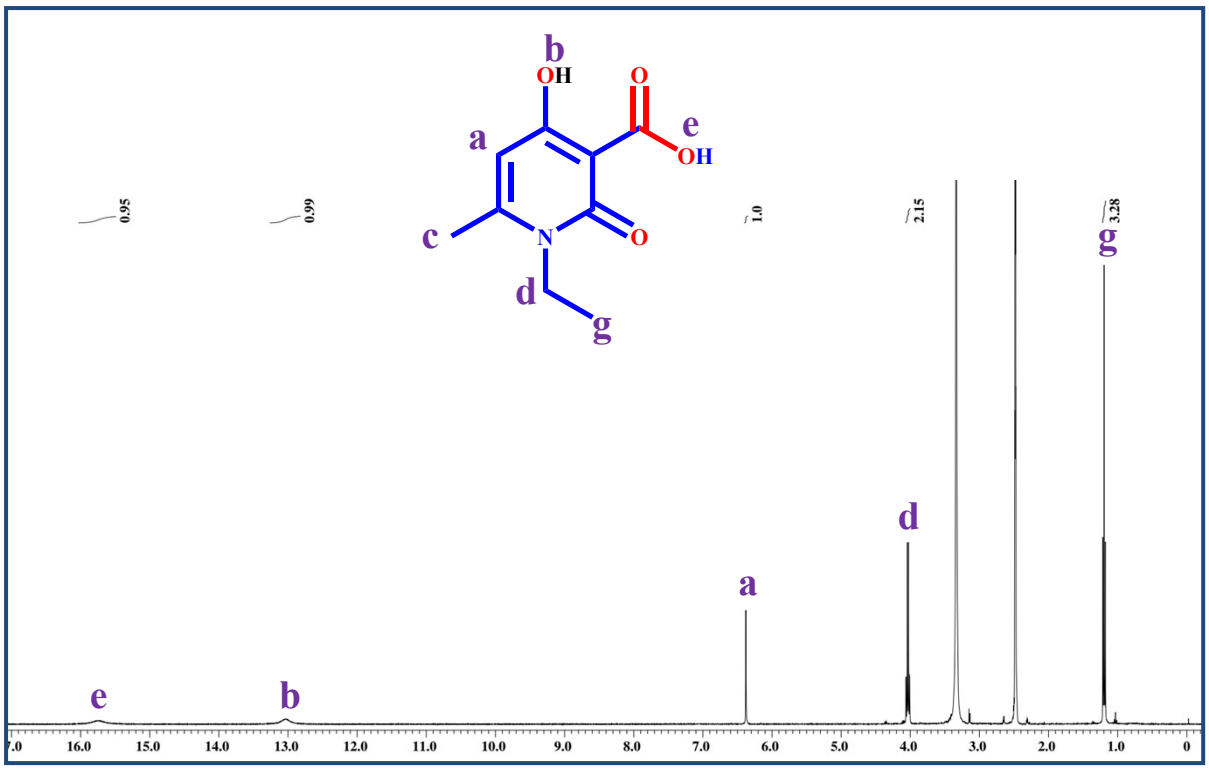

Fig. S19 ^{1}H NMR (DMSO-d_6, 400 MHz) spectrum of 1-ethyl-4-hydroxy-6-methyl-2-oxo-1,2-dihydropyridine-3-carboxylic acid obtained from carboxylation of 1-ethyl-4-hydroxy-6-methylpyridin-2(1H)-one by Ag_3-TAPT-COF under optimized conditions.

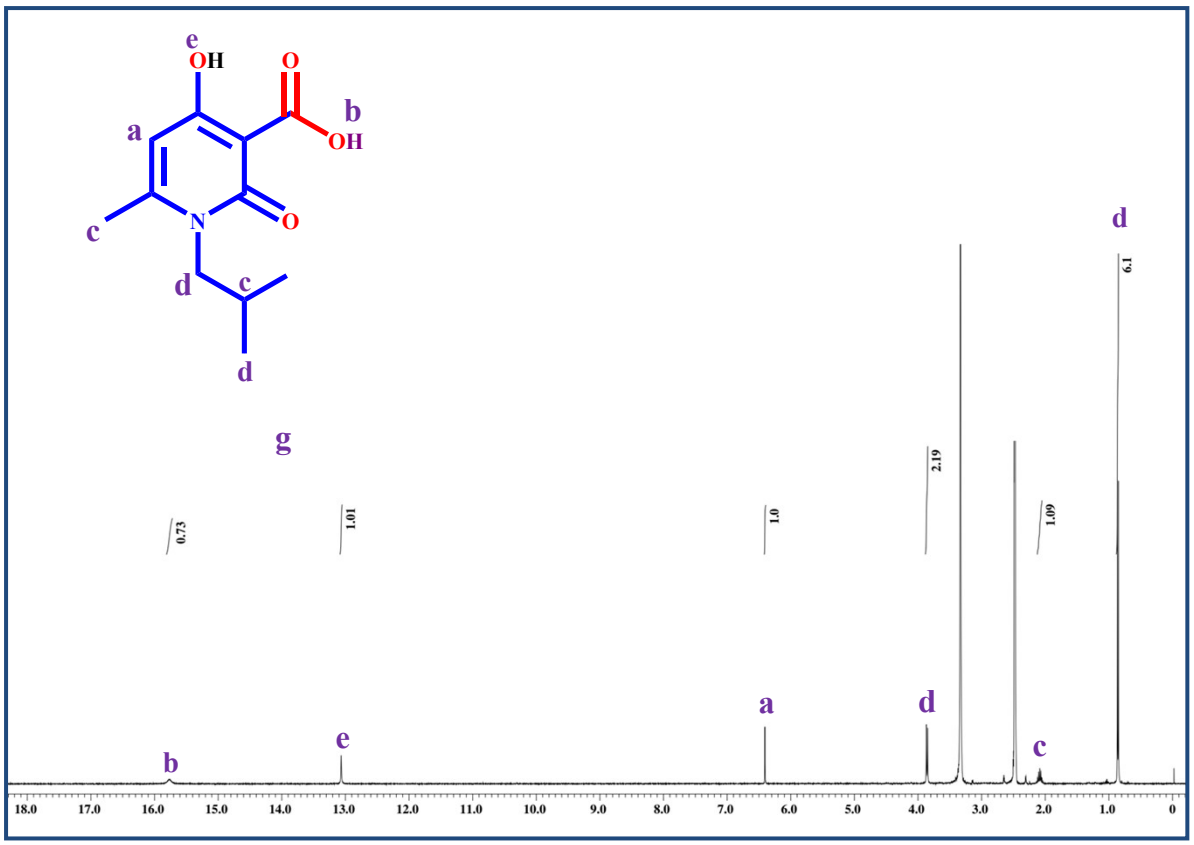

Fig. S20 ^{1}H NMR (DMSO-d_6, 400 MHz) spectrum of 4-hydroxy-1-isobutyl-6-methyl-2-oxo-1,2-dihydropyridine-3-carboxylic acid obtained from carboxylation of 4-hydroxy-1-isobutyl-6-methylpyridin-2(1H)-one by Ag_3-TAPT-COF under optimized conditions.

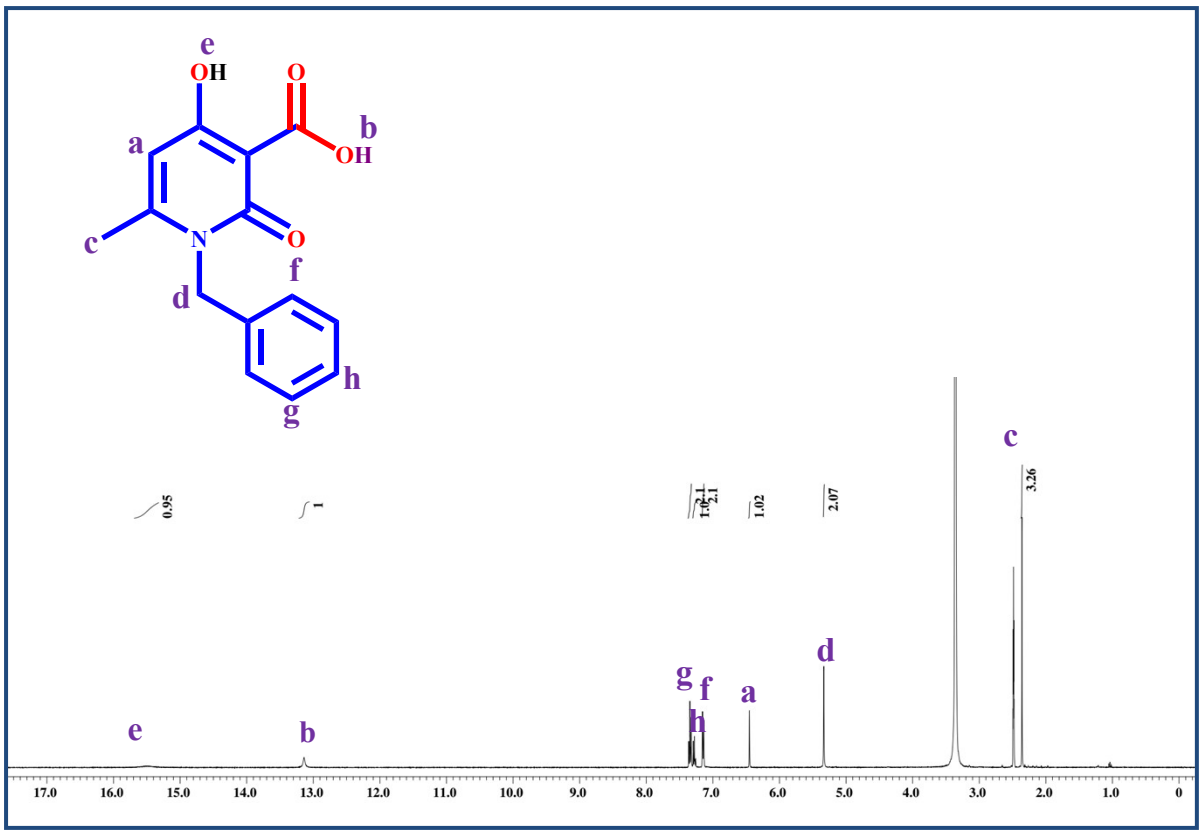

Fig. S21 ^{1}H NMR (DMSO-d_6, 400 MHz) spectrum of 1-benzyl-4-hydroxy-6-methyl-2-oxo-1,2-dihydropyridine-3-carboxylic acid obtained from carboxylation of 1-benzyl-4-hydroxy-6-methylpyridin-2(1H)-one by Ag_3-TAPT-COF under optimized conditions.

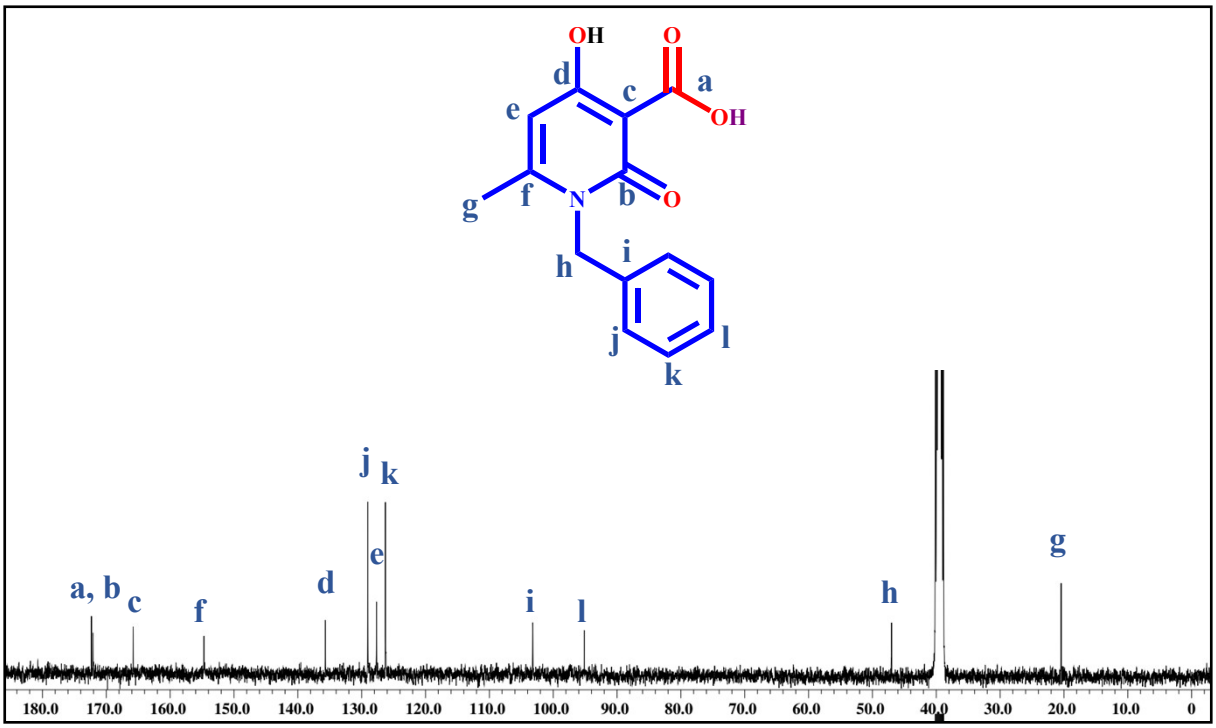

Fig. S22 ^{13}C NMR (DMSO-d_6, 101 MHz) spectrum of 1-benzyl-4-hydroxy-6-methyl-2-oxo-1,2-dihydropyridine-3-carboxylic acid obtained from carboxylation of 1-benzyl-4-hydroxy-6-methylpyridin-2(1H)-one by Ag_3-TAPT-COF under optimized conditions.

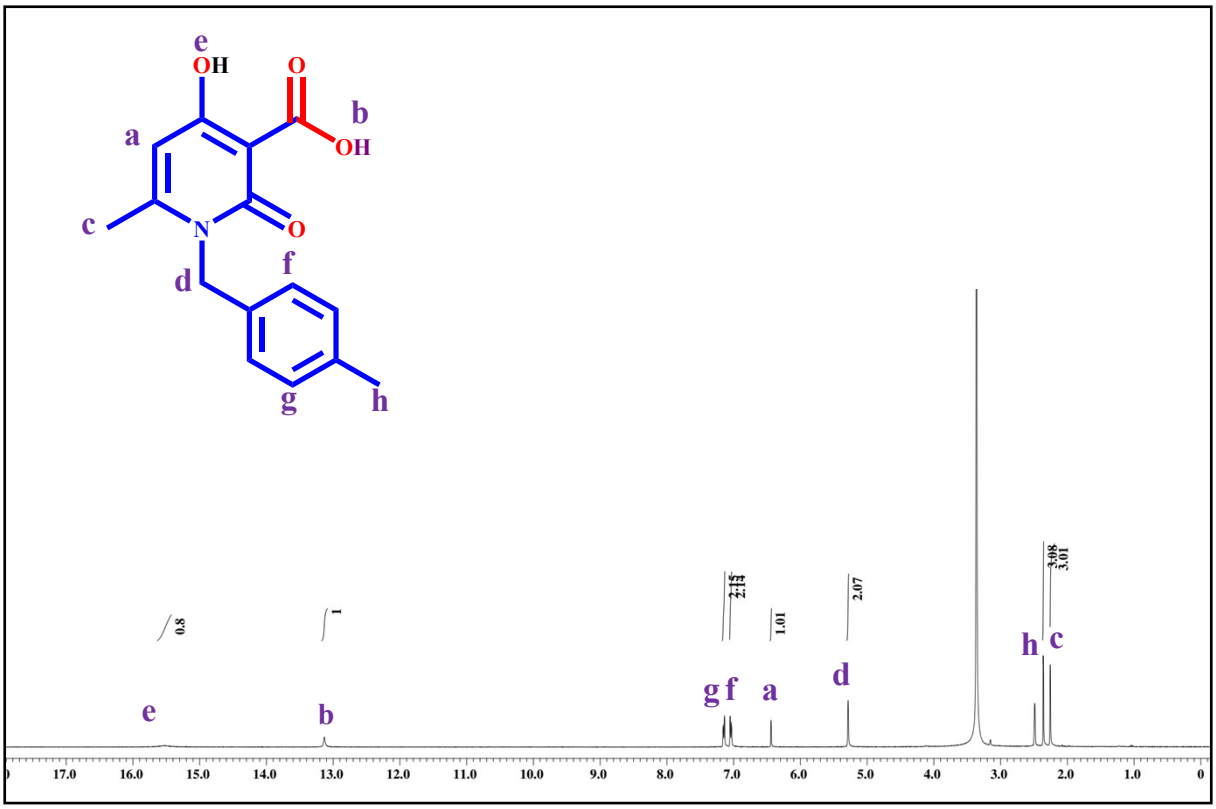

Fig. S23 ^{1}H NMR (DMSO-d_6, 400 MHz) spectrum of 4-hydroxy-6-methyl-1-(4-methylbenzyl)-2-oxo-1,2-dihydropyridine-3-carboxylic acid obtained from carboxylation of 4-hydroxy-6-methyl-1-(4-methylbenzyl)pyridin-2(1H)-one by Ag_3-TAPT-COF under optimized conditions.

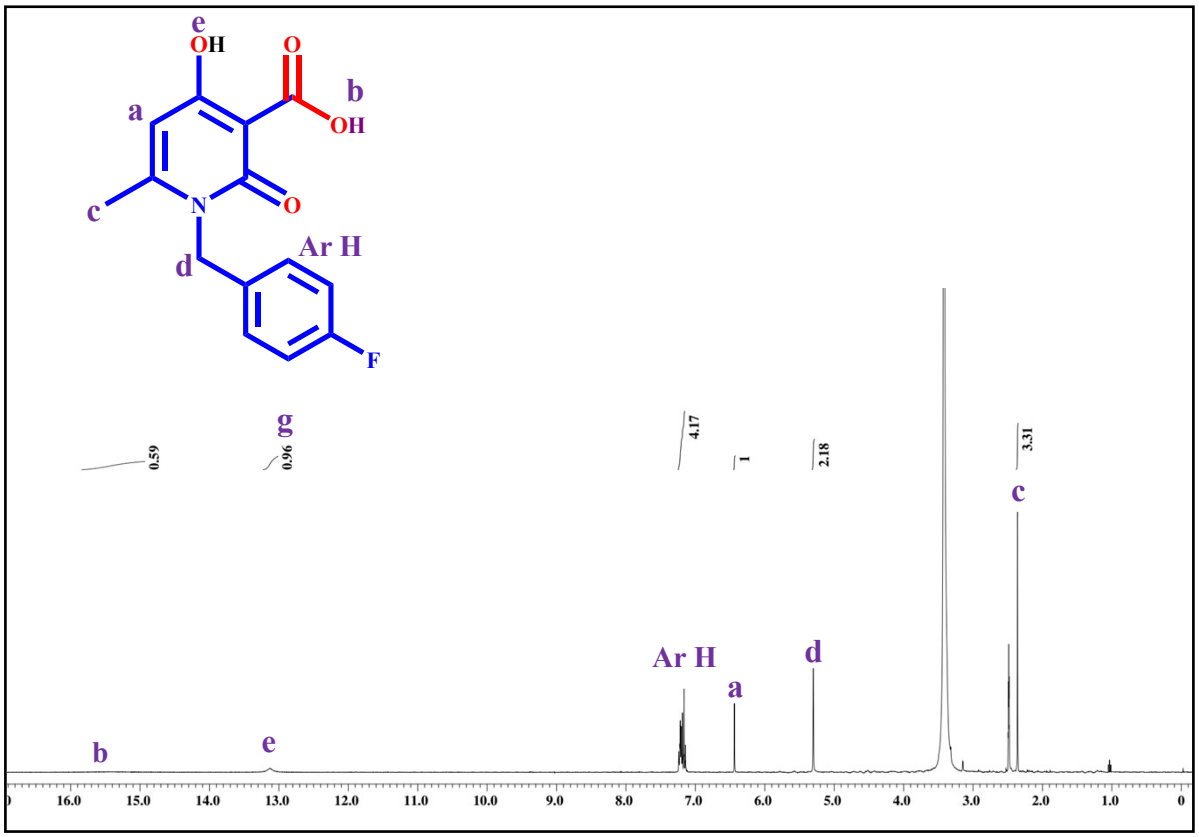

Fig. S24 ^{1}H NMR (DMSO-d_6, 400 MHz) spectrum of 1-(4-fluorobenzyl)-4-hydroxy-6-methyl-2-oxo-1,2-dihydropyridine-3-carboxylic acid obtained from carboxylation of 1-(4-fluorobenzyl)-4-hydroxy-6-methylpyridin-2(1H)-one by Ag_3-TAPT-COF under optimized conditions.

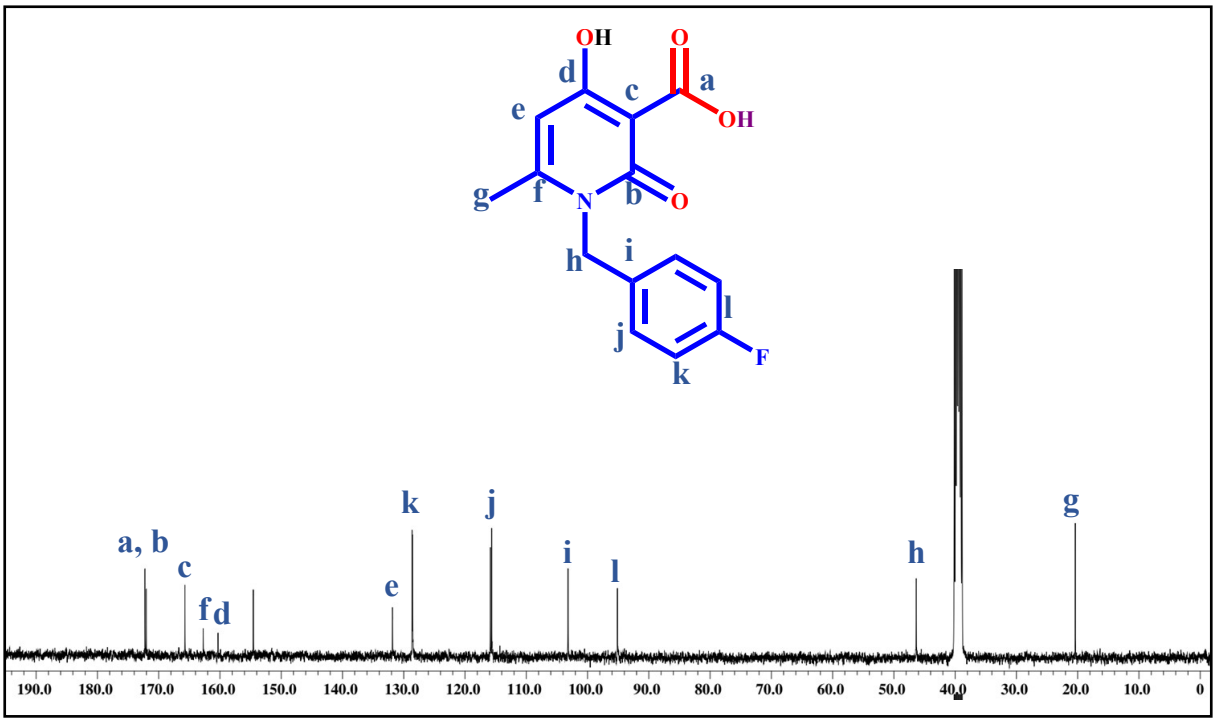

Fig. S25 ^{13}C NMR (DMSO-d_6, 101 MHz) spectrum of 1-(4-fluorobenzyl)-4-hydroxy-6-methyl-2-oxo-1,2-dihydropyridine-3-carboxylic acid obtained from carboxylation of 1-(2-((4-chlorophenyl)ethynyl)phenyl)ethan-1-one by Ag_3-TAPT-COF under optimized conditions.

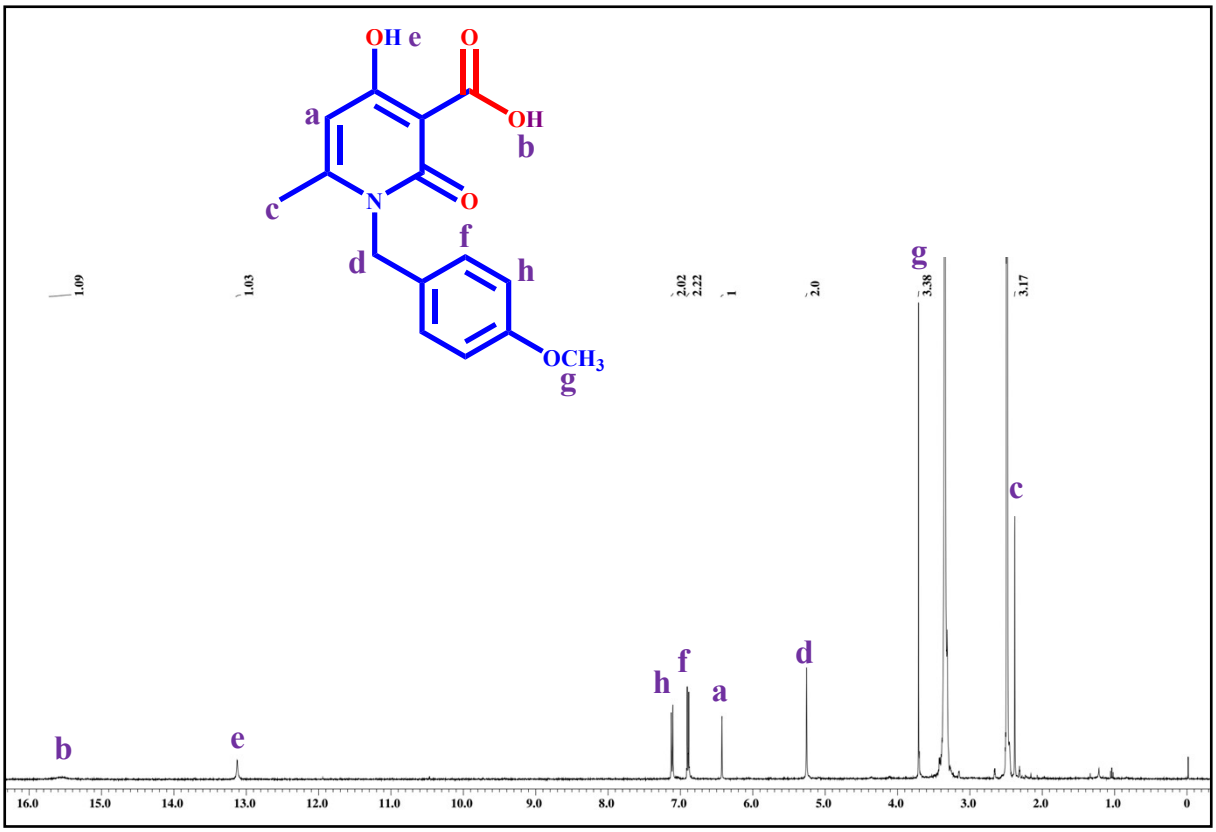

Fig. S26 ^{1}H NMR (DMSO-d_6, 400 MHz) spectrum of 4-hydroxy-1-(4-methoxybenzyl)-6-methyl-2-oxo-1,2-dihydropyridine-3-carboxylic acid obtained from carboxylation of 4-hydroxy-1-(4-methoxybenzyl)-6-methylpyridin-2(1H)-one by Ag_3-TAPT-COF under optimized conditions.

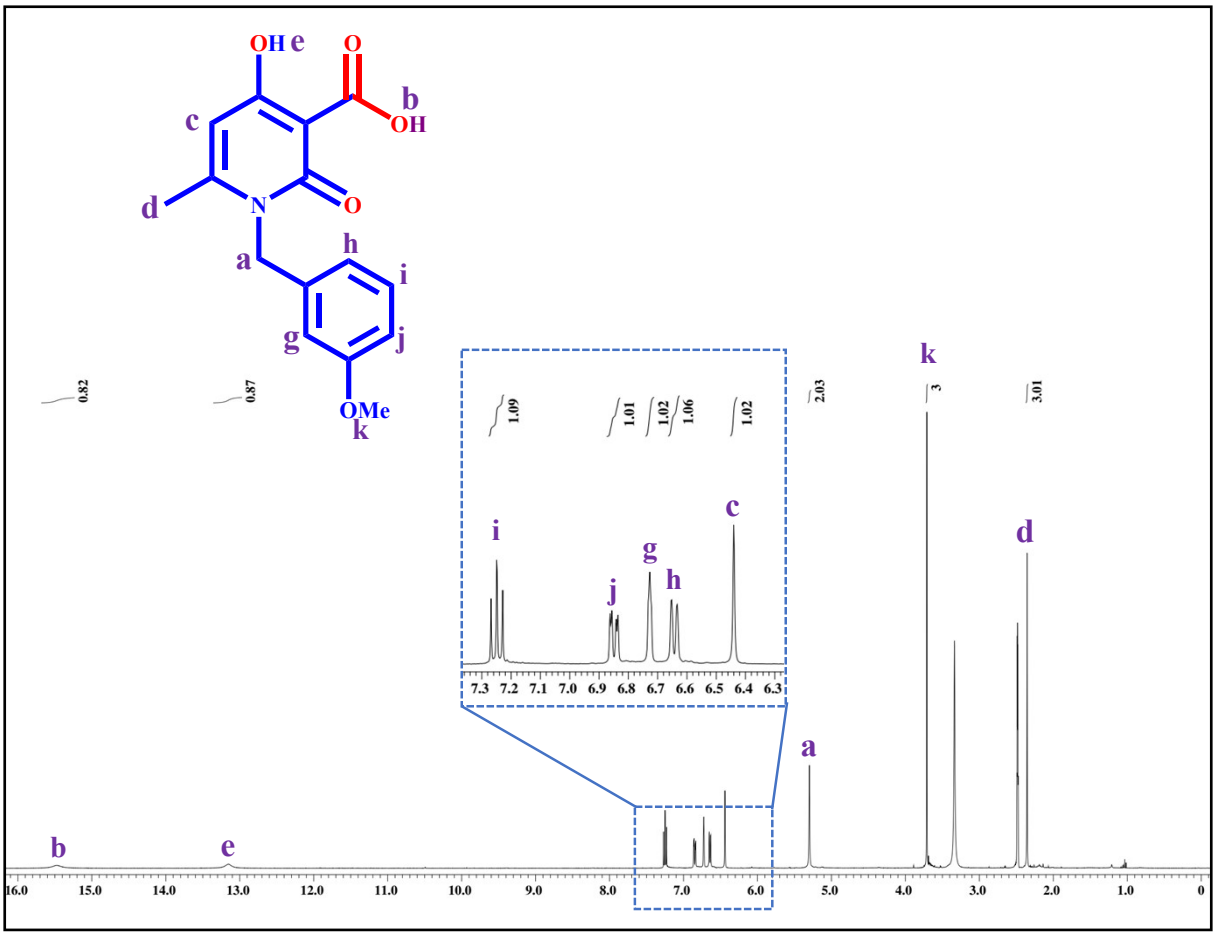

Fig. S27 ^{1}H NMR (DMSO-d_6, 400 MHz) spectrum of 4-hydroxy-1-(3-methoxybenzyl)-6-methyl-2-oxo-1,2-dihydropyridine-3-carboxylic acid obtained from carboxylation of 4-hydroxy-1-(3-methoxybenzyl)-6-methylpyridin-2(1H)-one by Ag_3-TAPT-COF under optimized conditions.

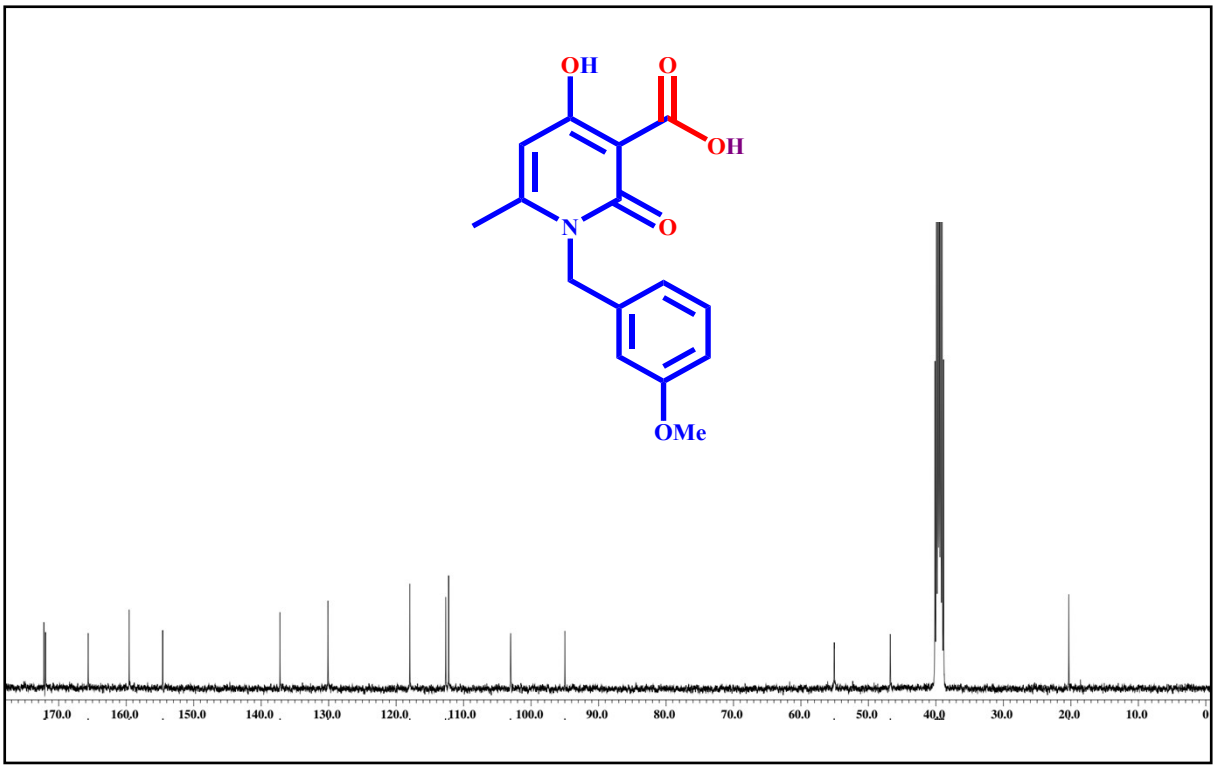

Fig. S28 ^{13}C NMR (DMSO-d_6, 101 MHz) spectrum of 4-hydroxy-1-(3-methoxybenzyl)-6-methyl-2-oxo-1,2-dihydropyridine-3-carboxylic acid obtained from carboxylation of 4-hydroxy-1-(3-methoxybenzyl)-6-methylpyridin-2(1H)-one by Ag_3-TAPT-COF under optimized conditions.

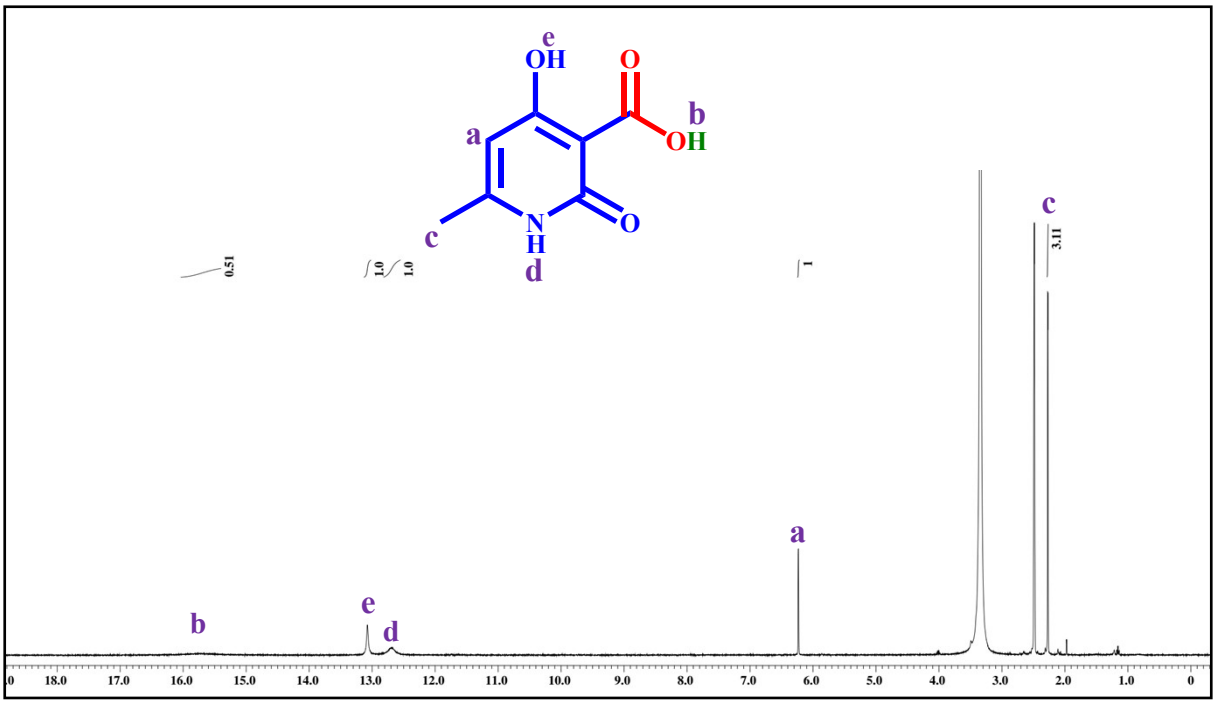

Fig. S29 ^{1}H NMR (DMSO-d_6, 400 MHz) spectrum of 4-hydroxy-6-methyl-2-oxo-1,2-dihydropyridine-3-carboxylic acid obtained from carboxylation of 4-hydroxy-6-methyl pyridin-2(1H)-one by Ag_3-TAPT-COF under K_2CO_3 as a base.

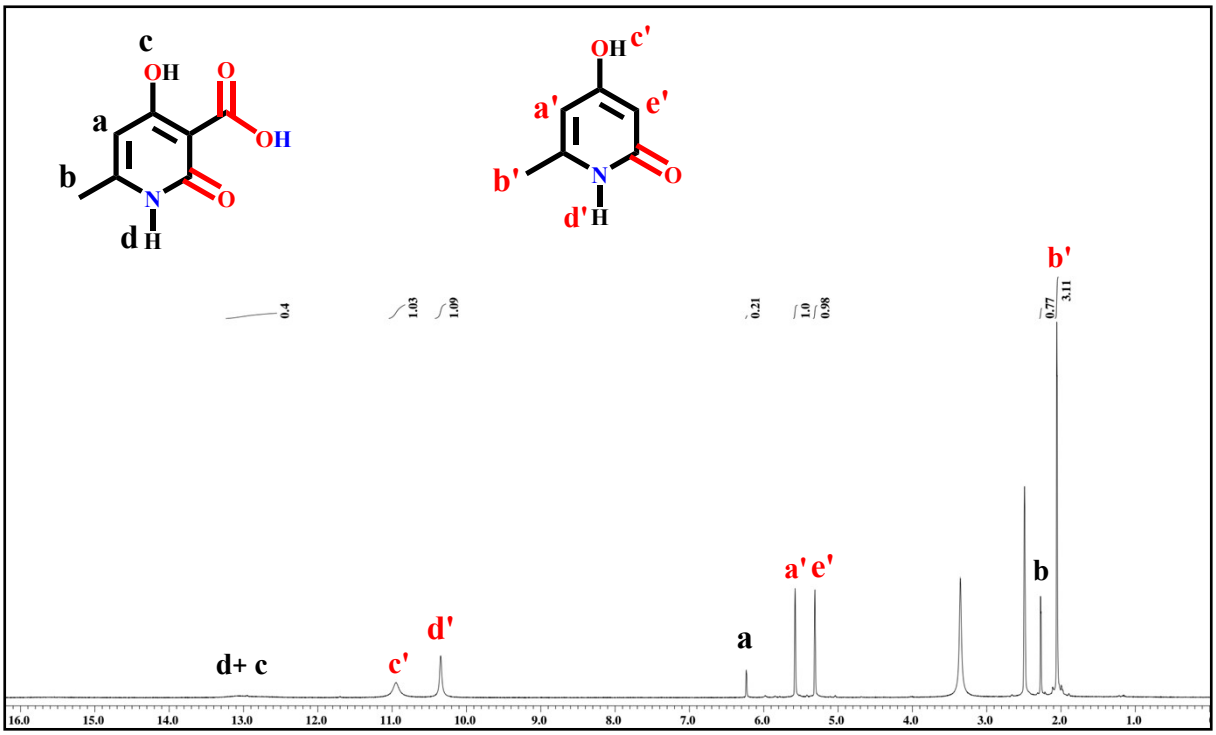

Fig. S30 ^{1}H NMR (DMSO-d_6, 400 MHz) spectrum of 4-hydroxy-6-methyl-2-oxo-1,2-dihydropyridine-3-carboxylic acid obtained from carboxylation of 4-hydroxy-6-methyl pyridin-2(1H)-one by $AgNO_3$ with CO_2 under optimized conditions.

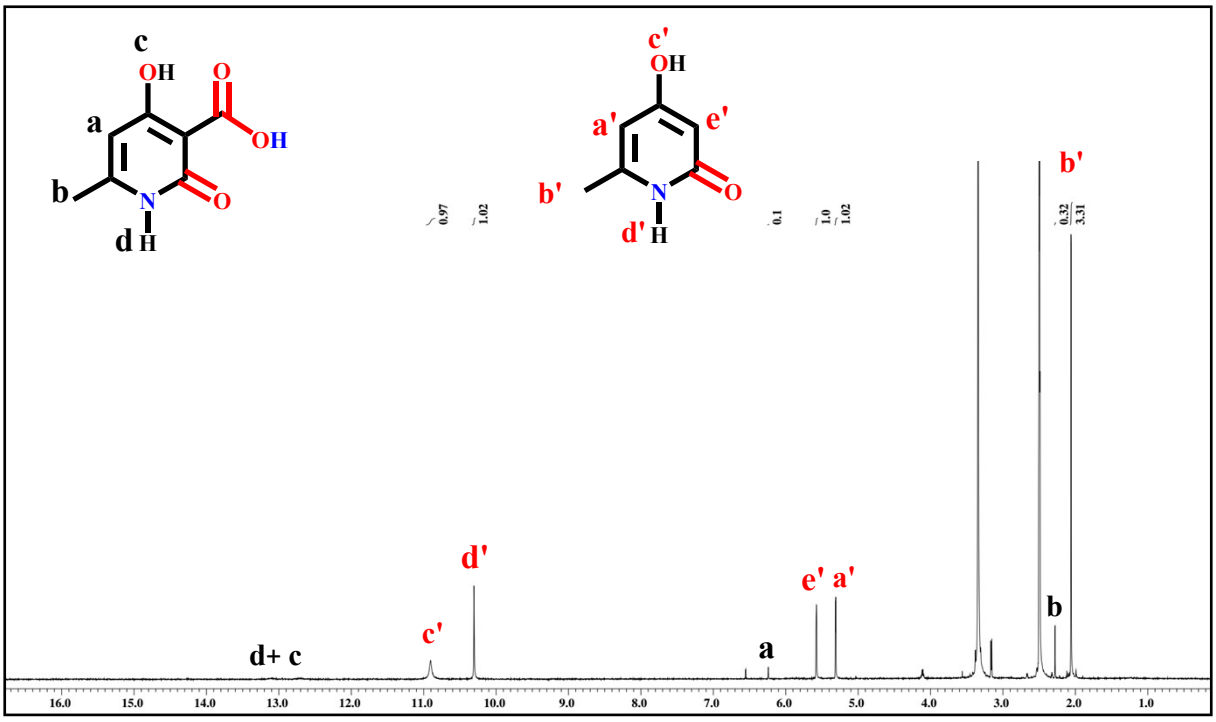

Fig. S31 ^{1}H NMR (DMSO-d_6, 400 MHz) spectrum of 4-hydroxy-6-methyl-2-oxo-1,2-dihydropyridine-3-carboxylic acid obtained from carboxylation of 4-hydroxy-6-methyl pyridin-2(1H)-one by Ag NPs with CO_2 under optimized conditions.

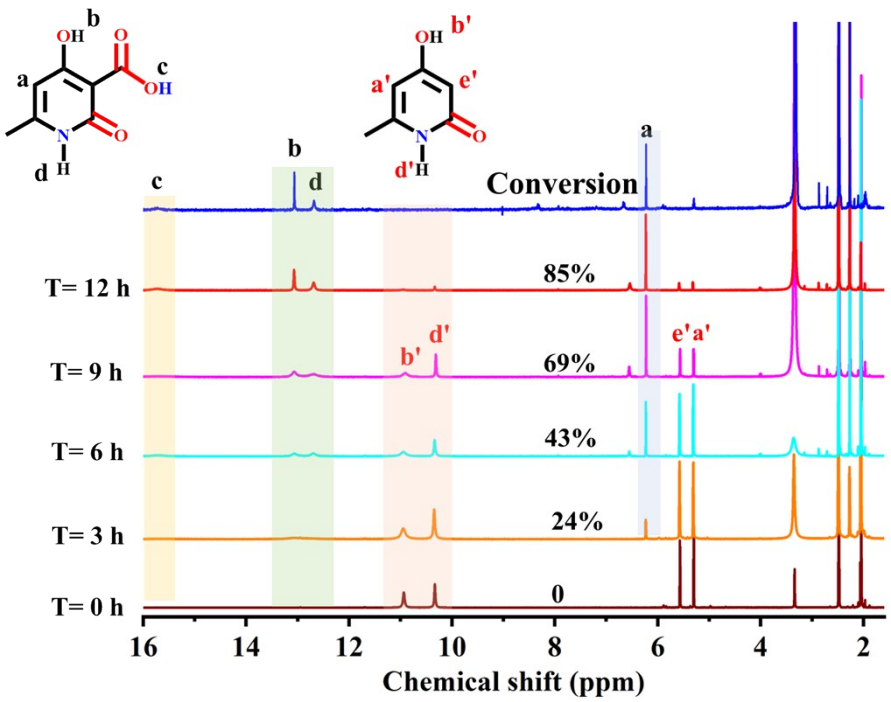

Fig. S32 ^{1}H NMR (DMSO-d_6, 400 MHz) stack plot for the carboxylation reaction of 4-hydroxy-6-methyl pyridin-2(1H)-one with CO_2 catalyzed by Ag_3-TAPT-COF under optimised conditions with 3, 6, 9, and 12 h.

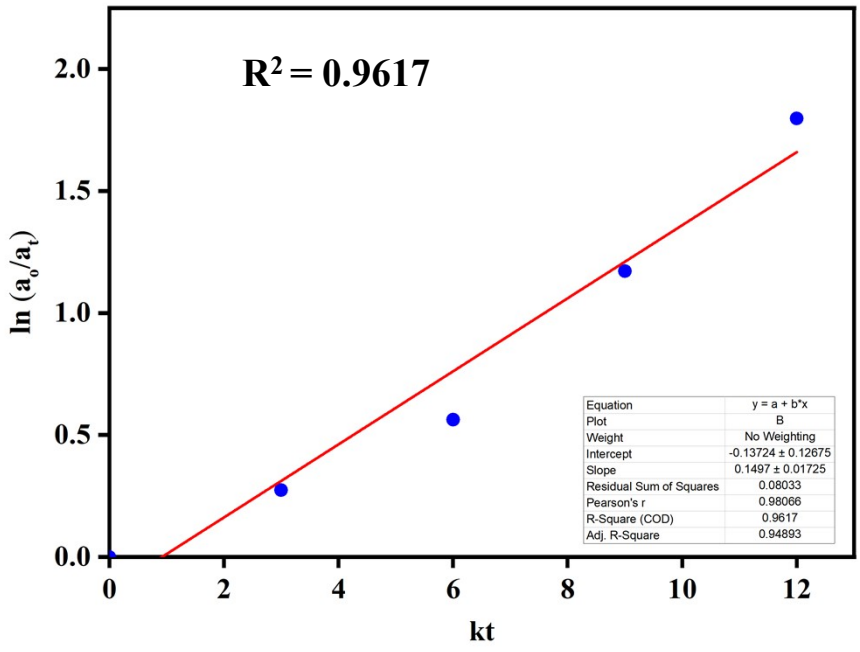

Fig. S33 Kinetic plot for carboxylation reaction of hydroxy-6-methyl-2-pyridone-3-acid under optimized conditions.

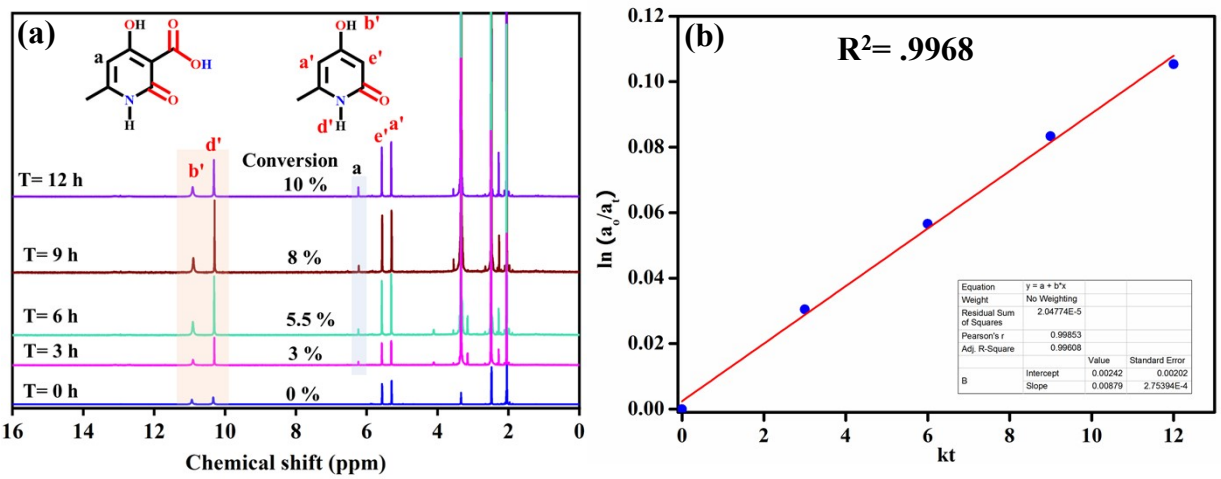

Fig. S34 ^{1}H NMR (DMSO-d_6, 400 MHz) stack plot for the carboxylation reaction of 4-hydroxy-6-methyl pyridin-2(1H)-one with CO_2 catalyzed by Ag NPs under optimised conditions with 3, 6, 9, and 12 h. (b) Kinetic plot for the carboxylation reaction of hydroxy-6-methyl-2-pyridone-3-acid with CO_2 under optimized conditions.

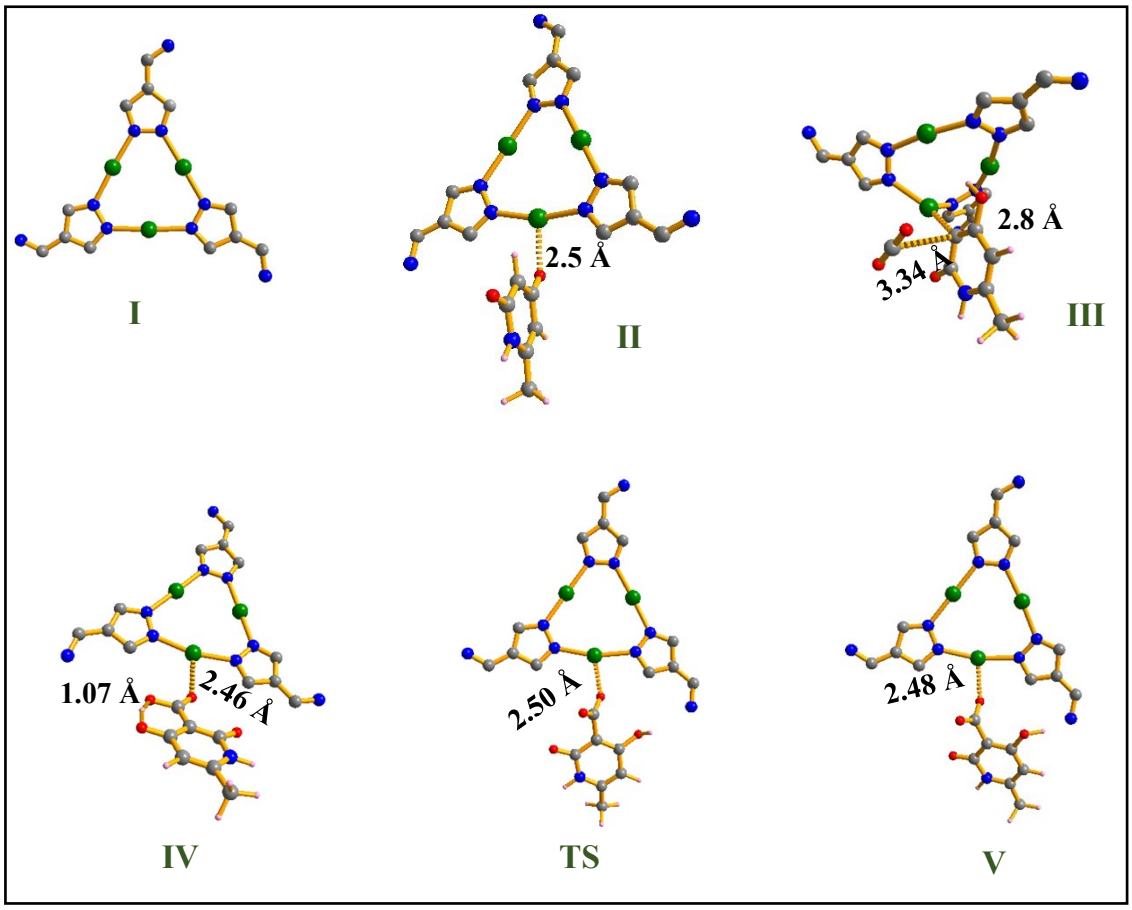

Fig. S35 Optimized structures of intermediates and transition state for sp^2 C-H carboxylation of 4-hydroxy-6-methyl pyridin-2(1H)-one with CO_2 catalyzed by Ag_3-TAPT-COF (bond distances are in Å).

Table S3 Synthesis of 1-(2-(phenylethynyl)phenyl)ethan-1-one from various phenyl acetylene derivatives.

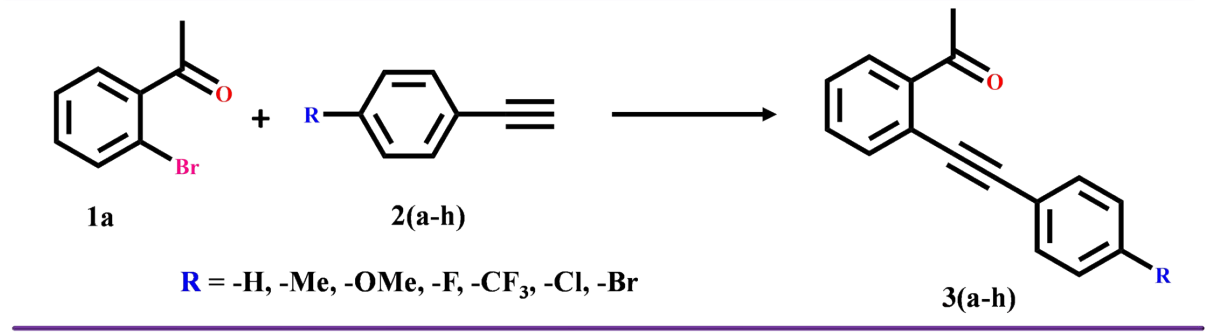

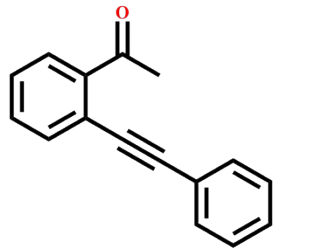

3a(85%)

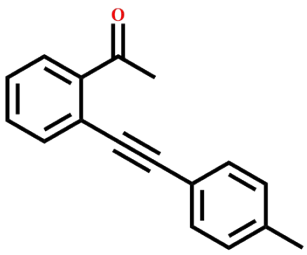

3b(88%)

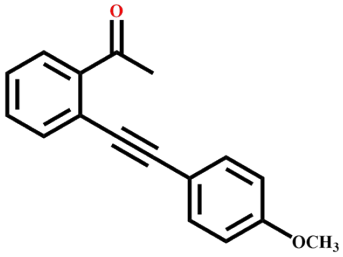

3c (91%)

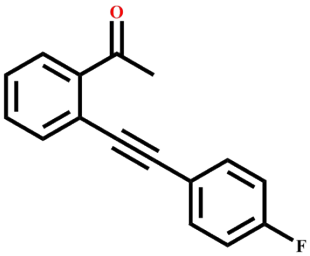

3d (82%)

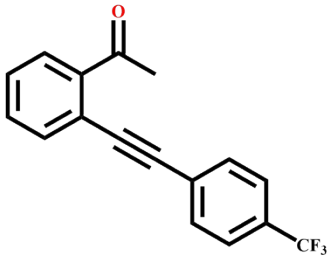

3e (78%)

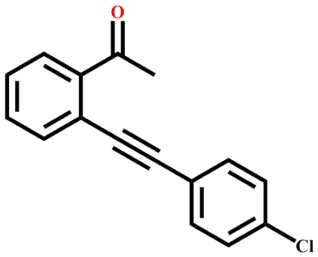

3f (75%)

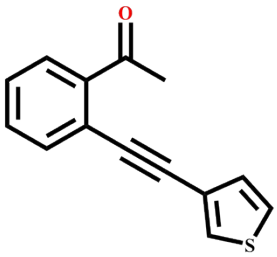

3g (72%)

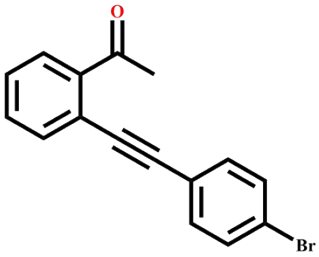

3h (65%)

Reaction Conditions: 2′-Bromoacetophenone (0.27 ml, 2.0 mmol, 1.0 equiv), phenylacetylene (0.22 ml, 2.0 mmol, 1.0 equiv), $PdCl_2(PPh_3)_2$ (28.1 mg, 0.04 mmol, 0.02 equiv), and CuI (7.618 mg, 0.04 mmol, 0.02 equiv), 24 h, 70 °C, and Et_3N (3mL).

Table S4 NMR spectral data of (phenylethynyl)phenyl)ethan-1-one derivatives prepared from various terminal alkynes.

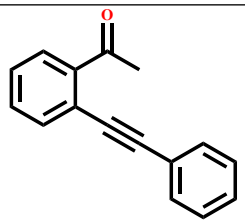	**1-(2-(phenylethynyl)phenyl)ethan-1-one** ^{1}H NMR (400 MHz; $CDCl_3$): δ (ppm) = 7.73-7.75 (dd, 1H), 7.60-7.62 (dd, 1H), 7.52-7.54 (m, 2H), 7.44-7.48 (td, 1H), 7.34-7.40 (m, 4H), 2.78 (s, 3H).
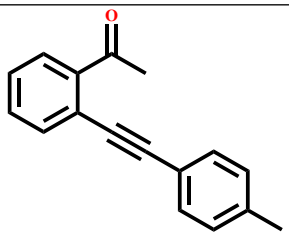	**1-(2-(p-tolylethynyl)phenyl)ethan-1-one** ^{1}H NMR (400 MHz, $CDCl_3$): δ (ppm) = 7.71-7.74 (dd, 1H), 7.58-7.61 (dd, 1H), 7.41-7.47 (m, 3H), 7.34-7.38 (td, 1H), 7.14-7.16 (d, 2H), 2.77 (s, 3H), 2.36 (s, 3H).
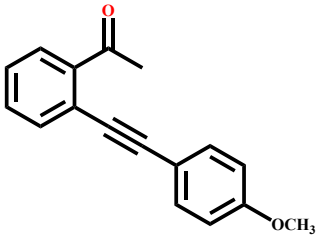	**1-(2-((4-methoxyphenyl)ethynyl)phenyl)ethan-1-one** ^{1}H NMR (400 MHz; $CDCl_3$): δ (ppm) = 7.74-7.76 (dd, 1H), 7.60-7.62 (dd, 1H), 7.44-7.51 (m, 3H), 7.36-7.40 (td, 1H), 6.89-6.91 (d, 2H), 3.84 (s, 3H), 2.79 (s, 3H).
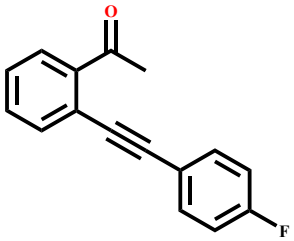	**1-(2-((4-fluorophenyl)ethynyl)phenyl)ethan-1-one** ^{1}H NMR (400 MHz, $CDCl_3$): δ (ppm) = 7.72-7.74 (dd, 1H), 7.58-7.60 (dd, 1H), 7.49-7.53 (m, 2H), 7.44-7.48 (td, 1H), 7.36-7.40 (td, 1H), 7.02-7.06 (t, 2H), 2.74 (s, 3H). ^{19}F NMR ($CDCl_3$, 376 MHz): δ (ppm) -109.64.
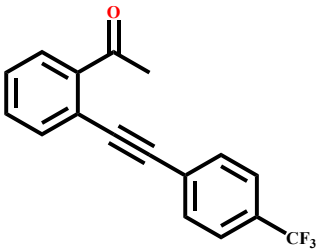	**1-(2-((4-(trifluoromethyl)phenyl)ethynyl)phenyl)ethan-1-one** ^{1}H NMR (400 MHz, $CDCl_3$): δ (ppm) = 7.77-7.79 (dd, 1H), 7.61-7.67 (m, 5H), 7.49-7.53 (td, 1H), 7.43-7.47 (td, 1H), 2.76 (s, 3H). ^{19}F NMR ($CDCl_3$, 376 MHz): δ (ppm) -61.21.
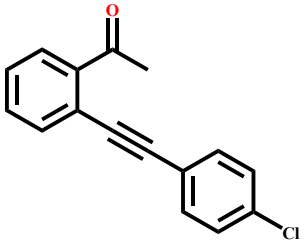	**1-(2-((4-chlorophenyl)ethynyl)phenyl)ethan-1-one** ^{1}H NMR (400 MHz, $CDCl_3$): δ (ppm) = 7.75-7.77 (dd, 1H), 7.61-7.63 (dd, 1H), 7.47-7.50 (m, 3H), 7.39-7.44 (td, 1H), 7.33-7.35 (d, 2H), 2.76 (s, 3H).

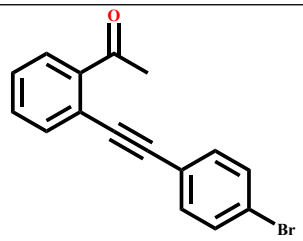	**1-(2-((4-bromorophenyl)ethynyl)phenyl)ethan-1-one** ^{1}H NMR (400 MHz; $CDCl_3$): δ (ppm) = 7.75-7.77 (dd,1H), 7.64-7.61 (dd, 1H), 7.47-7.53 (m, 4H), 7.40-7.44 (td, 2H), 2.76 (s, 3H).
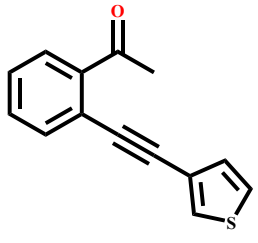	**1-(2-(thiophen-3-ylethynyl)phenyl)ethan-1-one** ^{1}H NMR (400 MHz; $CDCl_3$): δ (ppm) = 7.74-7.76 (dd, 1H), 7.60-7.62 (dd, 1H), 7.56-7.57 (m, 1H), 7.45-7.49 (td, 1H), 7.38-7.42 (td, 1H), 7.32-7.34 (m, 1H), 7.21-7.22 (dd, 1H), 2.78 (s, 3H).

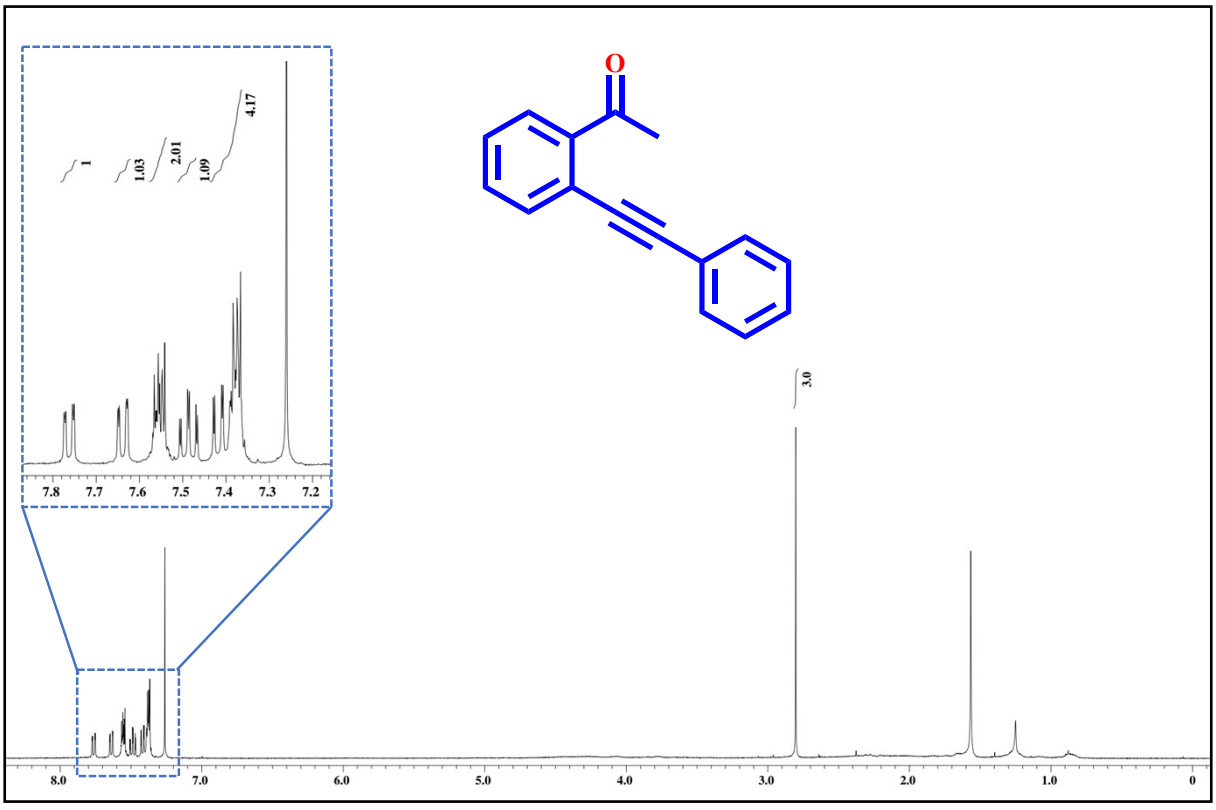

Fig. S36 ^{1}H NMR ($CDCl_3$, 400 MHz) spectrum of 1-(2-(phenylethynyl)phenyl)ethan-1-one.

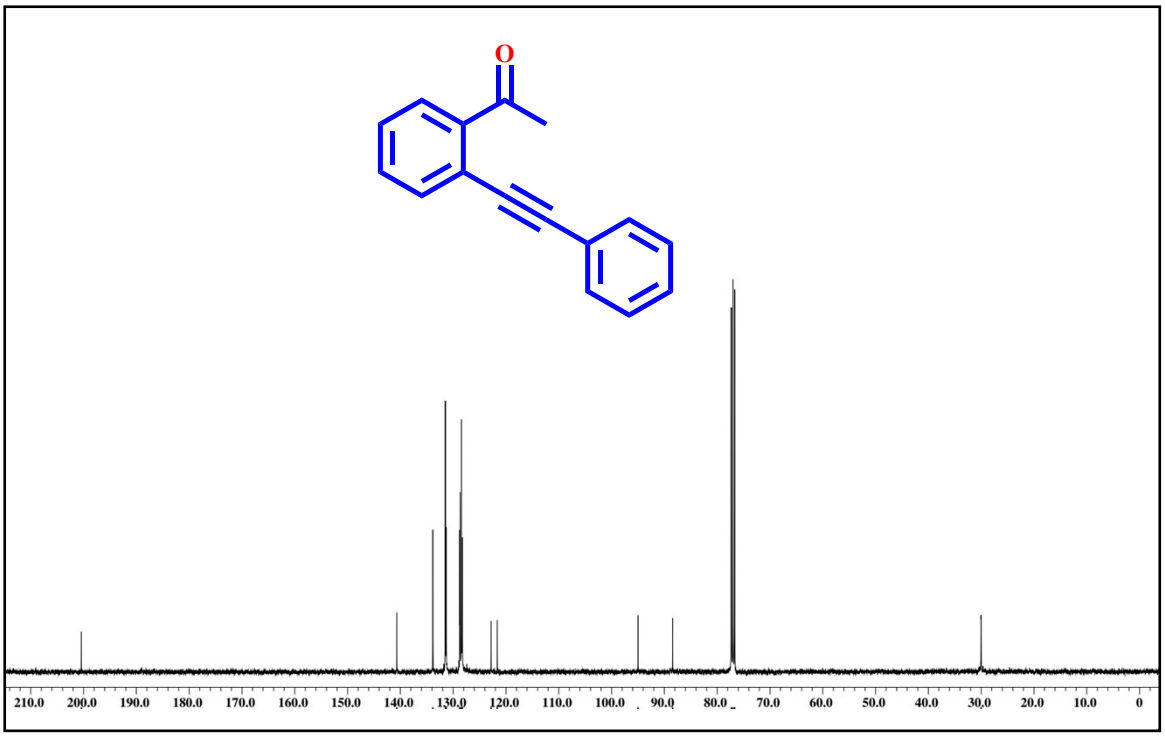

Fig. S37 ^{13}C NMR ($CDCl_3$, 101 MHz) spectrum of 1-(2-(phenylethynyl)phenyl)ethan-1-one.

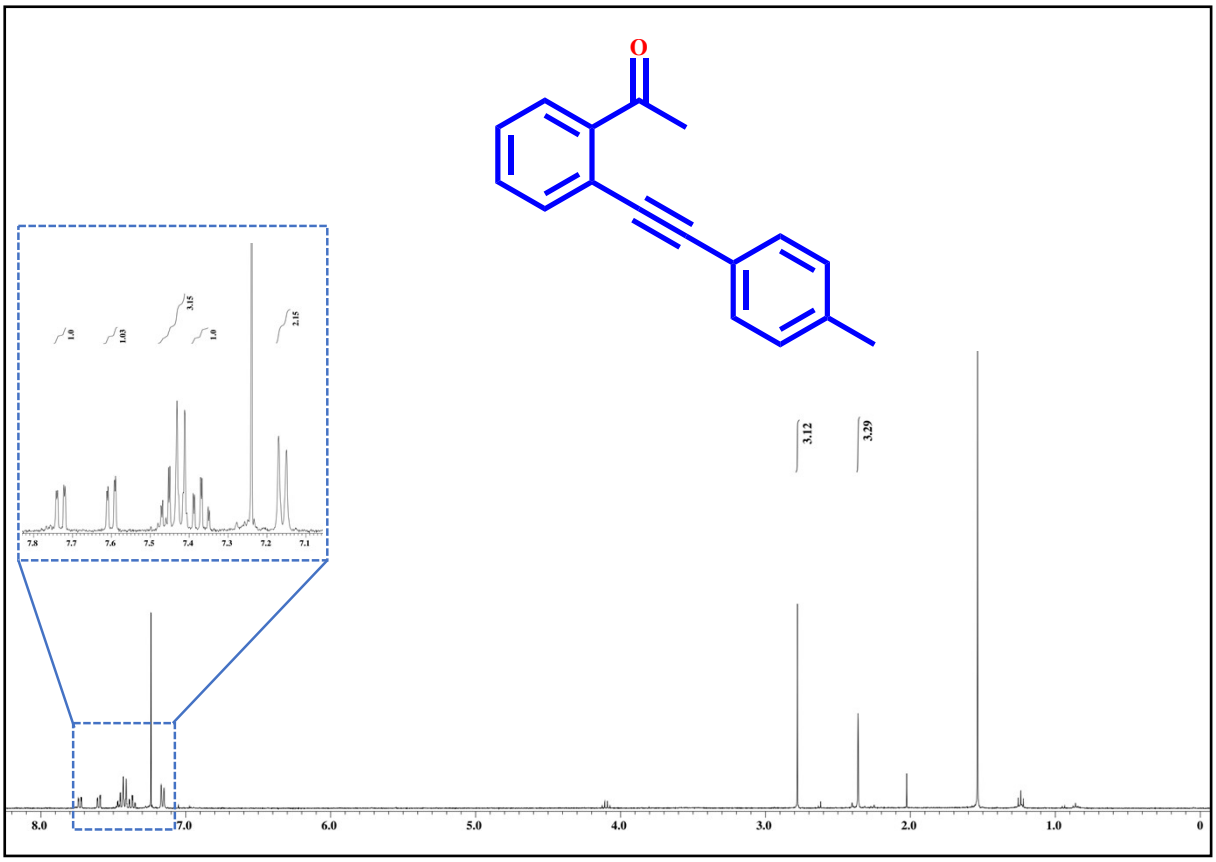

Fig. S38 ^{1}H NMR ($CDCl_3$, 400 MHz) spectrum of 1-(2-(p-tolylethynyl)phenyl)ethan-1-one.

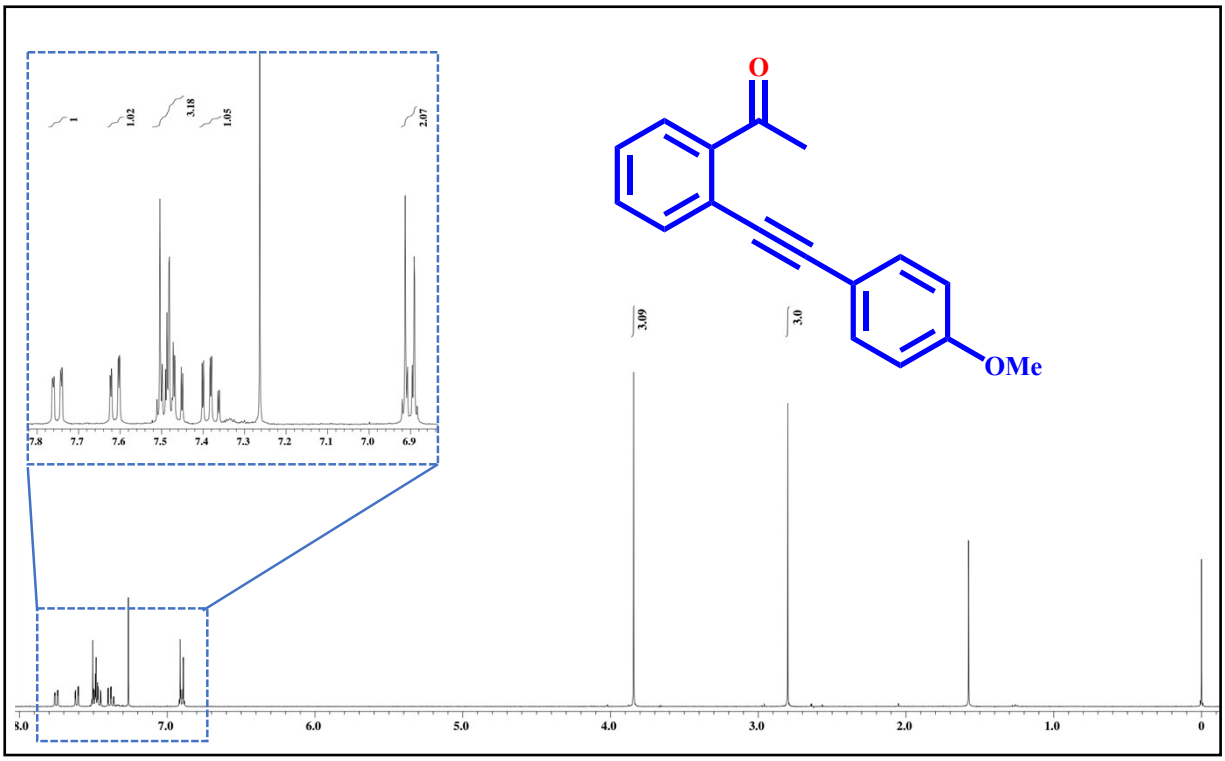

Fig. S39 ^{1}H NMR ($CDCl_3$, 400 MHz) spectrum of 1-(2-((4-methoxyphenyl)ethynyl)phenyl)ethan-1-one.

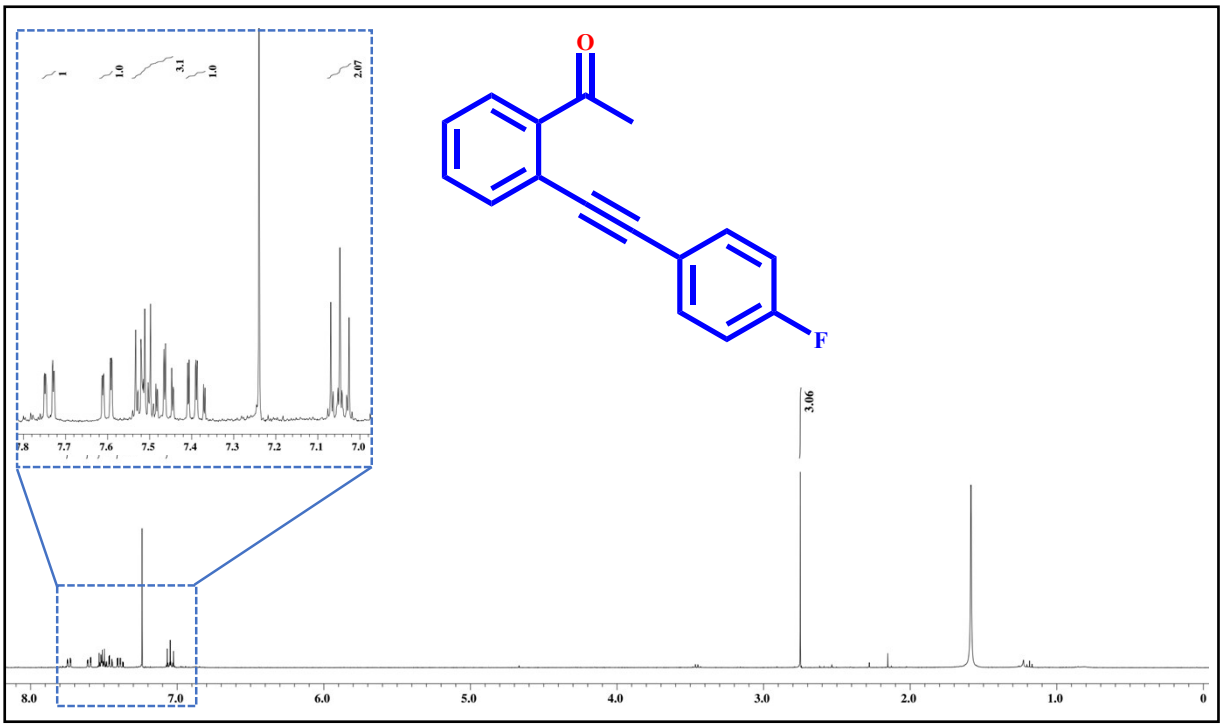

Fig. S40 ^{1}H NMR ($CDCl_3$, 400 MHz) spectrum of 1-(2-((4-fluorophenyl)ethynyl)phenyl)ethan-1-one.

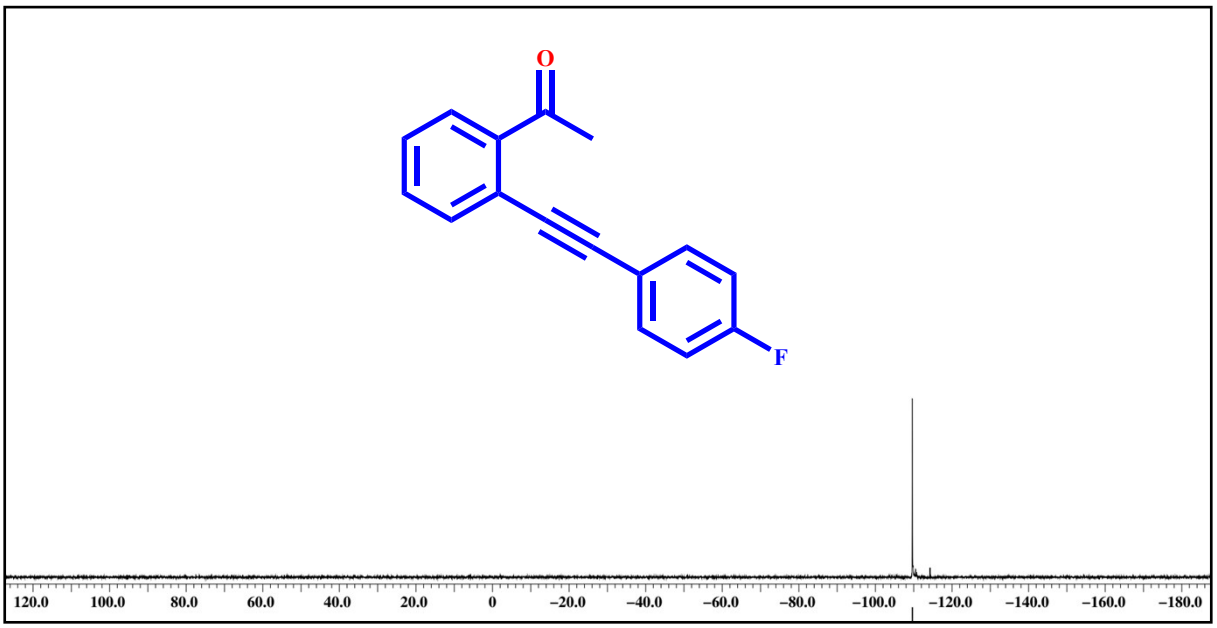

Fig. S41 ^{19}F NMR ($CDCl_3$, 376 MHz) spectrum of 1-(2-((4-fluorophenyl)ethynyl)phenyl)ethan-1-one.

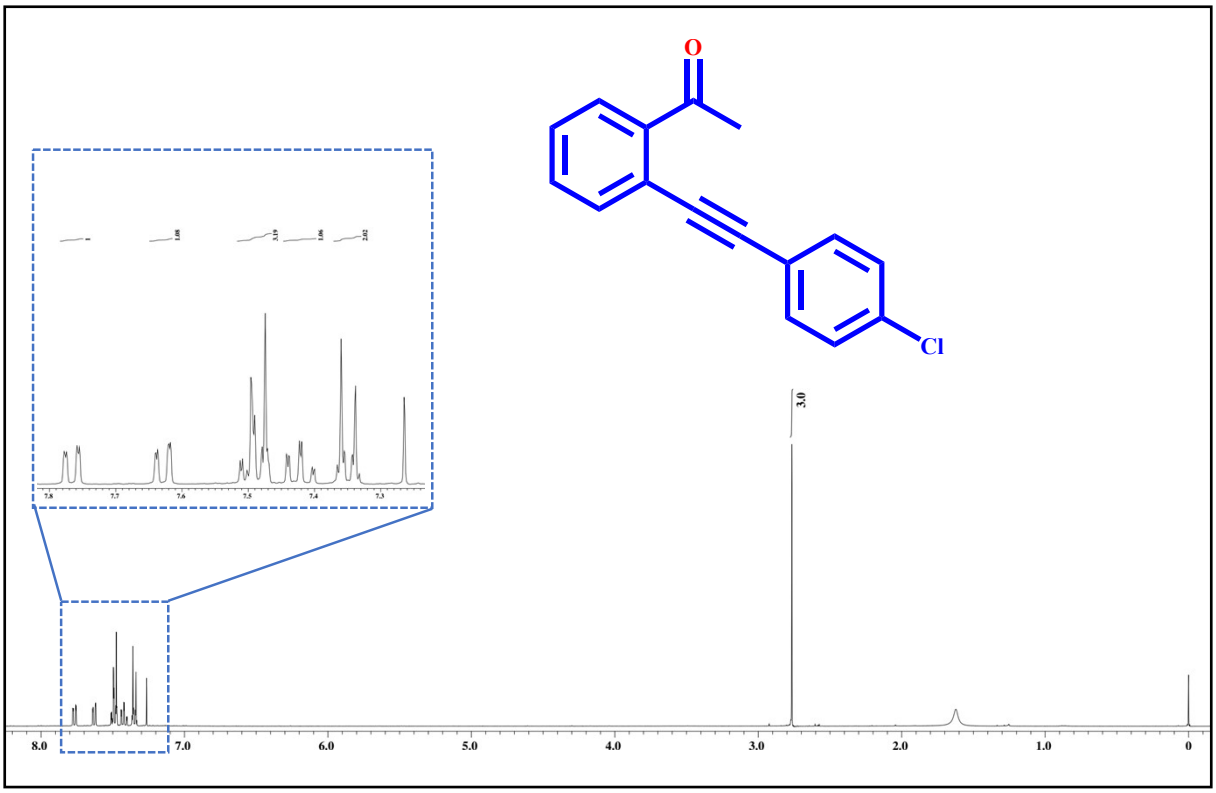

Fig. S42 ^{1}H NMR ($CDCl_3$, 400 MHz) spectrum of 1-(2-((4-chlorophenyl)ethynyl)phenyl)ethan-1-one.

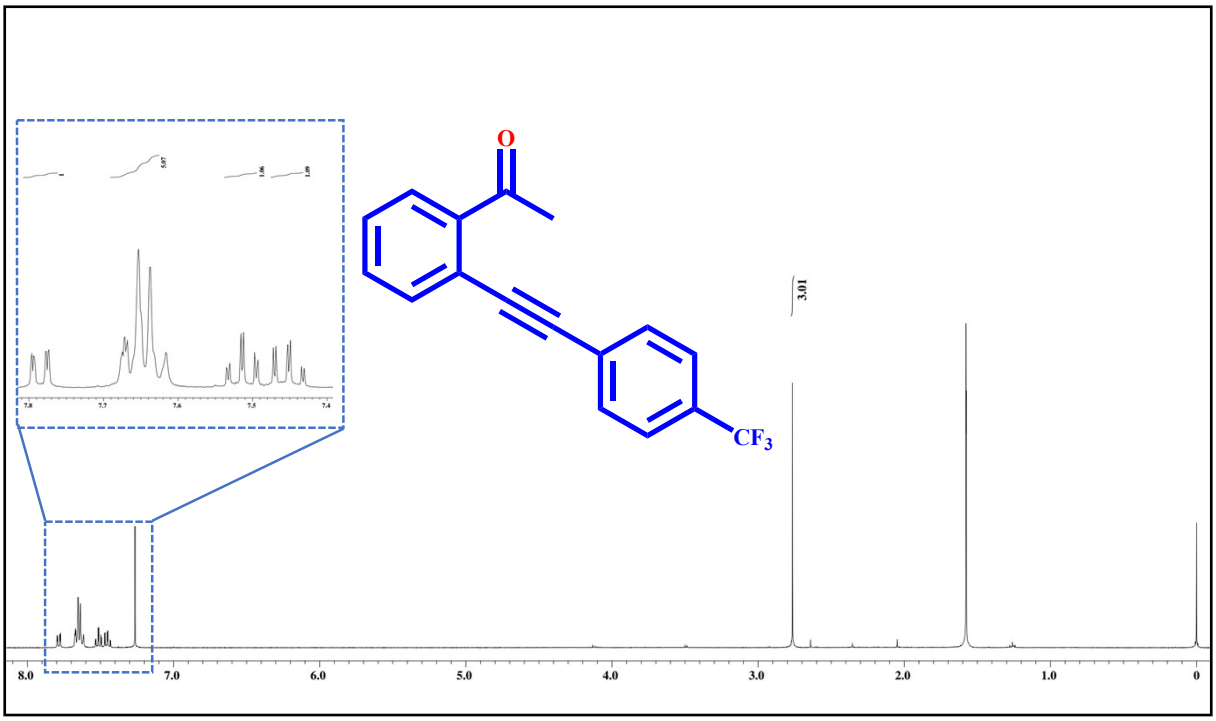

Fig. S43 ^{1}H NMR ($CDCl_3$, 400 MHz) spectrum of 1-(2-((4-(trifluoromethyl)phenyl)ethynyl)phenyl)ethan-1-one.

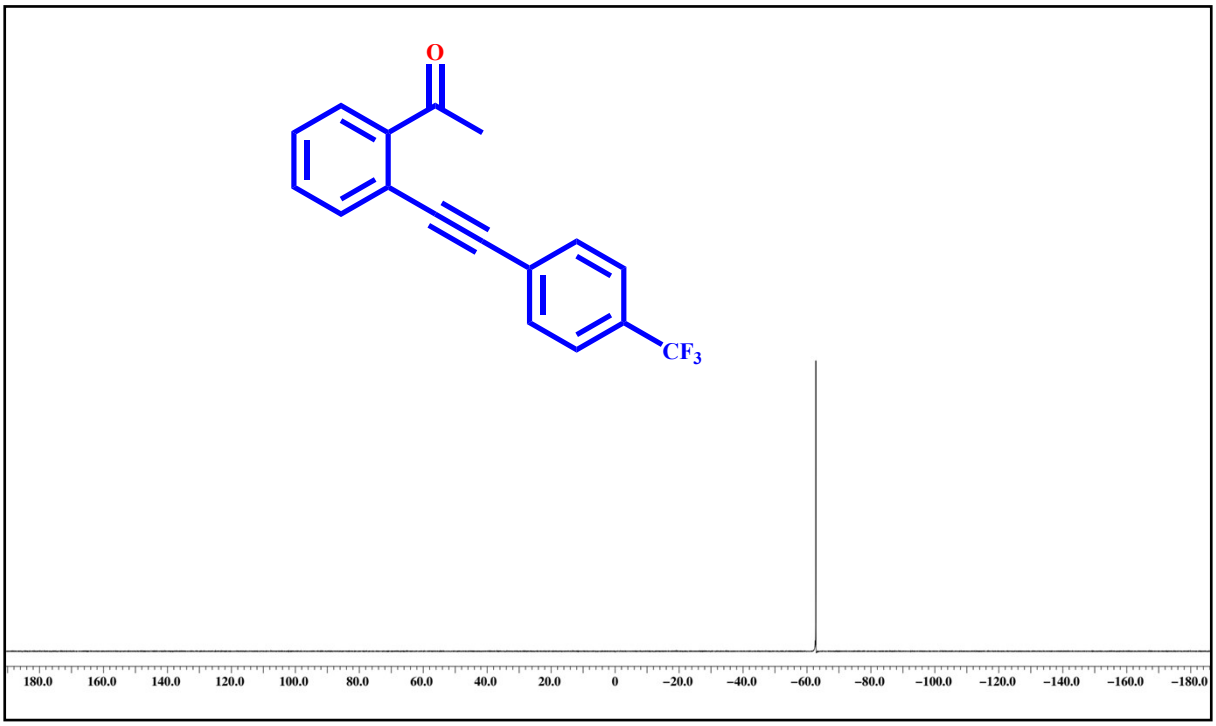

Fig. S44 ^{19}F NMR ($CDCl_3$, 376 MHz) spectrum of 1-(2-((4-(trifluoromethyl)phenyl)ethynyl)phenyl)ethan-1-one.

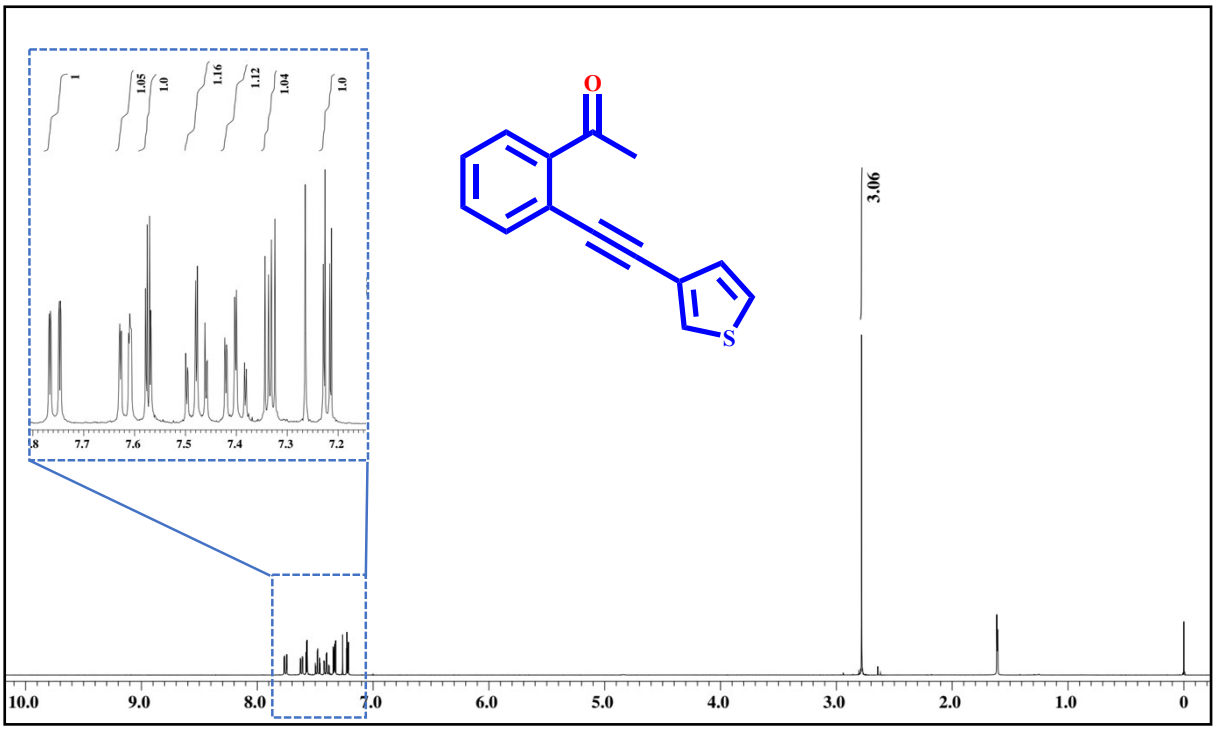

Fig. S45 ^{1}H NMR ($CDCl_3$, 400 MHz) spectrum of 1-(2-(thiophen-3-ylethynyl)phenyl)ethan-1-one.

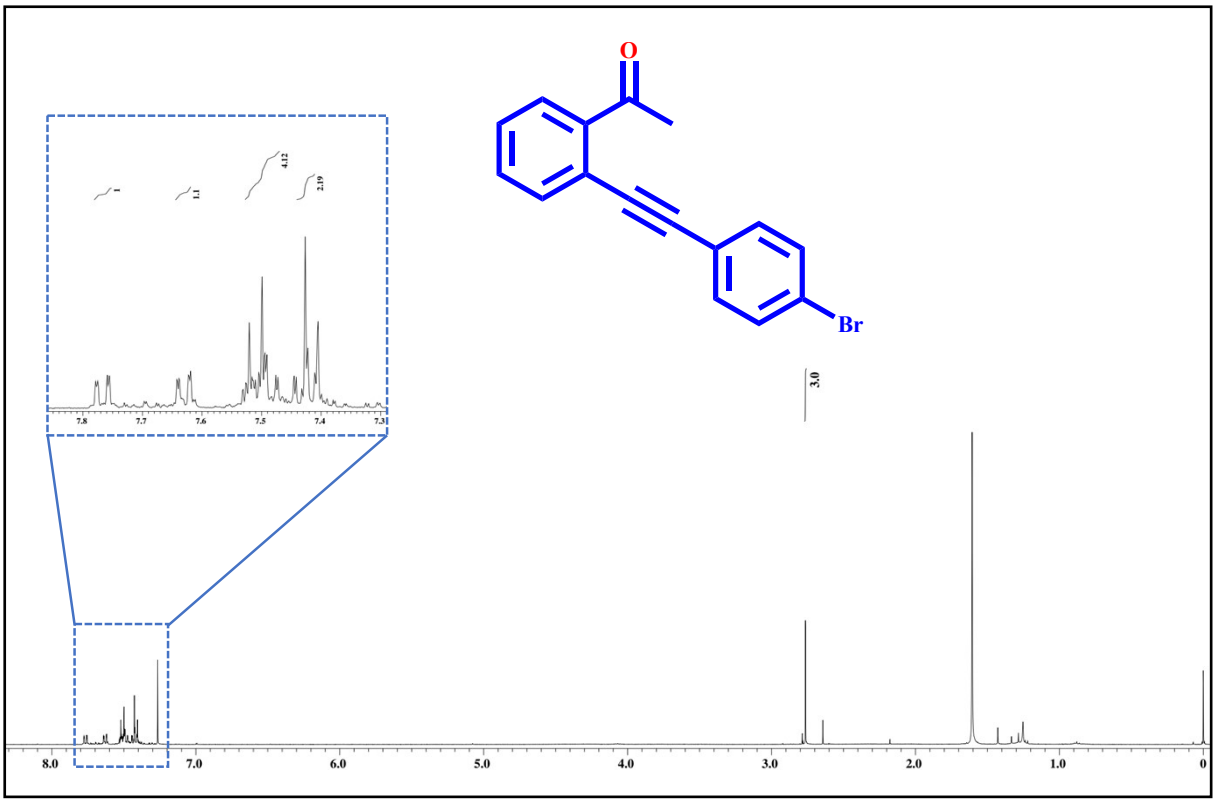

Fig. S46 ^{1}H NMR ($CDCl_3$, 400 MHz) spectrum of 1-(2-((4-bromophenyl)ethynyl)phenyl)ethan-1-one.

Table S5 Optimization of catalytic reaction conditions for the carboxylation of 1-(2-(phenylethynyl)phenyl)ethan-1-one with CO_2 catalyzed by Ag_3-TAPT-COF.

S. No.	Catalyst	Base	Temp. (°C)	Time (h)	Yield (%) [b]
1.	Ag_3-TAPT-COF	-	50	12	-
2.	-	DBU	50	12	10
3.	Ag_3-TAPT-COF	LiHMDS	50	12	29
4.	Ag_3-TAPT-COF	K_2CO_3	50	12	34
5.	Ag_3-TAPT-COF	Cs_2CO_3	50	12	45
6.	Ag_3-TAPT-COF	DBU	RT	12	25
7.	Ag_3-TAPT-COF	DBU	50	8	67
8.	Ag_3-TAPT-COF	DBU	50	12	88
9.	Ag_3-TAPT-COF	DBU	40	12	73
10[c].	Ag_3-TAPT-COF	DBU	50	12	trace

Reaction Conditions: 1-(2-(phenylethynyl)phenyl)ethan-1-one (1 mmol), DBU (1.5 mmol), 50 °C, 12 h, DMF (5mL), Catalyst (Ag_3-TAPT-COF) 10 mg, CO_2 balloon. [c]N_2 (balloon).

Table S6 NMR spectral data of isobenzofuranacetic acids prepared from various 1-(2-(phenylethynyl)phenyl)ethan-1-one substrates.

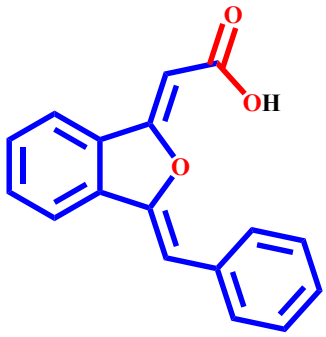	**2-((Z)-3-((Z)-benzylidene)isobenzofuran-1(3H)-ylidene)acetic acid** ^{1}H NMR (400 MHz; DMSO-d_6): δ (ppm) 12.09 (s, 1H), 8.04-8.06 (d, 3H), 7.99-8.01 (d, 1H), 7.66-7.70 (t, 1H), 7.55-7.59 (t, 1H), 7.39-7.42 (t, 2H), 7.28-7.31 (t, 1H), 6.73 (s, 1H), 5.93 (s, 1H), ^{13}C NMR (101 MHz, DMSO-d_6) δ (ppm) 89.69, 103.11, 120.46, 122.11, 127.47, 128.69, 129.28, 129.95, 131.41, 132.05, 134.12, 134.55, 150.28, 161.10, 165.93.
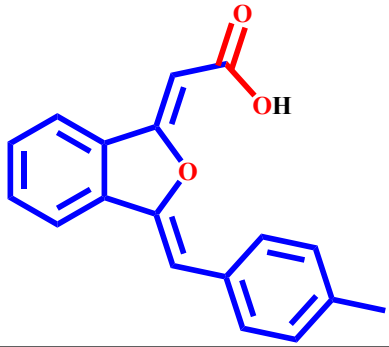	**2-((Z)-3-((Z)-4-methylbenzylidene)isobenzofuran-1(3H)-ylidene)acetic acid** ^{1}H NMR (400 MHz; DMSO-d_6): δ (ppm) 12.04 (s, 1H) 7.99-8.01 (d, 1H), 7.90-7.96 (m, 3H), 7.62-7.66 (t, 1H), 7.50-7.54 (t, 1H), 7.18-7.20 (d, 2H), 6.67 (s, 1H), 5.88 (s, 1H), 2.31 (s, 3H).
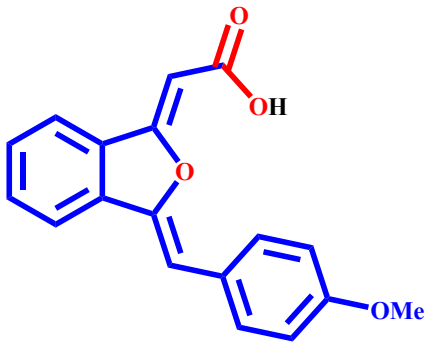	**2-((Z)-3-((Z)-4-fluorobenzylidene)isobenzofuran-1(3H)-ylidene)acetic acid** ^{1}H NMR (400 MHz; DMSO-d_6): δ (ppm) 11.98 (s, 1H), 7.97-8.01 (m, 3H), 7.92-7.94 (d, 1H), 7.61-7.65 (t, 1H), 7.49-7.53 (t, 1H), 6.94-7.96 (d, 2H), 6.67 (s, 1H), 5.87 (s, 1H), 3.78 (s, 3H) 6.73(s, 1H); ^{13}C NMR (101 MHz, DMSO-d_6): δ (ppm) 55.22, 89.03, 103.20, 114.24, 120.17, 122.06, 126.77, 129.52, 130.90, 131.07, 132.04, 134.88, 148.78, 158.77, 161.43, 166.05.

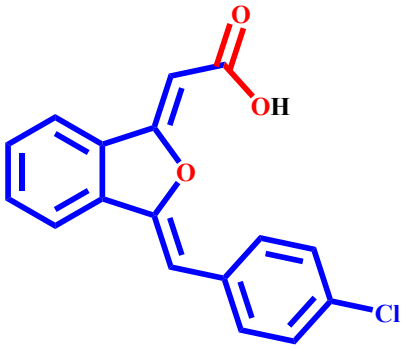	**2-((Z)-3-((Z)-4-methoxybenzylidene)isobenzofuran-1(3H)-ylidene)acetic acid** ^{1}H NMR (400 MHz; DMSO-d_6): δ (ppm) 12.5 (s, 1H) 8.02-8.04 (dd, 2H), 7.95-7.97 (d, 1H), 7.64-6.67 (t, 1H), 7.53-7.57 (t, 1H), 7.40-7.43 (d, 1H), 6.72 (s, 1H), 5.94 (s, 1H); ^{13}C NMR (101 MHz, DMSO-d_6): δ (ppm) 90.05, 101.72, 120.58, 122.18, 128.65, 130.18, 130.78, 131.50, 131.70, 132.12, 133.12, 134.36, 150.92, 160.99, 165.94.
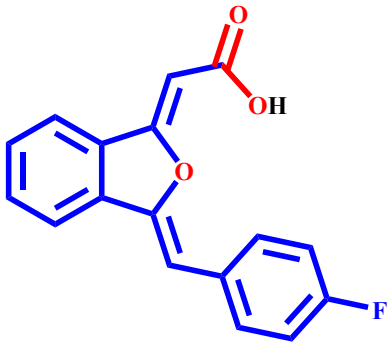	**2-((Z)-3-((Z)-4-fluorobenzylidene)isobenzofuran-1(3H)-ylidene)acetic acid** ^{1}H NMR (400 MHz; DMSO-d_6): δ (ppm) 12.05 (s,1H) 8.06-8.10 (d, 2H), 8.02-8.04 (d, 1H), 7.95-7.97 (d, 1H), 7.64-7.68 (t, 1H), 7.53-7.57 (t, 1H), 7.19-7.24 (t, 2H), 6.74 (s, 1H), 5.92 (s, 1H), 5.93 (s, 1H), 12.04 (s br, 1H); ^{13}C NMR (101 MHz, DMSO-d_6):δ (ppm) 89.81, 102.17, 115.63, 115.88, 120.58, 122.27, 130.15, 131.41, 132.19, 134.56, 150.06, 160.24, 161.33, 162.69, 166.02; ^{19}F NMR (DMSO-d$_6$, 376 MHz):δ (ppm) -42.62.
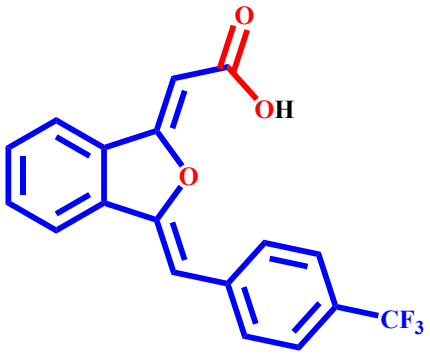	**2-((Z)-3-((Z)-4-(trifluoromethyl)benzylidene)isobenzofuran-1(3H)-ylidene)acetic acid** ^{1}H NMR (400 MHz; DMSO-d_6): δ (ppm) 12.21 (s, 1H), 8.20-8.23 (d, 2H), 8.01-8.08 (d, 2H), 7.67-7.71 (t, 3H), 7.58-7.62 (t, 1H), 6.84 (s, 1H), 6.00 (s, 1H); ^{13}C NMR (101 MHz, DMSO-d_6) 90.79, 101.33, 120.91, 122.22, 123.02, 125.36, 126.74, 129.46, 130.61, 131.77, 132.21, 134.18, 138.31, 152.17, 160.80, 165.73; ^{19}F NMR (DMSO-d$_6$, 376 MHz): δ (ppm) -60.90.

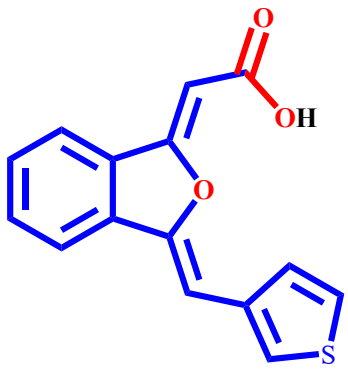	**2-((1Z,3Z)-3-(thiophen-3-ylmethylene)isobenzofuran-1(3H)-ylidene)acetic acid** ^{1}H NMR (400 MHz; DMSO-d_6): δ (ppm) 12.04 (s, 1H) 8.06-8.07 (d, 1H), 8.00-8.02 (d, 1H), 7.91-7.93 (d, 1H), 7.75-7.76 (dd, 1H), 7.62-7.65 (t, 1H), 7.58-7.61(m, 1H), 7.50-7.54 (t, 1H), 6.81 (s, 1H), 5.89 (s, 1H); ^{13}C NMR (101 MHz, DMSO-d_6): δ (ppm) 89.43, 98.44, 120.51, 122.37, 125.23, 126.52, 129.04, 130.04, 131.68, 132.39, 134.46, 135.37, 149.58, 161.49, 166.31.
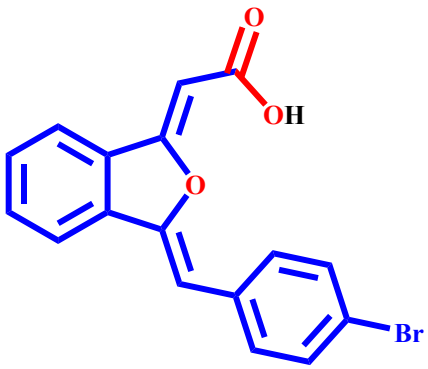	**2-((Z)-3-((Z)-4-bromobenzylidene)isobenzofuran-1(3H)-ylidene)acetic acid** ^{1}H NMR (400 MHz; DMSO-d_6): δ (ppm) 12.12 (s, 1H) 8.03-8.05 (d, 1H), 7.96-7.98 (d, 3H), 7.65-7.69 (t, 1H), 7.55-7.59 (dd, 1H), 7.62-7.65 (t, 1H), 7.58-7.61(m, 1H), 7.50-7.54 (t, 1H), 6.81 (s, 1H), 5.89 (s, 1H); ^{13}C NMR (101 MHz, DMSO-d_6): δ (ppm) 89.43, 98.44, 120.51, 122.37, 125.23, 126.52, 129.04, 130.04, 131.68, 132.39, 134.46, 135.37, 149.58, 161.49, 166.31.

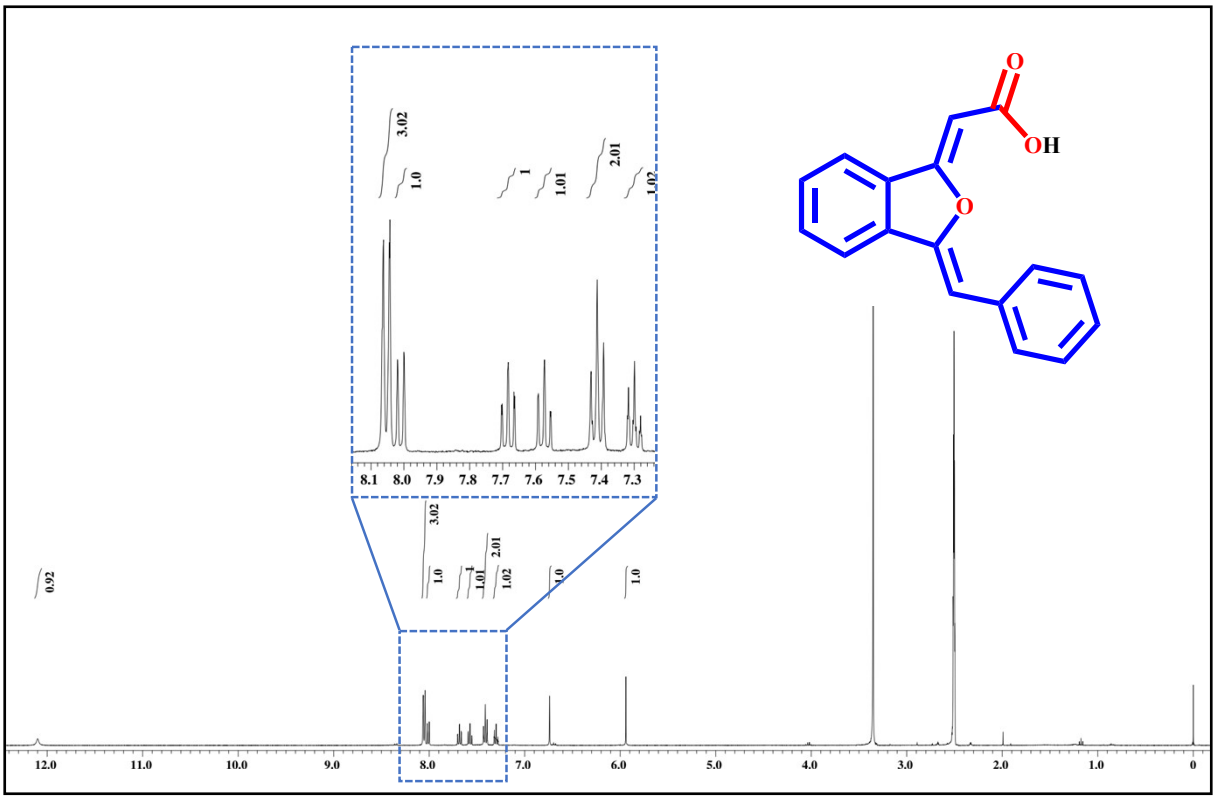

Fig. S47 ^{1}H NMR (DMSO-d_6, 400 MHz) spectrum of 2-((Z)-3-((Z)-benzylidene)isobenzofuran-1(3H)-ylidene)acetic acid obtained from carboxylation of 1-(2-(phenylethynyl)phenyl)ethan-1-one with CO_2 by Ag_3-TAPT-COF under optimized conditions.

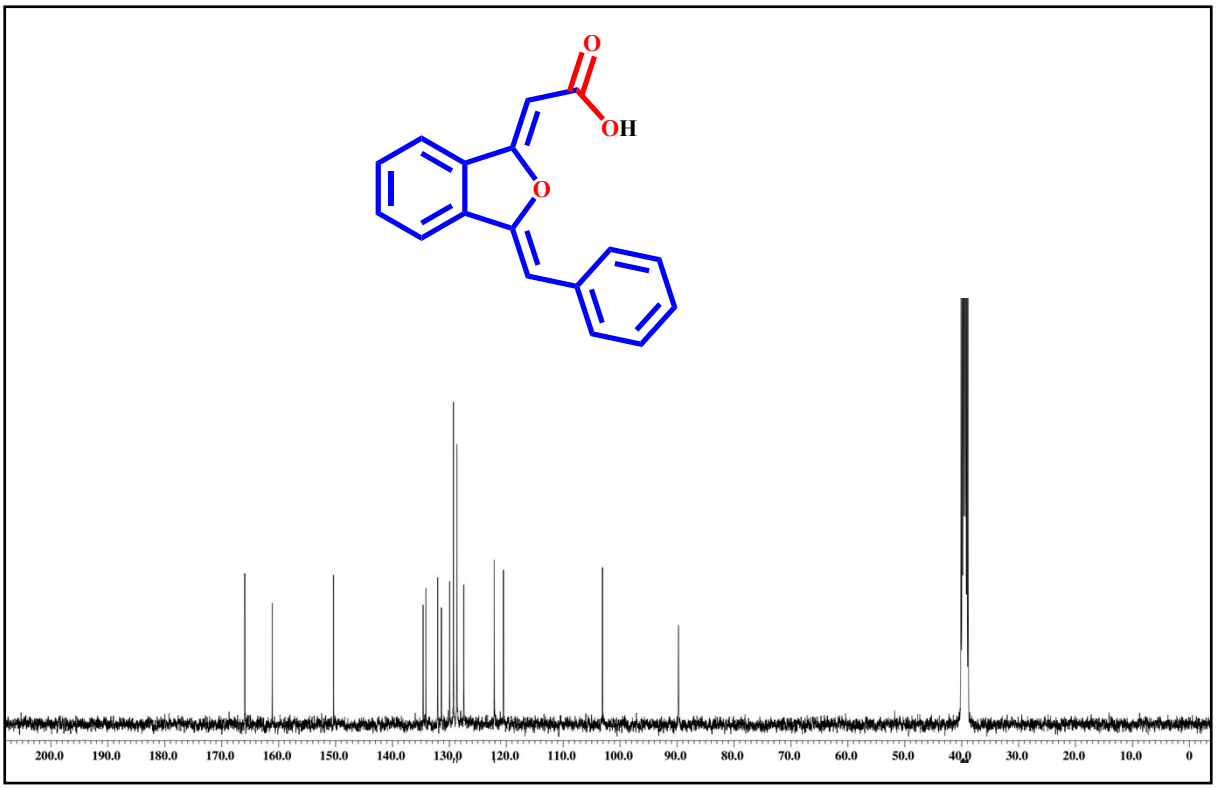

Fig. S48 ^{13}C NMR (DMSO-d_6, 101 MHz) spectrum of 2-((Z)-3-((Z)-benzylidene)isobenzofuran-1(3H)-ylidene)acetic acid obtained from carboxylation of 1-(2-(phenylethynyl)phenyl)ethan-1-one with CO_2 by Ag_3-TAPT-COF under optimized conditions.

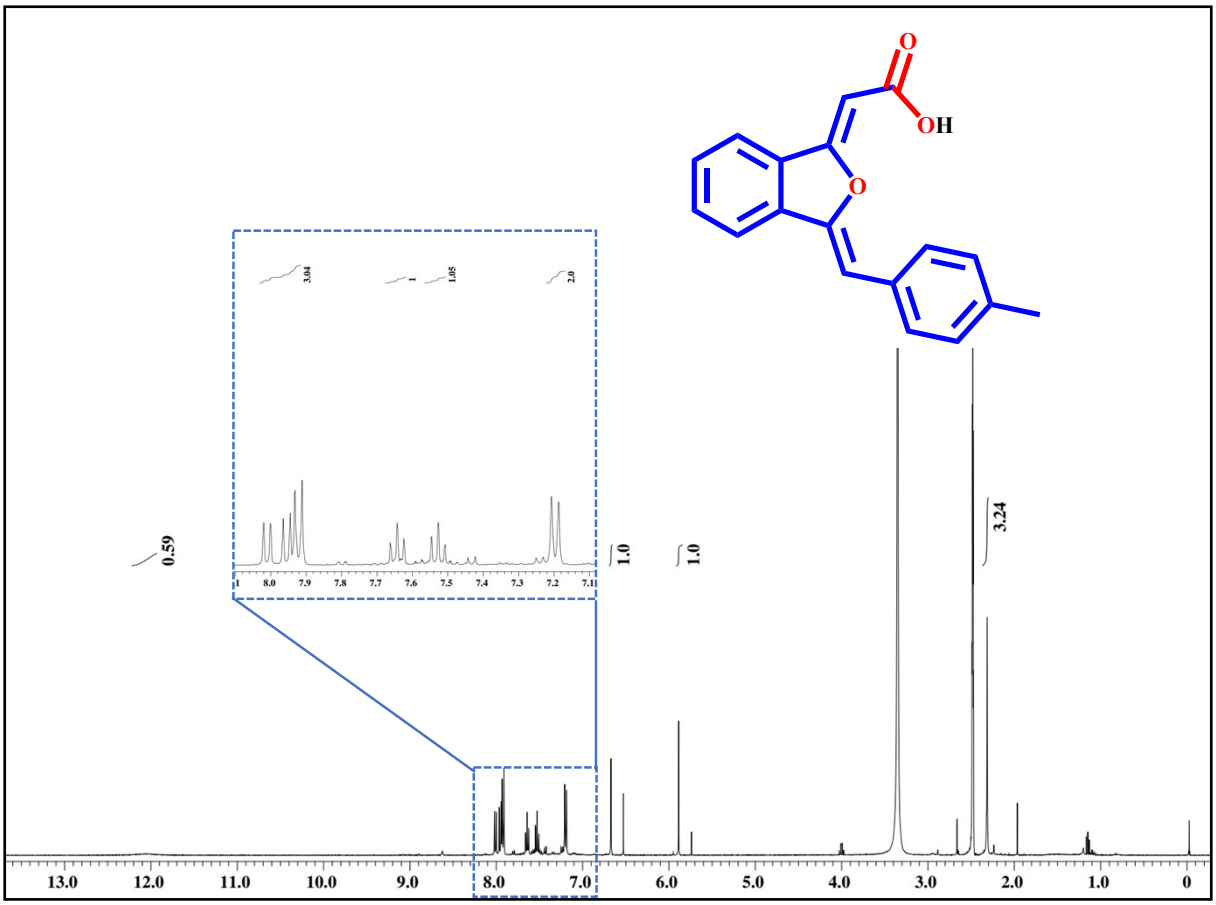

Fig. S49 ^{1}H NMR (DMSO-d_6, 400 MHz) spectrum of 2-((Z)-3-((Z)-4-methylbenzylidene)isobenzofuran-1(3H)-ylidene)acetic acid obtained from carboxylation of 1-(2-(p-tolylethynyl)phenyl)ethan-1-one with CO_2 by Ag_3-TAPT-COF under optimized conditions.

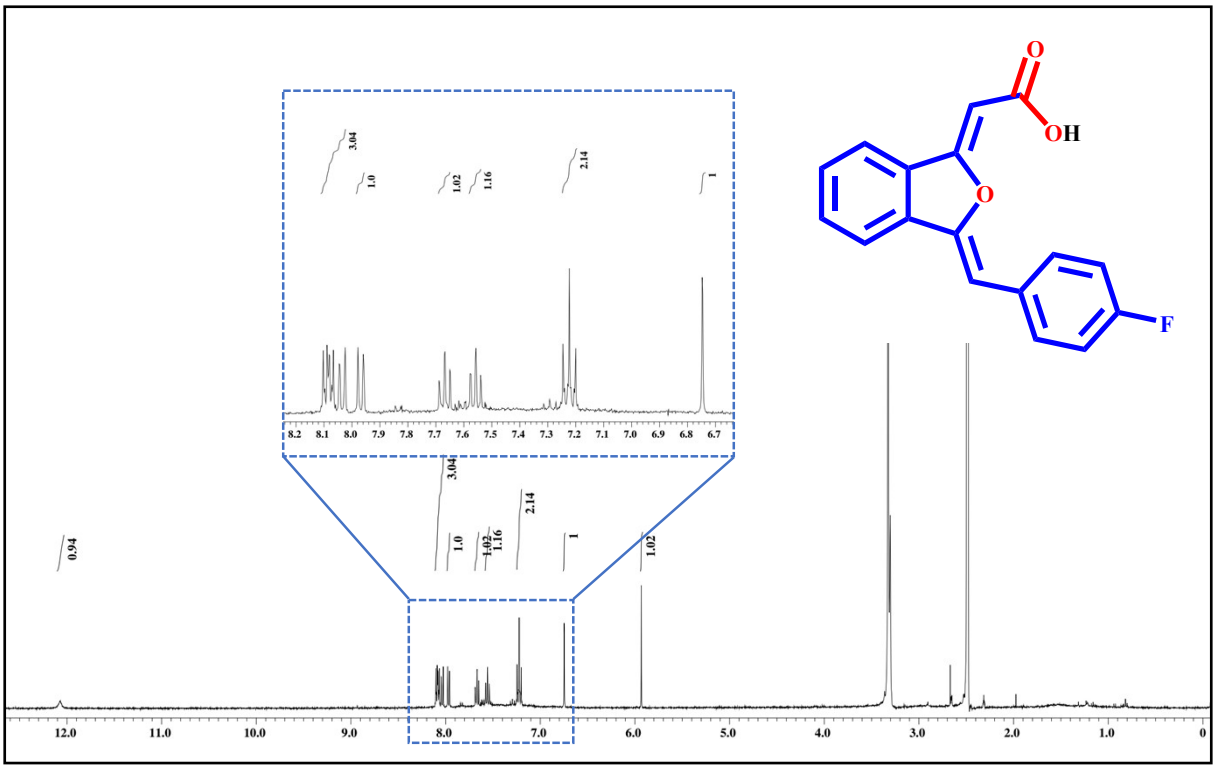

Fig. S50 ^{1}H NMR (DMSO-d_6, 400 MHz) spectrum of 2-((Z)-3-((Z)-4-fluorobenzylidene)isobenzofuran-1(3H)-ylidene)acetic acid obtained from carboxylation of 1-(2-((4-fluorophenyl)ethynyl)phenyl)ethan-1-one with CO_2 by Ag_3-TAPT-COF under optimized conditions.

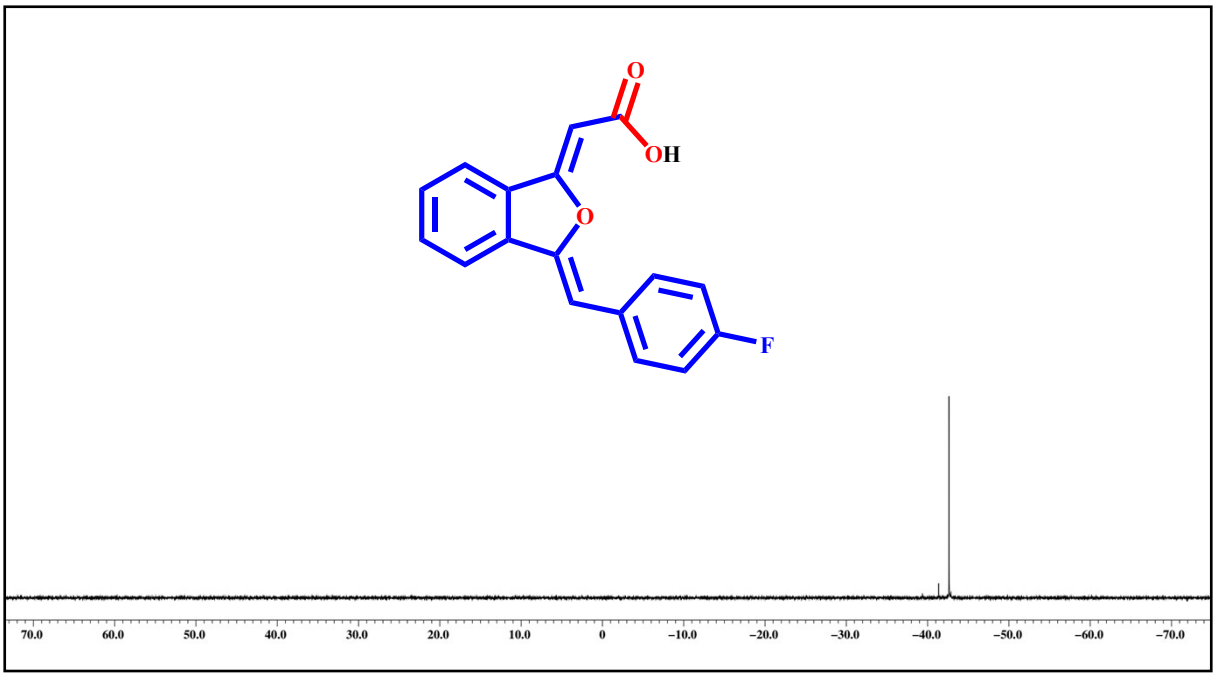

Fig. S51 ^{19}F NMR (DMSO-d_6, 376 MHz) spectrum of 2-((Z)-3-((Z)-4-fluorobenzylidene)isobenzofuran-1(3H)-ylidene)acetic acid obtained from carboxylation of 1-(2-((4-fluorophenyl)ethynyl)phenyl)ethan-1-one with CO_2 by Ag_3-TAPT-COF under optimized conditions.

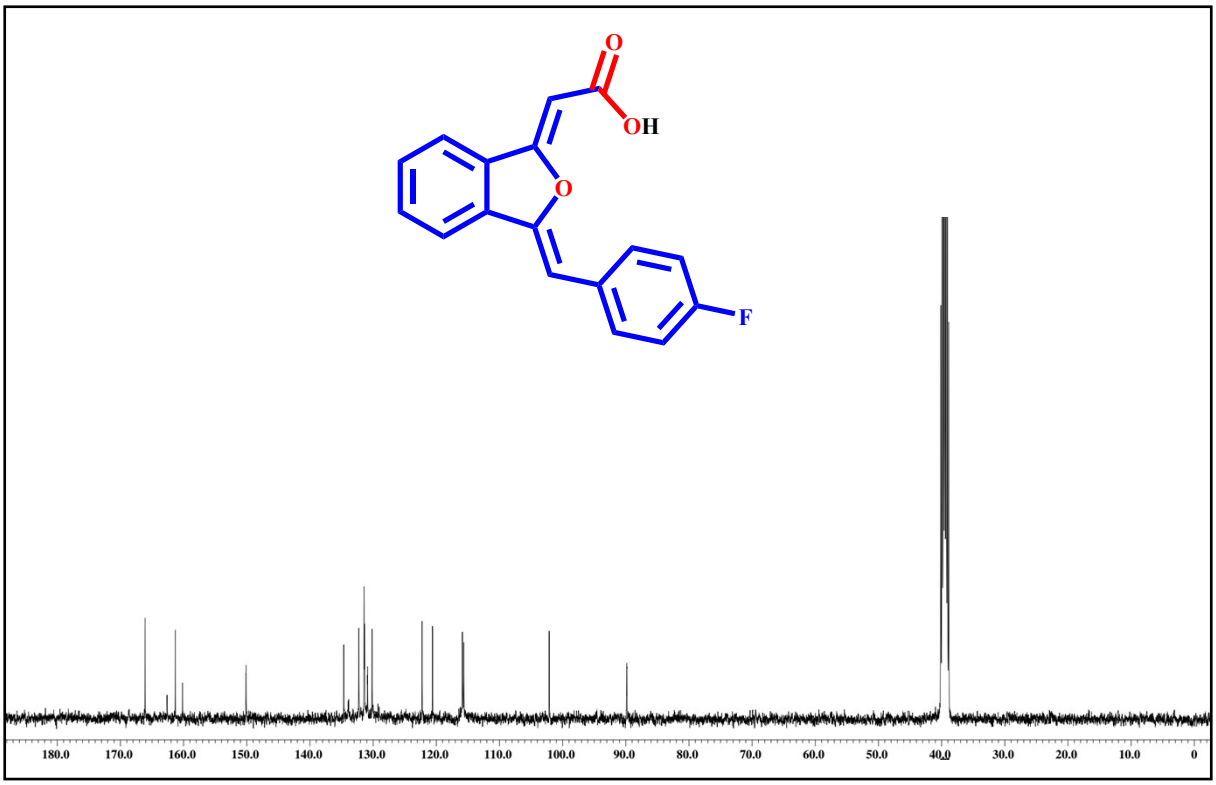

Fig. S52 ^{13}C NMR (DMSO-d_6, 101 MHz) spectrum of 2-((Z)-3-((Z)-4-fluorobenzylidene)isobenzofuran-1(3H)-ylidene)acetic acid obtained from carboxylation of 1-(2-((4-fluorophenyl)ethynyl)phenyl)ethan-1-one with CO_2 by Ag_3-TAPT-COF under optimized conditions.

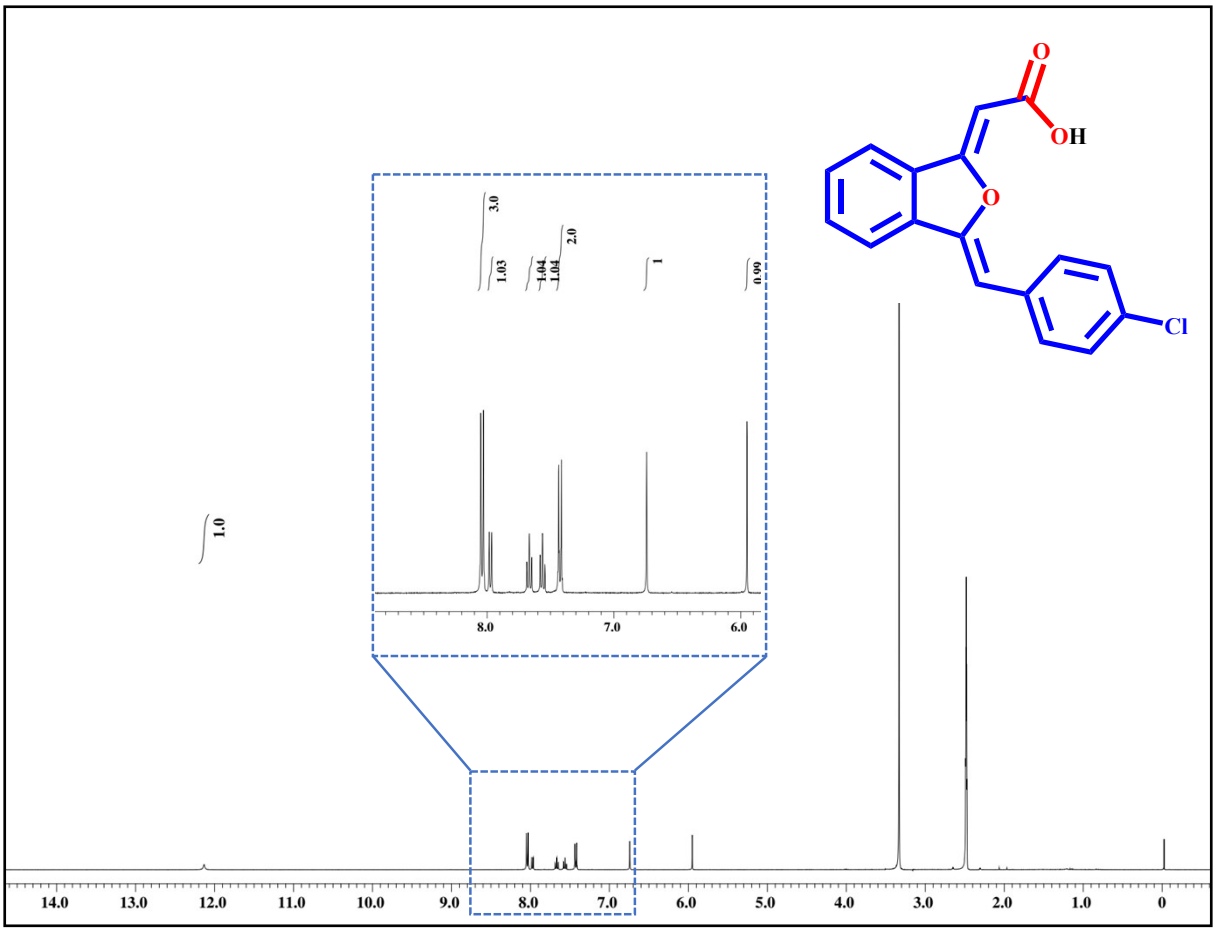

Fig. S53 ^{1}H NMR (DMSO-d_6, 400 MHz) spectrum of 2-((Z)-3-((Z)-4-chlorobenzylidene)isobenzofuran-1(3H)-ylidene)acetic acid obtained from carboxylation of 1-(2-((4-chlorophenyl)ethynyl)phenyl)ethan-1-one with CO_2 by Ag_3-TAPT-COF under optimized conditions.

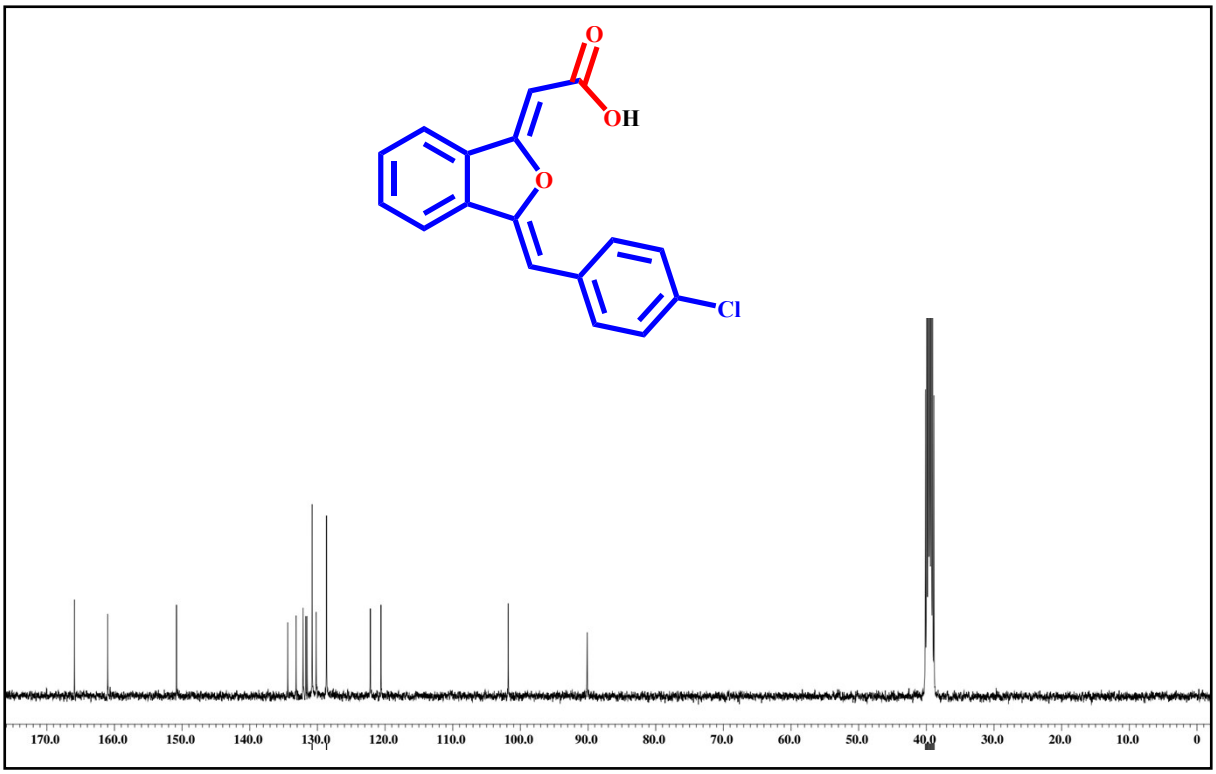

Fig. S54 ^{13}C NMR (DMSO-d_6, 101 MHz) spectrum of 2-((Z)-3-((Z)-4-chlorobenzylidene)isobenzofuran-1(3H)-ylidene)acetic acid obtained from carboxylation of 1-(2-((4-chlorophenyl)ethynyl)phenyl)ethan-1-one with CO_2 by Ag_3-TAPT-COF under optimized conditions.

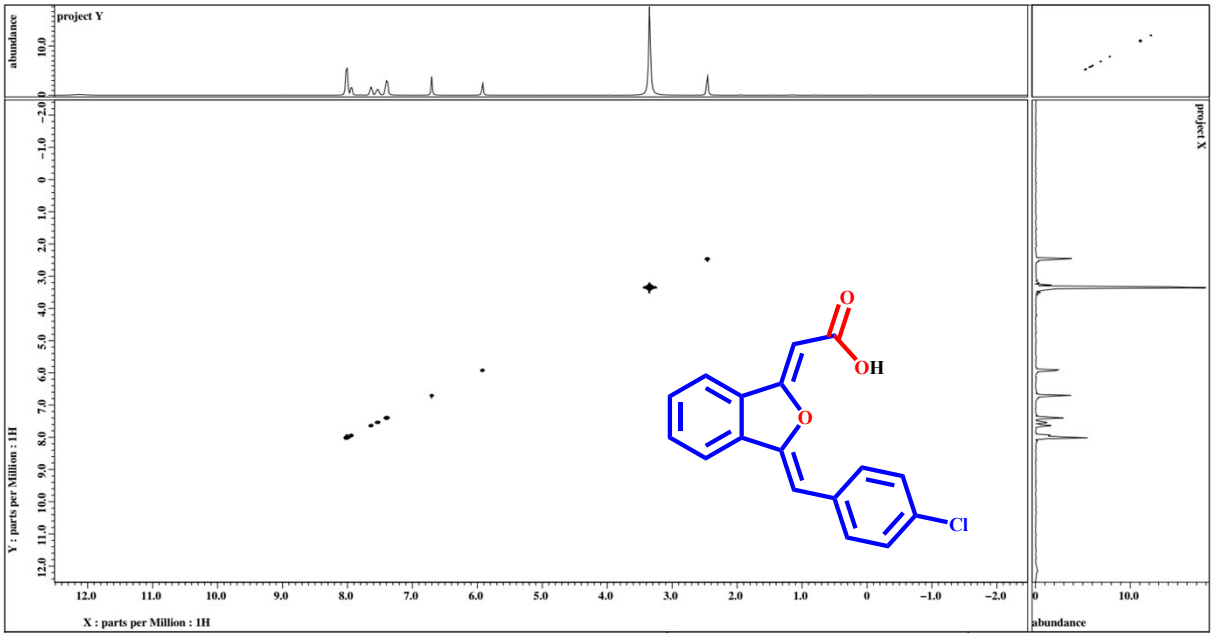

Fig. S55 ^{1}H-^{1}H 2D NMR (DMSO-d_6, 400 MHz) NOESY spectra of 2-((Z)-3-((Z)-4-chlorobenzylidene)isobenzofuran-1(3H)-ylidene)acetic acid.

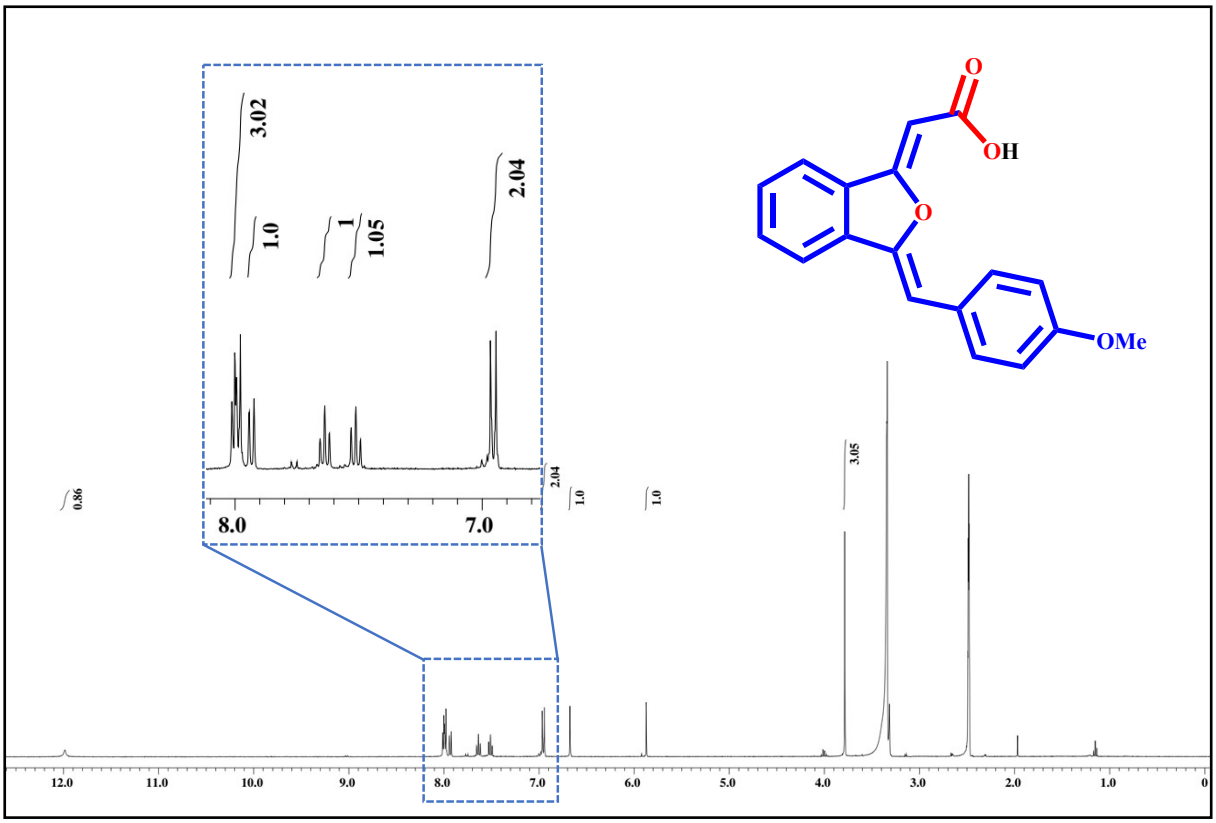

Fig. S56 ^{1}H NMR (DMSO-d_6, 400 MHz) spectrum of 2-((Z)-3-((Z)-4-methoxybenzylidene)isobenzofuran-1(3H)-ylidene)acetic acid obtained from carboxylation of 1-(2-((4-methoxyphenyl)ethynyl)phenyl)ethan-1-one with CO_2 by Ag_3-TAPT-COF under optimized conditions.

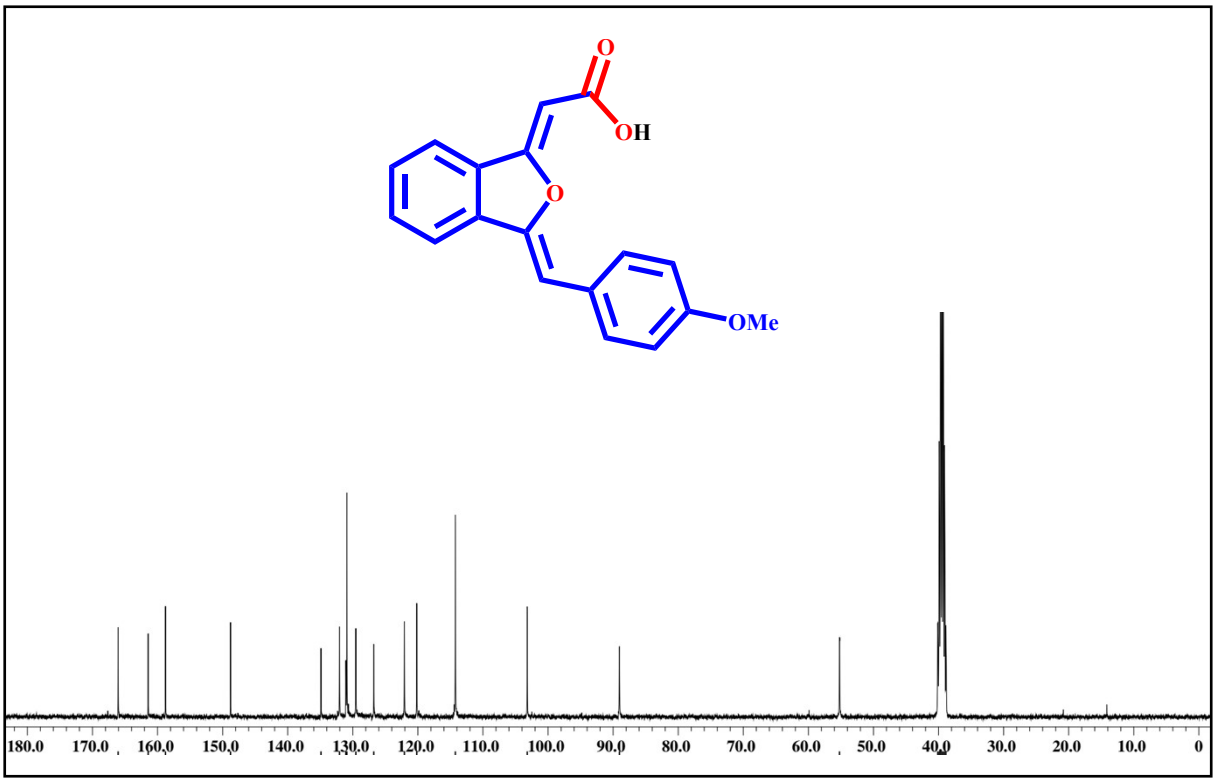

Fig. S57 ^{13}C NMR (DMSO-d_6, 101 MHz) spectrum of 2-((Z)-3-((Z)-4-methoxybenzylidene)isobenzofuran-1(3H)-ylidene)acetic acid obtained from carboxylation of 1-(2-((4-methoxyphenyl)ethynyl)phenyl)ethan-1-one with CO_2 by Ag_3-TAPT-COF under optimized conditions.

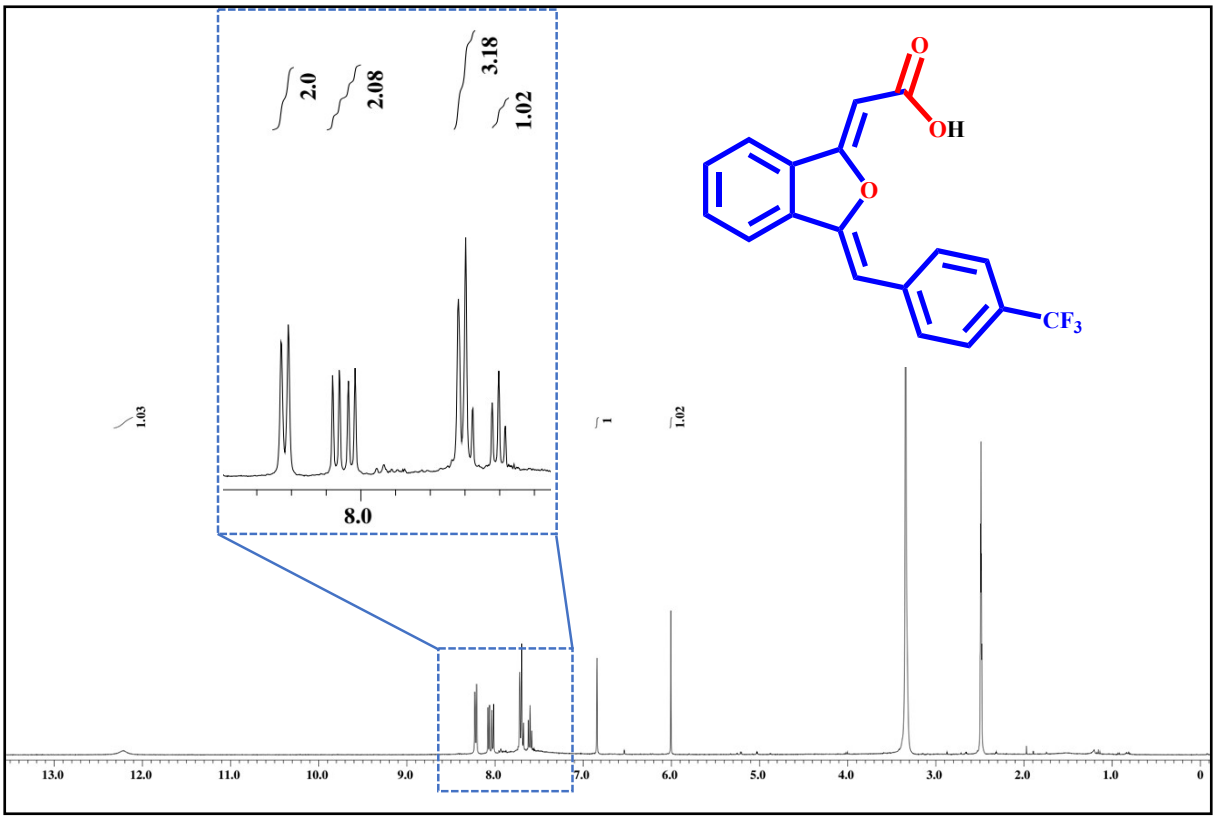

Fig. S58 ^{1}H NMR (DMSO-d_6, 400 MHz) spectrum of 2-((Z)-3-((Z)-4-(trifluoromethyl)benzylidene)isobenzofuran-1(3H)-ylidene)acetic acid obtained from carboxylation of 1-(2-((4-(trifluoromethyl)phenyl)ethynyl)phenyl)ethan-1-one with CO_2 by Ag_3-TAPT- COF under optimized conditions.

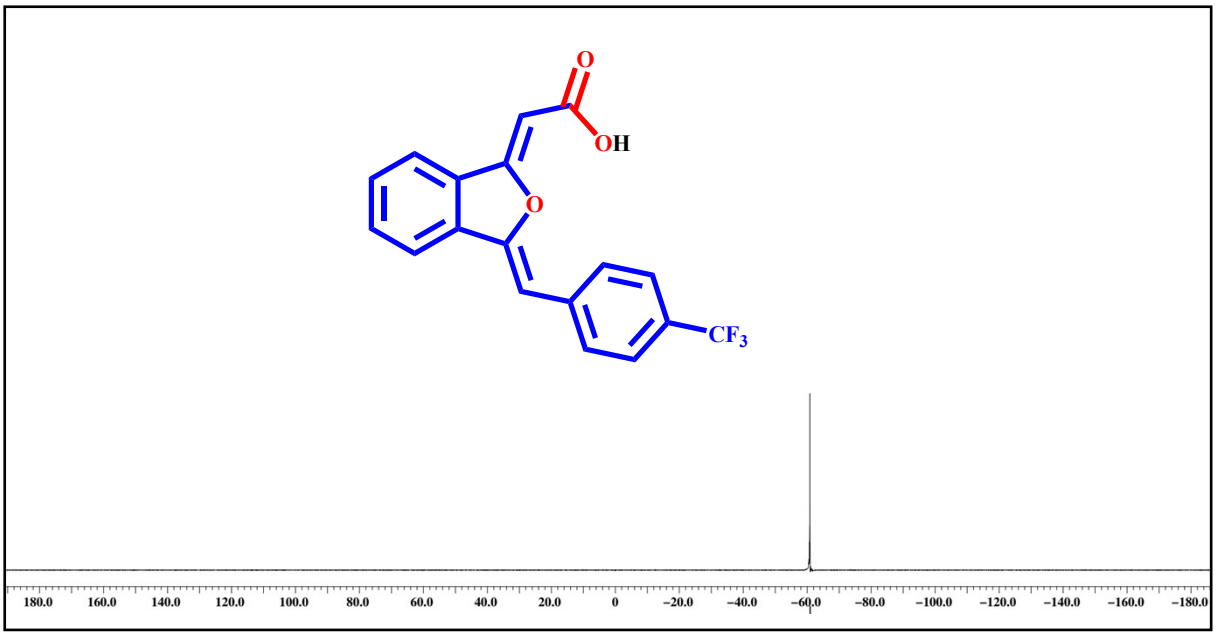

Fig. S59 ^{19}F NMR (DMSO-d_6, 376 MHz) spectrum of 2-((Z)-3-((Z)-4-(trifluoromethyl)benzylidene)isobenzofuran-1(3H)-ylidene)acetic acid obtained from carboxylation of 1-(2-((4-(trifluoromethyl)phenyl)ethynyl)phenyl)ethan-1-one with CO_2 by Ag_3-TAPT- COF under optimized conditions.

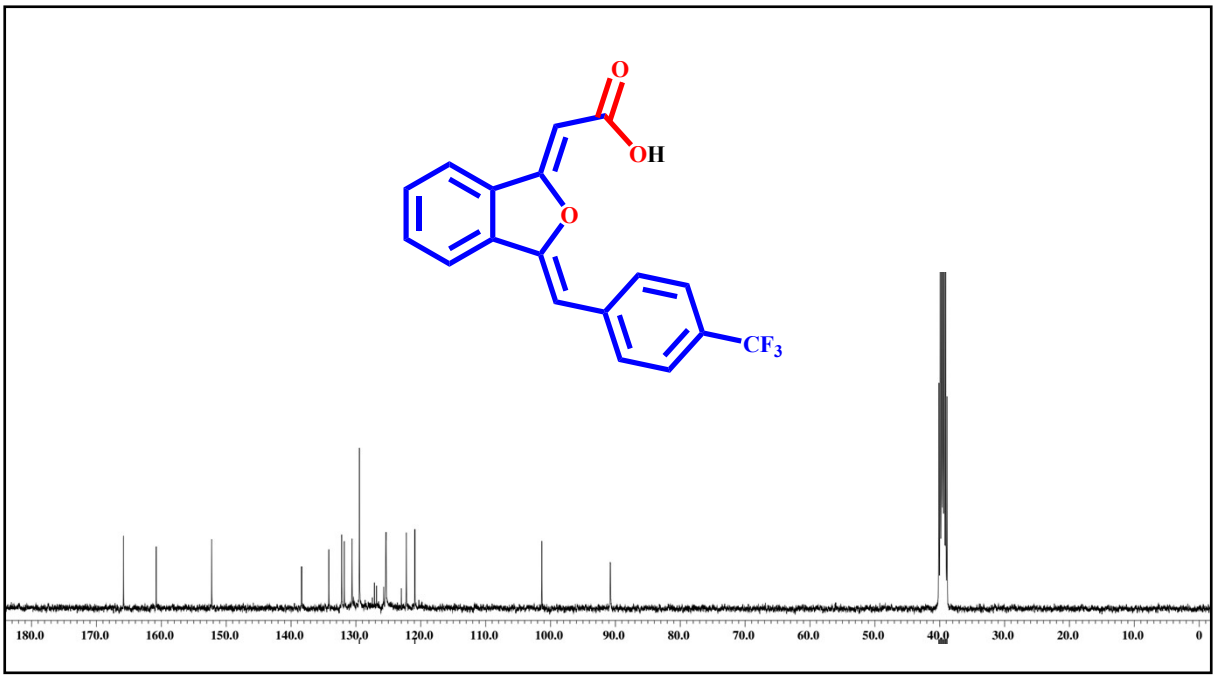

Fig. S60 ^{13}C NMR (DMSO-d_6, 101 MHz) spectrum of 2-((Z)-3-((Z)-4-(trifluoromethyl)benzylidene)isobenzofuran-1(3H)-ylidene)acetic acid obtained from carboxylation of 1-(2-((4-(trifluoromethyl)phenyl)ethynyl)phenyl)ethan-1-one with CO_2 by Ag_3-TAPT-COF under optimized conditions.

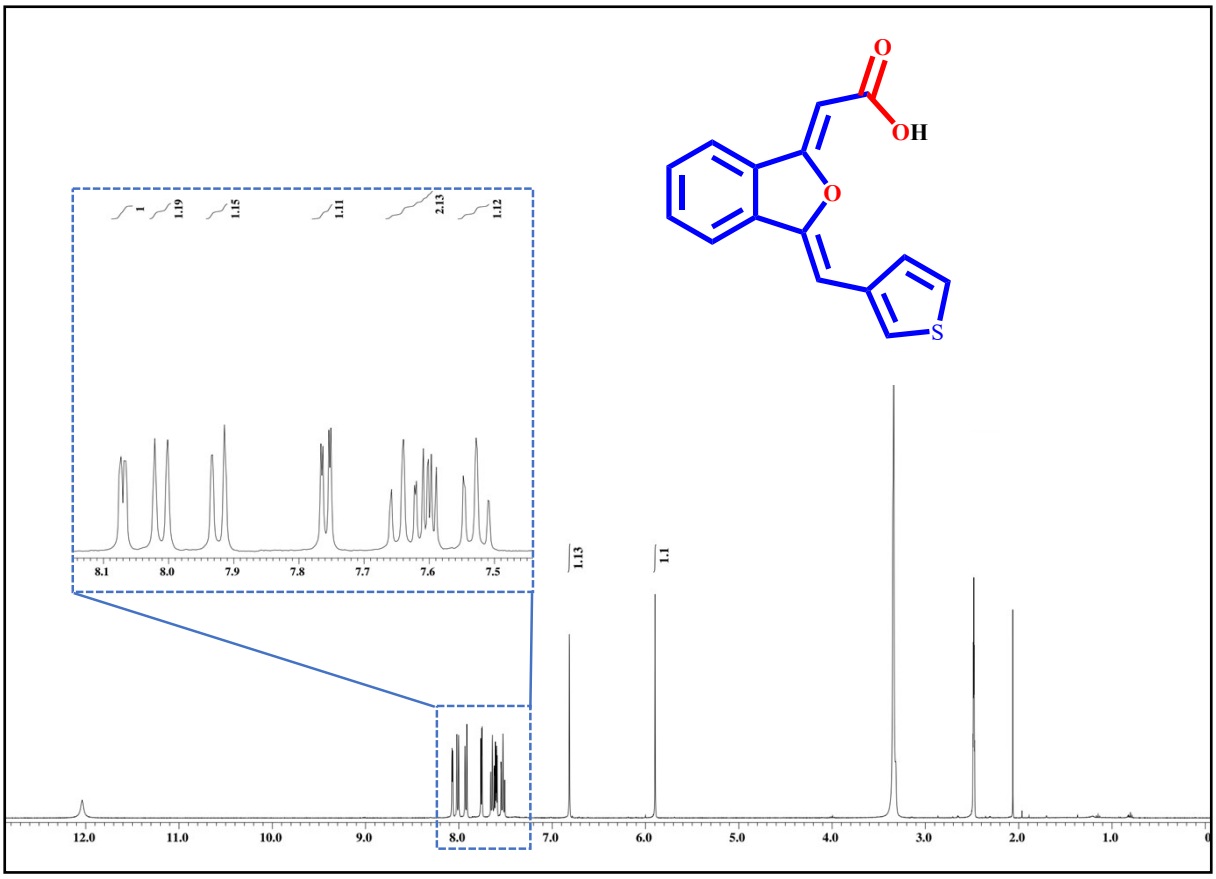

Fig. S61 ^{1}H NMR (DMSO-d_6, 400 MHz) spectrum of 2-((1Z,3Z)-3-(thiophen-3-ylmethylene)isobenzofuran-1(3H)-ylidene)acetic acid obtained from carboxylation of 1-(2-((4-(trifluoromethyl)phenyl)ethynyl)phenyl)ethan-1-one with CO_2 by Ag_3-TAPT-COF under optimized conditions.

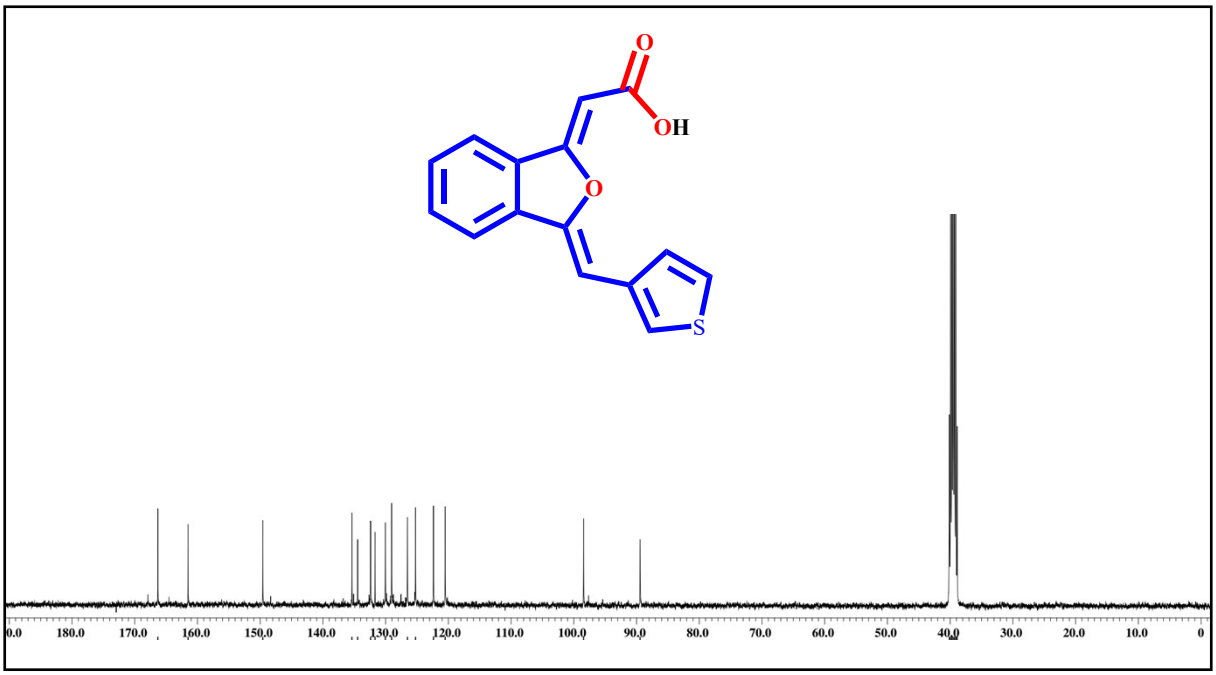

Fig. S62 ^{13}C NMR (DMSO-d_6, 101 MHz) spectrum of 2-((1Z,3Z)-3-(thiophen-3-ylmethylene)isobenzofuran-1(3H)-ylidene)acetic acid obtained from carboxylation of 1-(2-((4-(trifluoromethyl)phenyl)ethynyl)phenyl)ethan-1-one with CO_2 by Ag_3-TAPT-COF under optimized conditions.

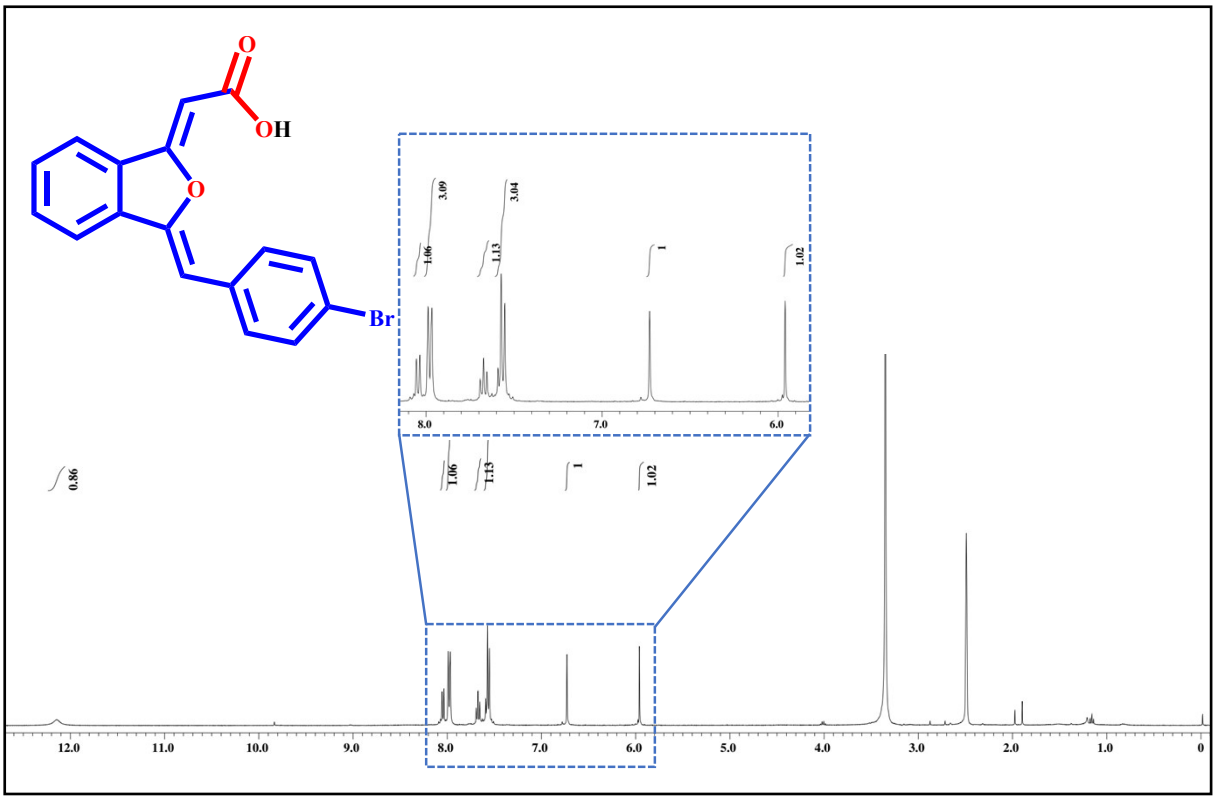

Fig. S63 ^{1}H NMR (DMSO-d_6, 400 MHz) spectrum of 2-((Z)-3-((Z)-4-bromobenzylidene)isobenzofuran-1(3H)-ylidene)acetic acid obtained from carboxylation of 1-(2-((4-bromophenyl)ethynyl)phenyl)ethan-1-one with CO_2 by Ag_3-TAPT-COF under optimized conditions.

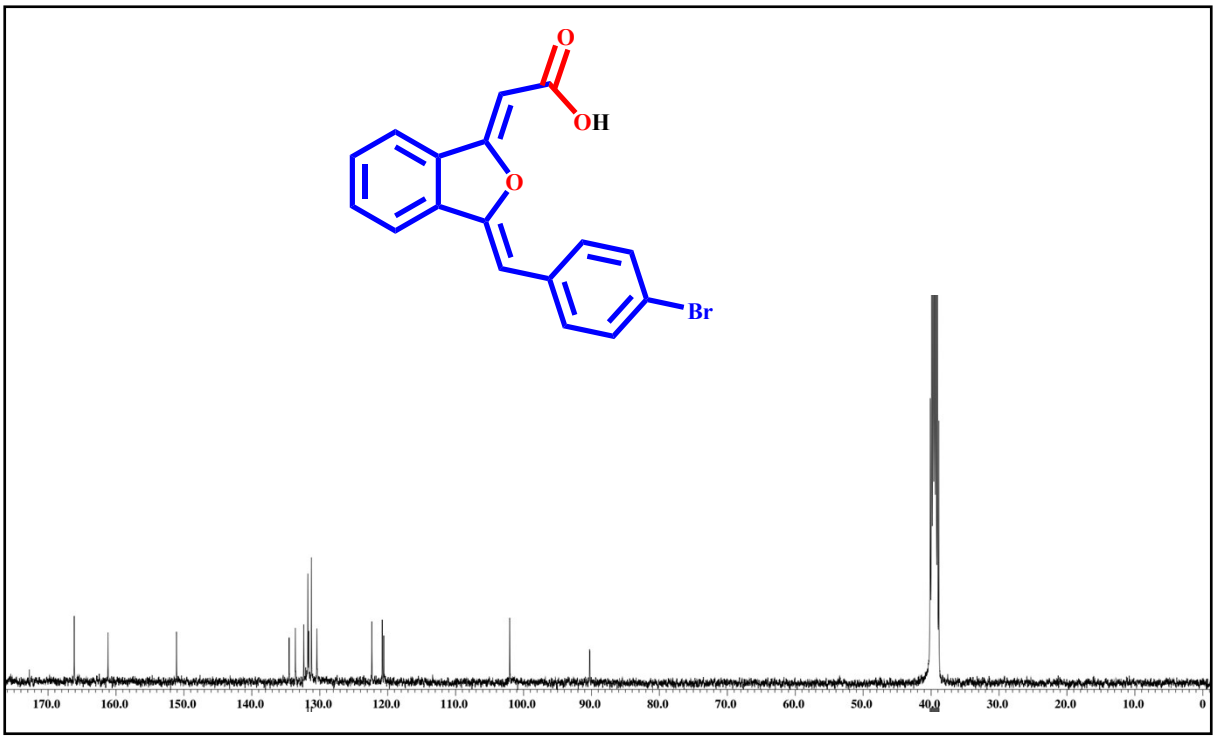

Fig. S64 ^{13}C NMR (DMSO-d_6, 101 MHz) spectrum of 2-((Z)-3-((Z)-4-bromobenzylidene)isobenzofuran-1(3H)-ylidene)acetic acid obtained from carboxylation of 1-(2-((4-bromophenyl)ethynyl)phenyl)ethan-1-one with CO_2 by Ag_3-TAPT-COF under optimized conditions.

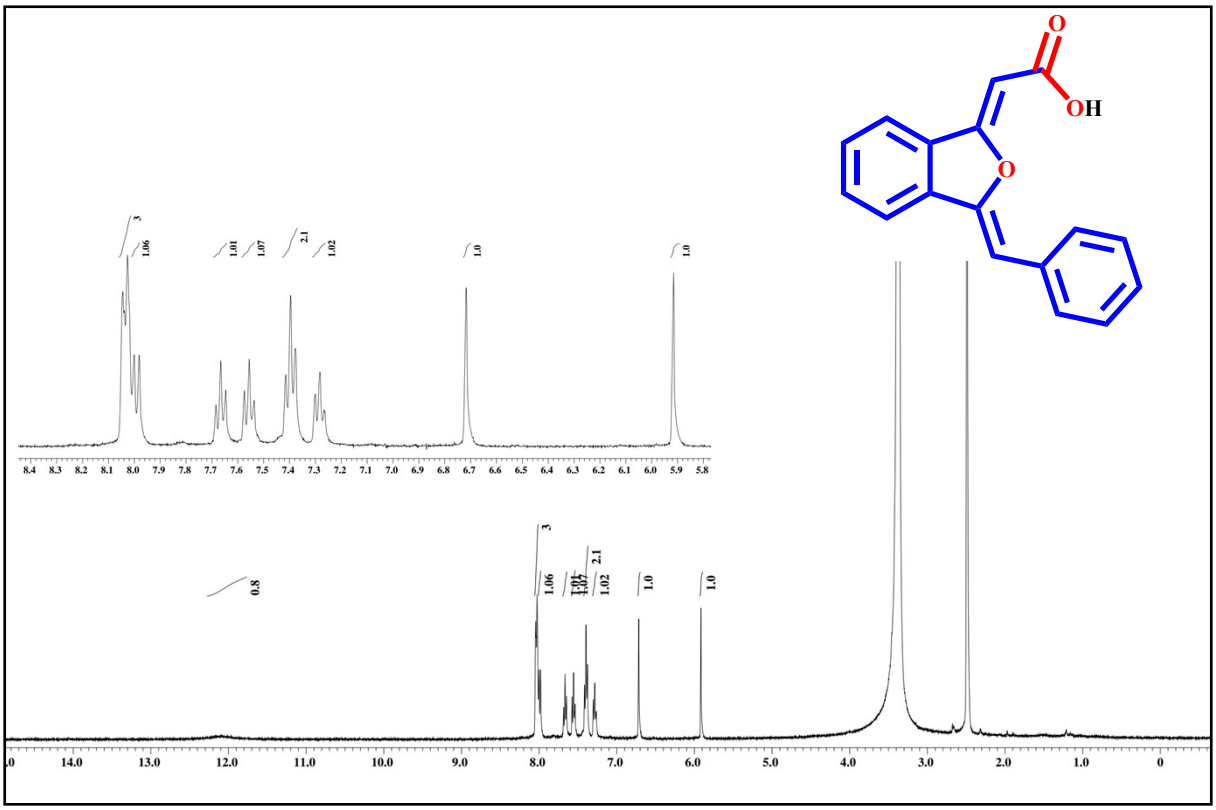

Fig. S65 ^{1}H NMR (DMSO-d_6, 400 MHz) spectrum of 2-((Z)-3-((Z)-benzylidene)isobenzofuran-1(3H)-ylidene)acetic acid obtained from carboxylation of 1-(2-(phenylethynyl)phenyl)ethan-1-one with CO_2 by Ag_3-TAPT-COF under K_2CO_3 basic conditions.

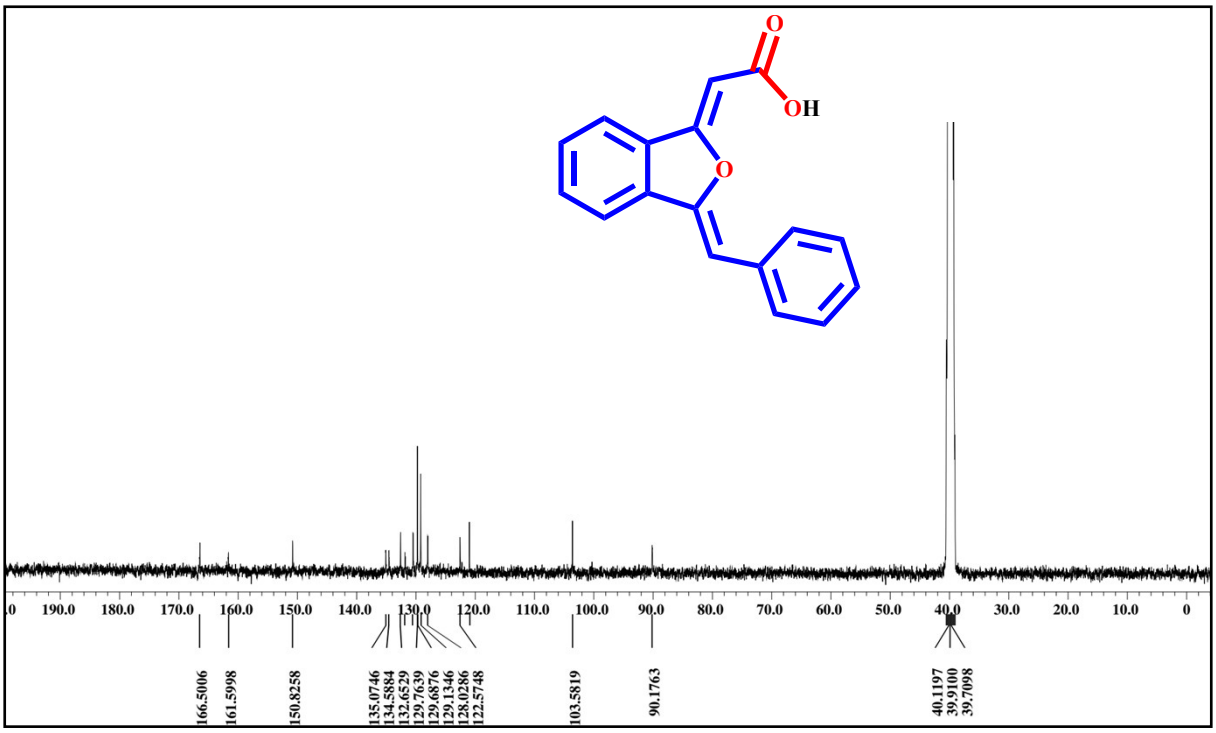

Fig. S66 ^{13}C NMR (DMSO-d_6, 101 MHz) spectrum of 2-((Z)-3-((Z)-benzylidene)isobenzofuran-1(3H)-ylidene)acetic acid obtained from carboxylation of 1-(2-(phenylethynyl)phenyl)ethan-1-one with CO_2 by Ag_3-TAPT-COF under K_2CO_3 basic conditions.

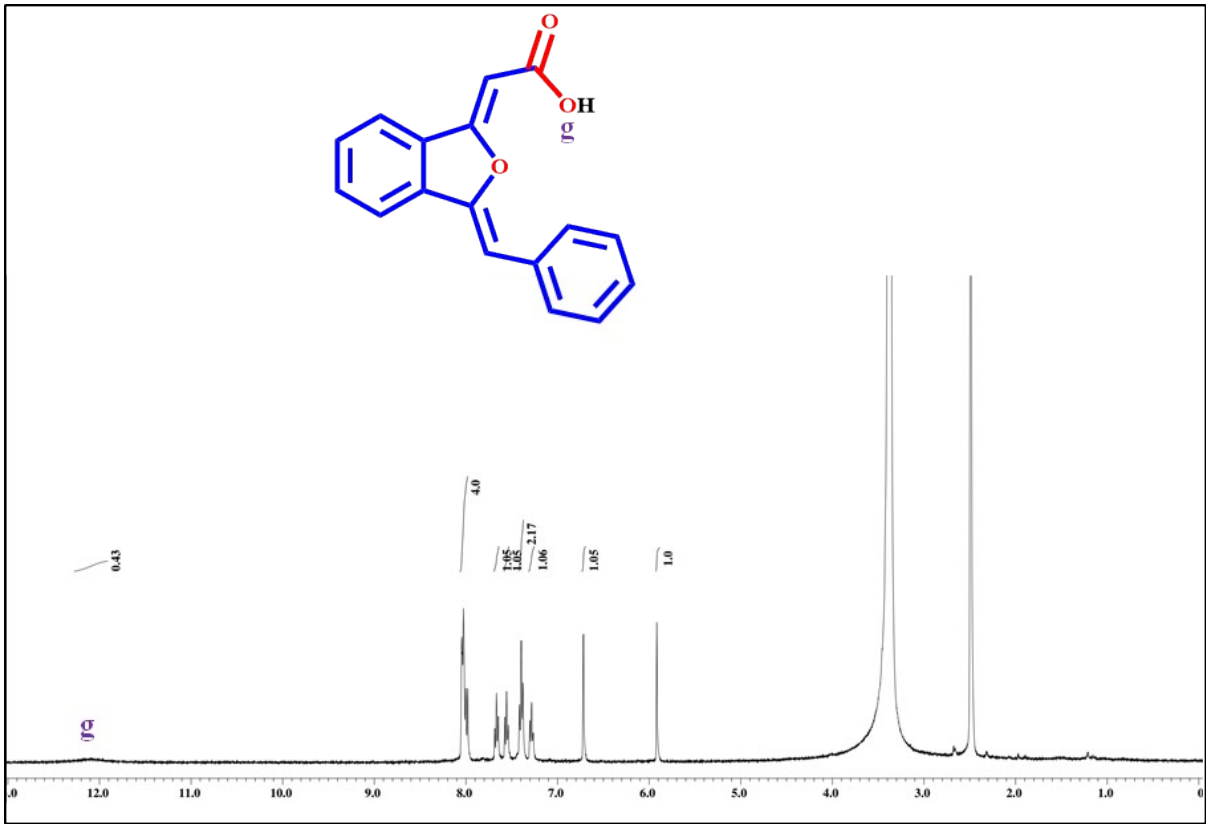

Fig. S67 ^{1}H NMR (DMSO-d_6, 400 MHz) spectrum of 2-((Z)-3-((Z)-benzylidene)isobenzofuran-1(3H)-ylidene)acetic acid obtained from carboxylation of 1-(2-(phenylethynyl)phenyl)ethan-1-one with CO_2 by $AgNO_3$ under optimised conditions.

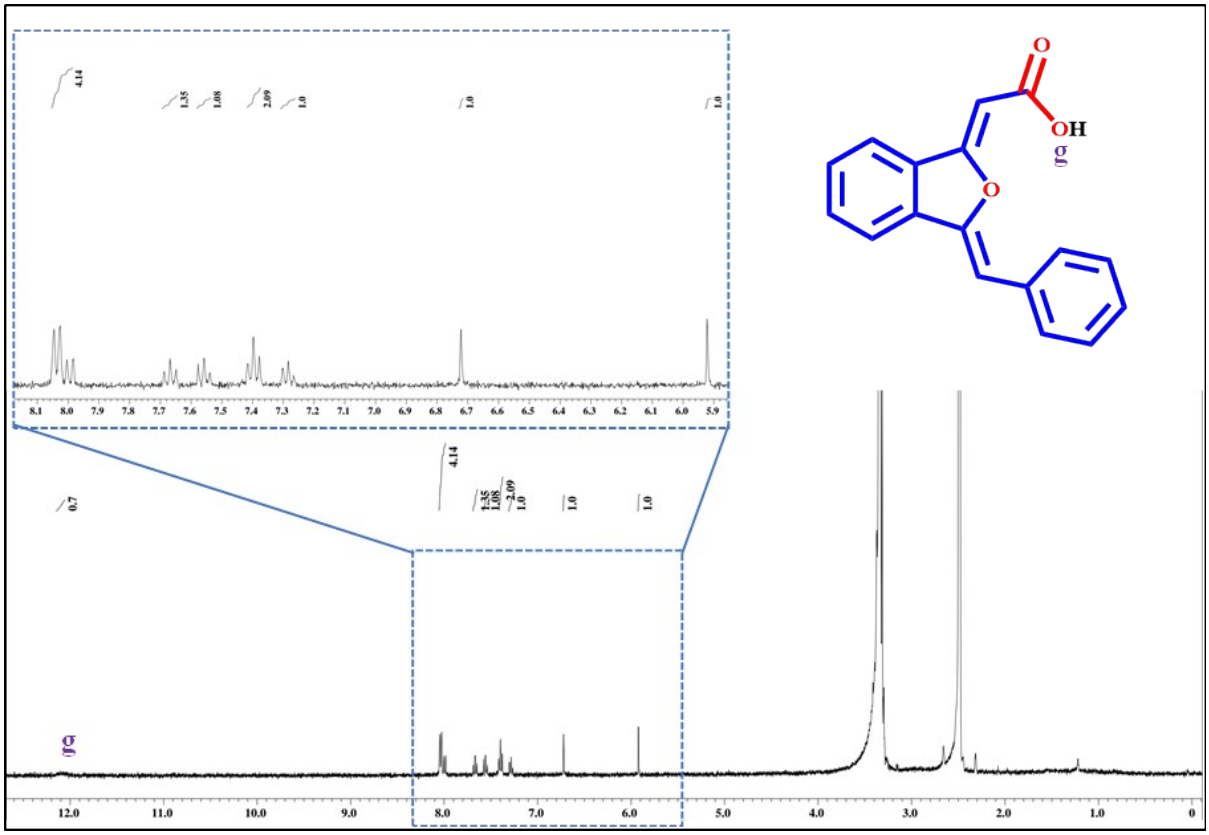

Fig. S68 ^{1}H NMR (DMSO-d_6, 400 MHz) spectrum of 2-((Z)-3-((Z)-benzylidene)isobenzofuran-1(3H)-ylidene)acetic acid obtained from carboxylation of 1-(2-(phenylethynyl)phenyl)ethan-1-one with CO_2 by Ag NPs under optimised conditions.

Table S7 Comparison of catalytic activity of Ag_3-TAPT-COF with reported catalysts for carboxylation of 1-(2-(phenylethynyl)phenyl)ethan-1-one with CO_2.

S. No.	Catalyst	Temp. (°C)	Time (h)	Pressure (bar)	Yield (%)	Ref.
1.	10 mol% AgOAc	30	3	10	92	4
2.	2 mol% $AgBF_4$	25	12	Balloon	75	5
3.	0.02 mmol CuI	60	24	20	54	6
4.	**0.00033 mmol Ag_3-TAPT-COF**	**50**	**12**	**balloon**	**88**	**This work**

Catalyst stability and recycling study

The heterogeneous nature of Ag_3-TAPT-COF was examined by recycling tests. The recycling experiments revealed the formation of silver nanoparticles (NPs), most likely due to the highly basic reaction environment.[1] We speculate that the deprotonated substrates, 4-hydroxy-pyridone or 1-(2-(phenylethynyl)phenyl)ethan-1-one in the presence of base LiHMDS or DBU, act as a reductant/ligand that reduces Ag(1) to Ag(0) NPs. To gain further support, the catalytic reaction was repeated using $Ag(NO_3)_2$ as a catalyst, and the characterization of the recovered catalyst unveiled the formation of Ag(0) NPs. To ruleout the effect of solvents in reduction of Ag(1) to Ag(0) NPs, COF stability was examined in various solvents, including THF, DMF, and ACN, which showed retention of the original framework structure (Fig. S69). These control experiments further support the stability of COF and in situ formation of Ag NPs during the catalytic reaction. Furthermore, Ag NPs were characterized by various techniques, including PXRD, XPS, FE-SEM, and HR-TEM analyses. The PXRD pattern (Fig. S70) displayed diffraction peaks at 2θ values of 38.2°, 44.3°, 64.5°, 77.6°, and 83.3°, which are assigned to (111), (200), (220), (311), and (331) crystallographic planes of metallic silver

(JCPDS 04-0783). Furthermore, the XPS survey spectrum confirmed the presence of all the expected elements, Ag, N, and C in the recycled sample (Fig. S70). From HR-TEM analyses, it was observed that the NPs are spherical in nature, with an average size of 50 nm. The SEAD patterns show the crystalline nature, and the lattice spacing of 0.235 nm corresponds to the (111) plane of the silver NP (Fig. S71).

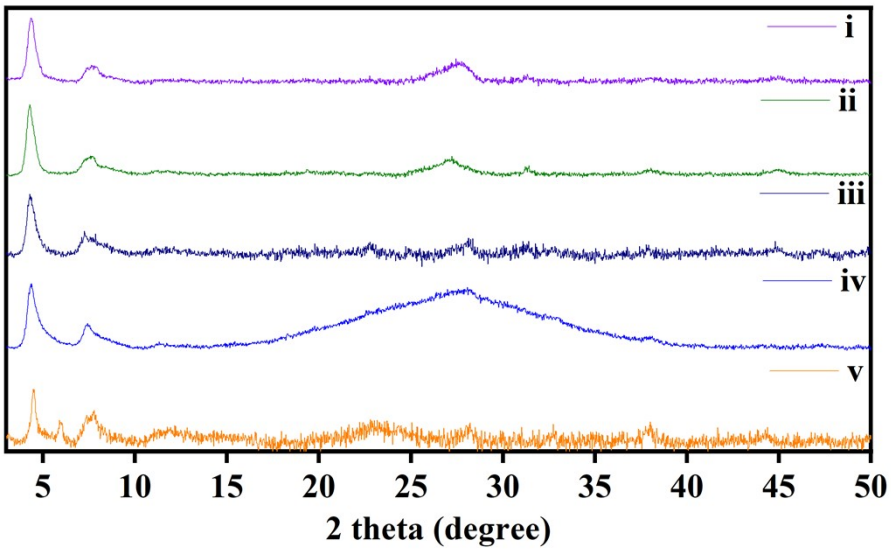

Fig. S69 PXRD patterns of Ag_3-TAPT-COF treated with (i) THF, (ii) ACN, (iii) DMF, (iv) DMF in the presence of DBU, and (v) DMF in the presence of DBU at 50 °C.

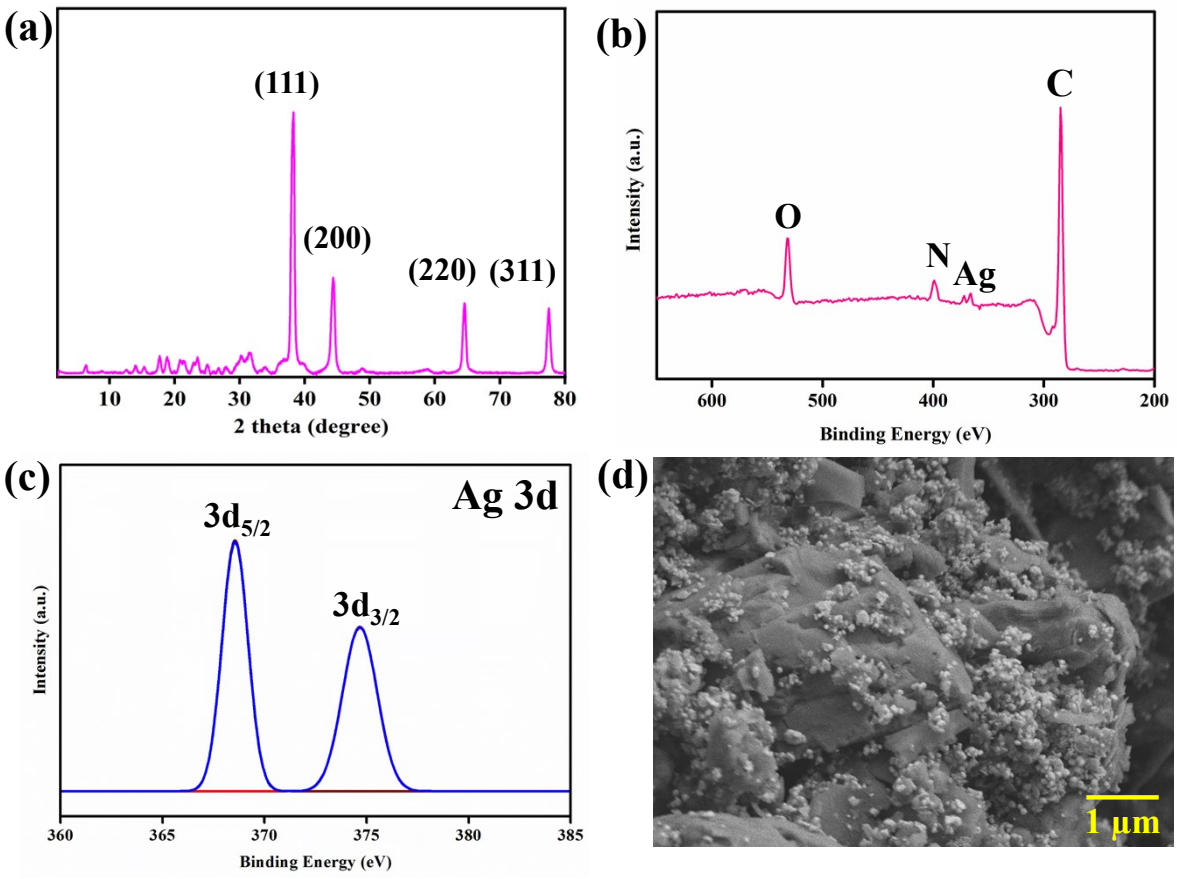

Fig. S70 (a) PXRD patterns of recycled Ag_3-TAPT-COF, (b and c) XPS survey scans Ag 3d spectra, and (d) FE-SEM image of recycled Ag_3-TAPT-COF.

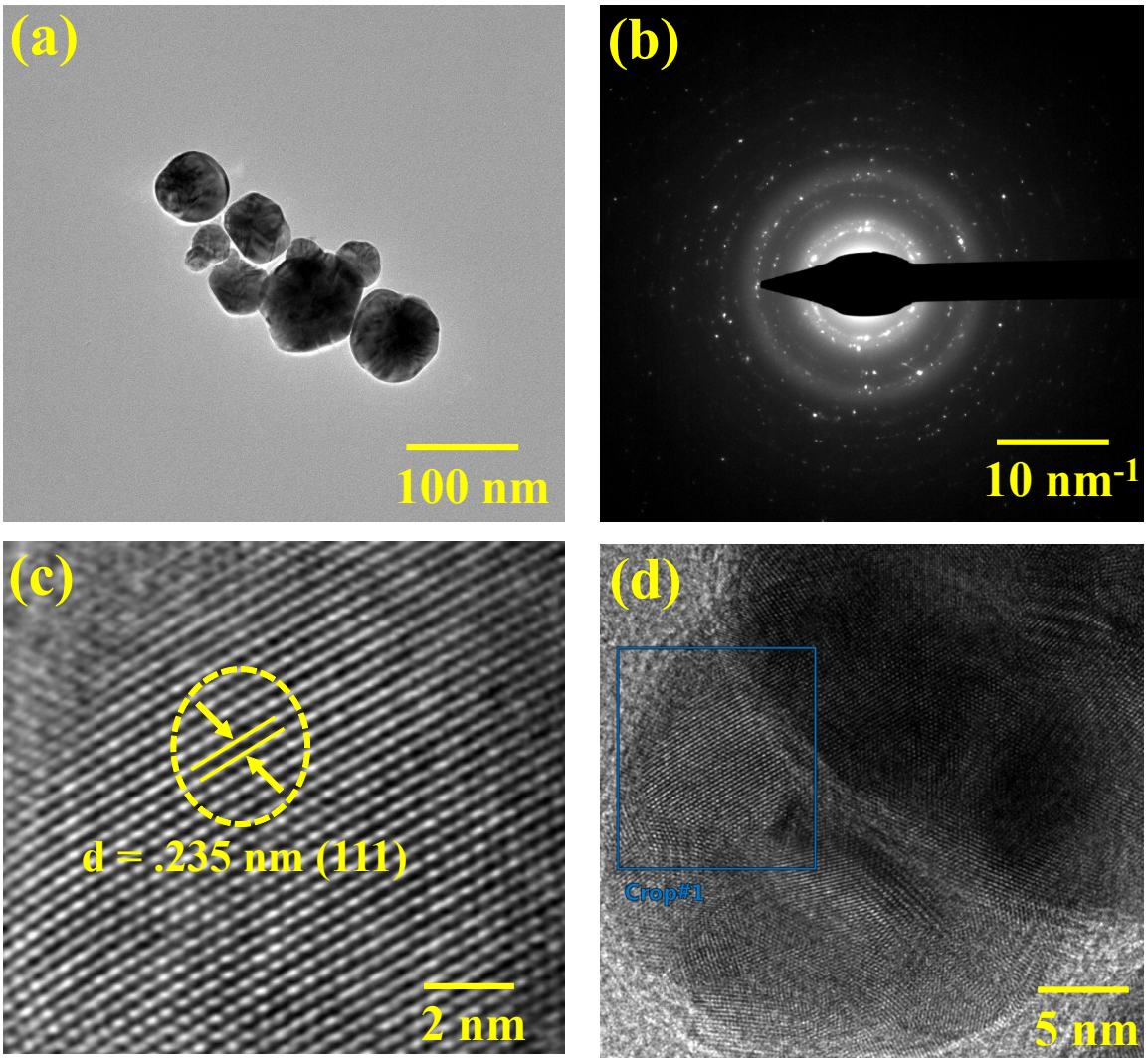

Fig. S71 (a) HR-TEM image of recycled Ag_3-TAPT-COF, (b) SAED pattern, (c and d) Lattice fringes of Ag.

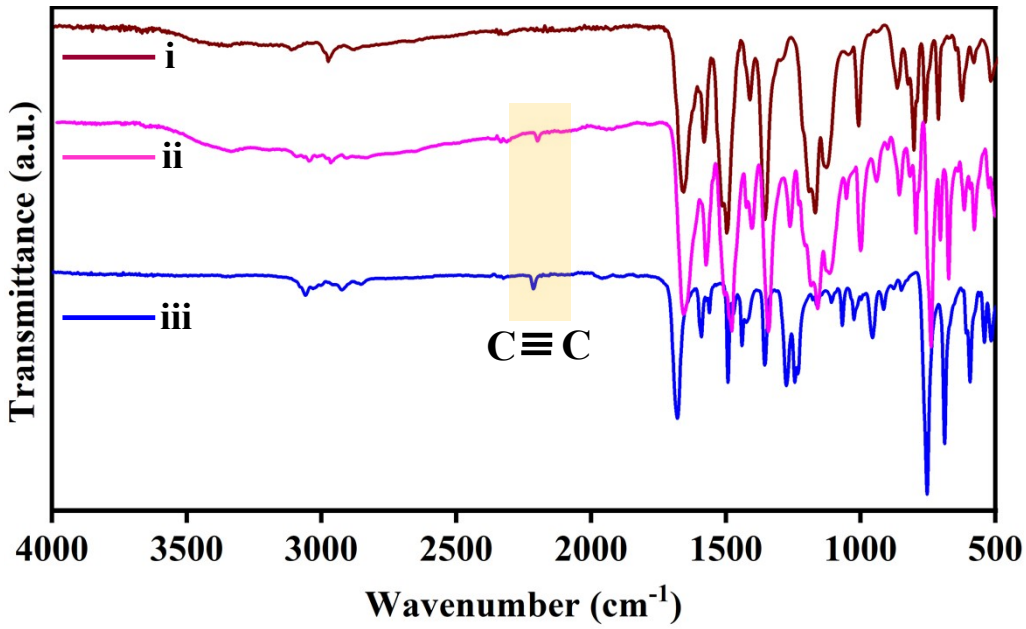

Fig. S72 FT-IR stack plot of Ag_3-TAPT-COF (i), Ag_3-TAPT-COF treated with 1-(2-(phenylethynyl)phenyl)ethan-1-one (ii), and 1-(2-(phenylethynyl)phenyl)ethan-1-one (iii).

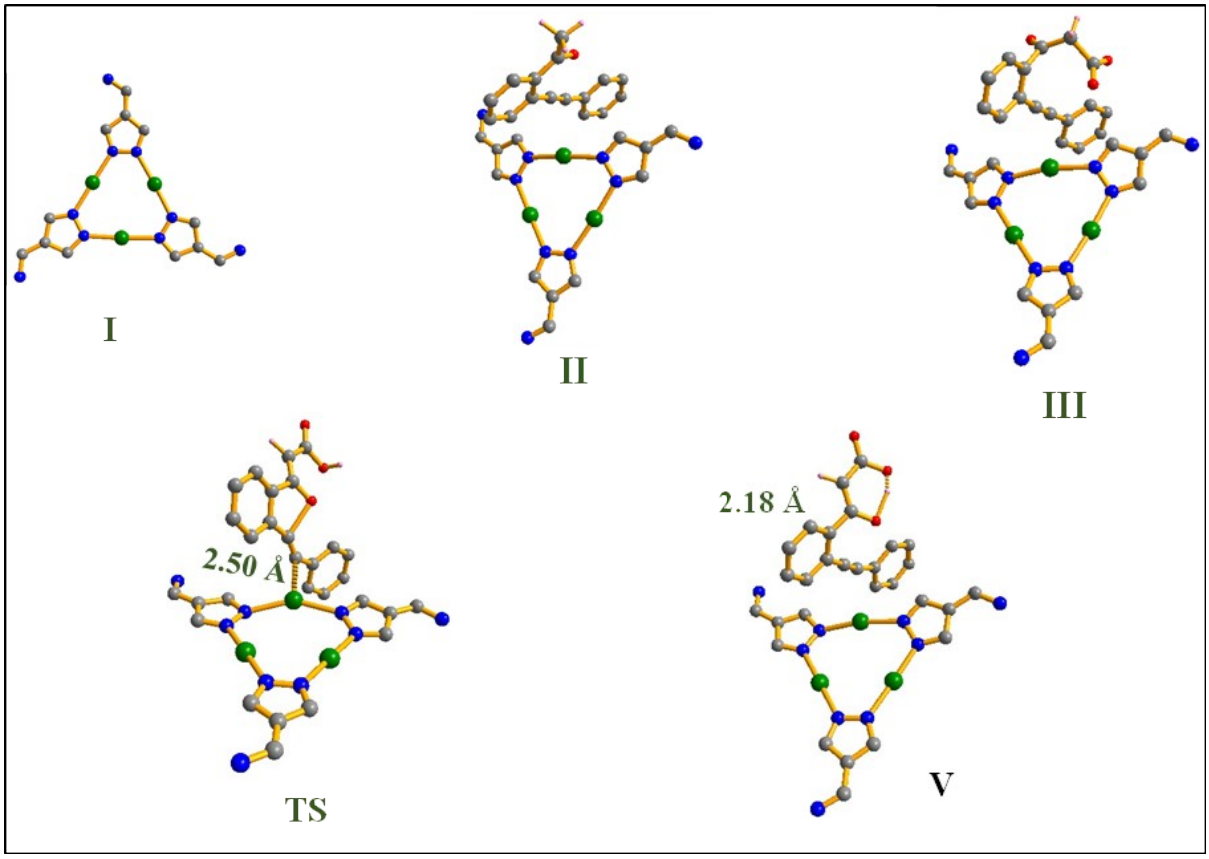

Figure S73. Optimized structures of intermediates and transition state for path A in the catalytic sp^3 C-H carboxylation of 1-(2-(phenylethynyl)phenyl)ethan-1-one with CO_2 catalyzed by Ag_3-TAPT-COF (bond distances are in Å).

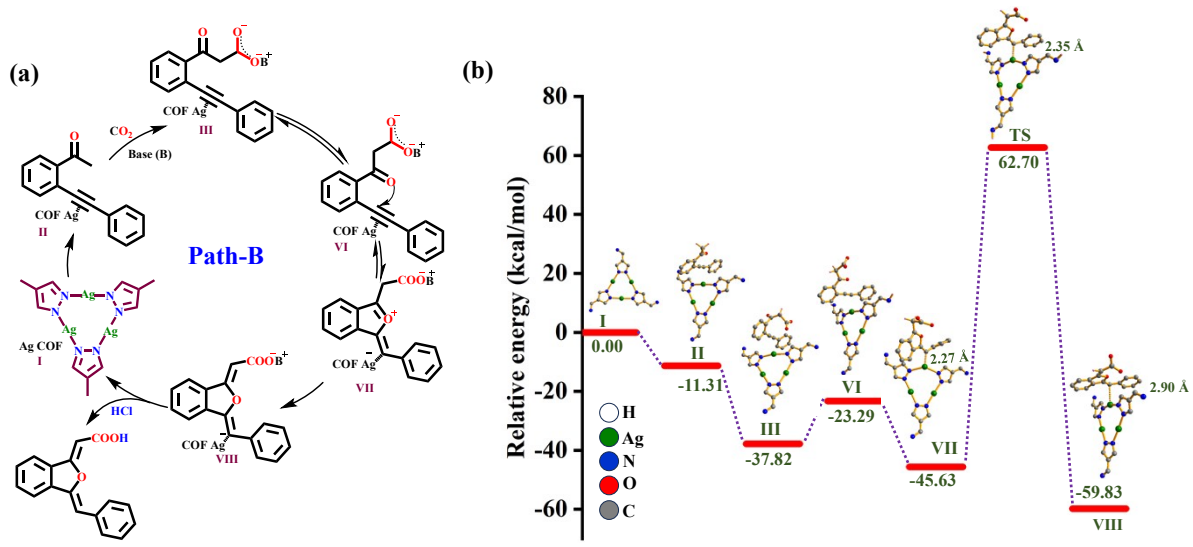

Fig. S74. (a) Plausible mechanism and (b) Theoretical energy profile diagram for path-B in carboxylation of 1-(2-(phenylethynyl)phenyl)ethan-1-one with CO_2 catalyzed by Ag_3-TAPT-COF.

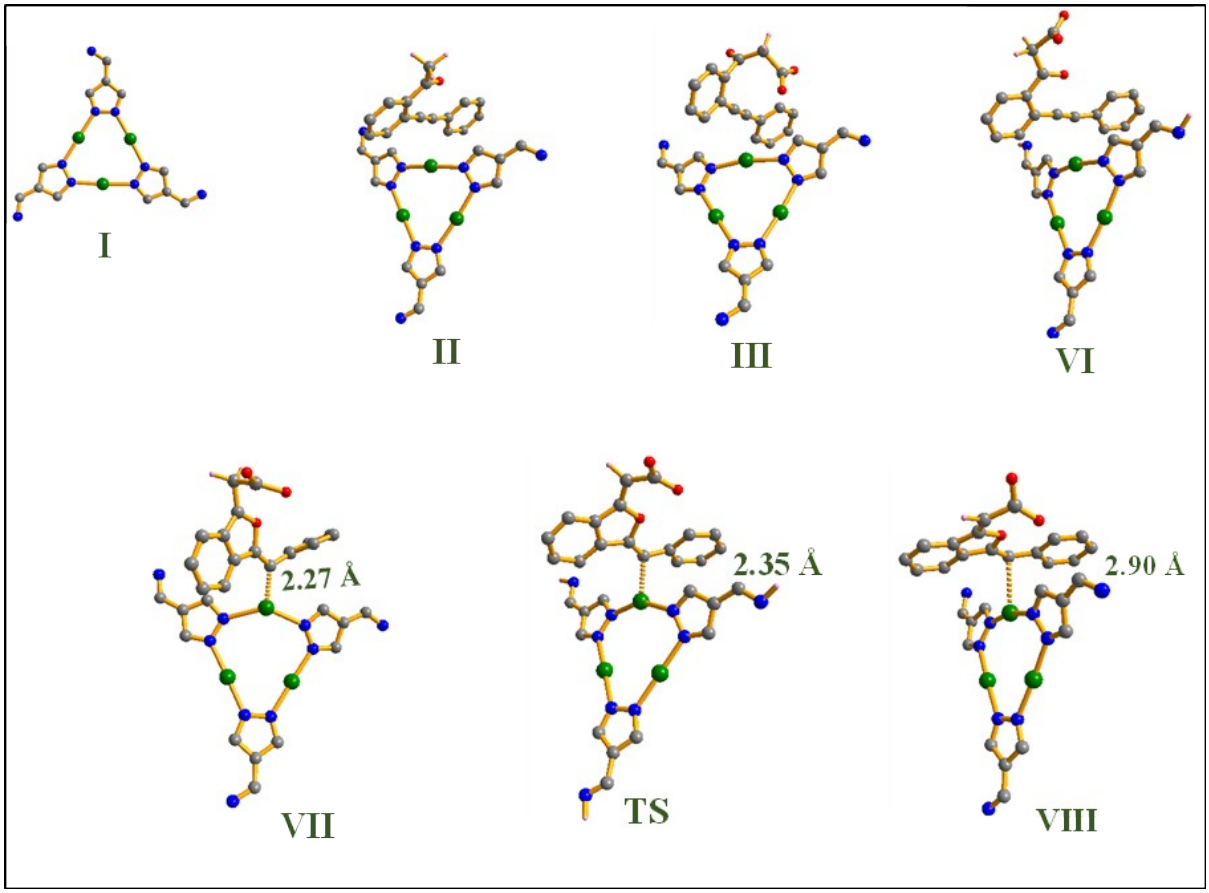

Fig. S75 Optimized structures of intermediates and transition state of path-Bin the catalytic sp^3 C-H carboxylation of 1-(2-(phenylethynyl)phenyl)ethan-1-one with CO_2 catalyzed by Ag_3-TAPT-COF (bond distances are in Å).

References

1. Y. -Y. Tang, X. Luo, R. -Q. Xia, J. Luo, S. -K. Peng, Z. -N. Liu, Q. Gao, M. Xie, R. -J. Wei, G. -H. Ning and D. Li, Molecular Engineering of Metal–Organic Frameworks for Boosting Photocatalytic Hydrogen Peroxide Production, *Angew. Chem. Int. Ed.*, 2024, **63**, e202408186.

2. D. R. Kishore, K. Goel, C. Shekhar and G. Satyanarayana, An Access to Benzo[*a*]fluorenes, Benzo[*b*]fluorenes, and Indenes Triggered by Simple Lewis Acid, *J Org Chem*, 2022, **87**, 2178-2203.

3. H. Pan, J. A. Ritter and P. B. Balbuena, Examination of the Approximations Used in Determining the Isosteric Heat of Adsorption from the Clausius-Clapeyron Equation, *Langmuir*, 1998, **14**, 6323–6327

4. K. Sekine, A. Takayanagi, S. Kikuchi and T. Yamada, Silver-catalyzed C–C bond formation with carbon dioxide: significant synthesis of dihydroisobenzofurans, *Chem. Commun.,* 2013, **49**, 11320.

5. W.-Z. Zhang, L.-L. Shi, C. Liu, X.-T. Yang, Y.-B. Wang, Y. Luo and X.-B. Lu, Sequential carboxylation/intramolecular cyclization reaction of o-alkynyl acetophenone with CO_2. *Org. Chem. Front.*, 2014, **1**, 275.

6. W.-Z. Zhang, M.-W. Yang, X.-T. Yang, L.-L. Shi, H.-B. Wang and X.-B. Lu, Double carboxylation of o-alkynyl acetophenone with carbon dioxide, *Org. Chem. Front.*, 2016, **3**, 217.